STUDIES ON ALUMINOSILICATE AND ALUMINOPHOSPHATE MOLECULAR SIEVES

A THESIS
SUBMITTED TO THE
UNIVERSITY OF POONA
FOR THE DEGREE OF
DOCTOR OF PHILOSOPHY
(IN CHEMISTRY)

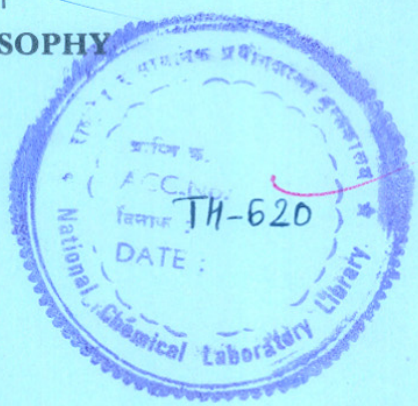

BY
S. PRASAD

INORGANIC CHEMISTRY DIVISION
NATIONAL CHEMICAL LABORATORY
PUNE-411 008 (INDIA)

JULY 1991

CERTIFICATE

Certified that the work incorporated in the thesis entitled "Studies on Aluminosilicate and Aluminophosphate Molecular Sieves" submitted by S. Prasad was carried out by the candidate under my supervision. Such material as has been obtained from other sources has been duly acknowledged in the thesis.

Research Guide

P. Ratnasamy

CONTENTS

ACKNOWLEDGEMENTS

I wish to express my deep sense of gratitude to Dr.P. Ratnasamy, Deputy Director, National Chemical Laboratory, Pune for his valuable guidance throughout the course of the investigation.

I am grateful to Dr.B.S. Rao and Dr.I. Balakrishnan for their constant encouragement and many stimulating discussions.

I thank Dr.R. Vetrivel for giving me an insight into Molecular Modelling studies and his help in the course this work.

My thanks are due to Mr. S. Mani for meticulous type–setting of the thesis and, friends and colleagues for their co–operation.

Finally, my thanks are due to Council of Scientific and Industrial Research, New Delhi, for the award of a fellowship and the Director, National Chemical Laboratory, Pune for permitting to submit this work in the form of a thesis.

S. Prasad

ABSTRACT

ZSM–5 zeolites have been modified by Chemical Vapour Deposition (CVD) and impregnation methods and the catalysts studied for the selective synthesis of para dialkylbenzenes.

A successive modification technique was used to coat the zeolite surface with layers of silica. The properties of the catalyst were studied as a function of the amount of silica deposited. The rate of sorption of o– and p–xylene was drastically reduced upon deposition of silica, but the surface area remained almost the same. As for the catalytic results, the activity dropped, para–selectivity improved and the B/DEB remained the same. The above results lead the conclusion that, by CVD, only the zeolite external surface and the pore mouth are modified leaving the internal structure intact. A trend in para–selectivity of PDEB > PET > PX was obtained with the silynated catalyst.

In alkylation of ethylbenzene, an aluminolanthanosilicate catalyst of ZSM–5 type showed higher para–selectivity on account of occluded lanthanum species inside the pores. The para–selectivity has been improved by modifying the catalyst with oxide of magnesium. The sorption, acidic, and catalytic properties of the modified catalyst were comparatively less.

Several alumionophosphates have been synthesized by modifying the synthesis parameters such as source of aluminium, crystallization period and temperature, concentration of the amine etc.

The medium pore aluminophosphate molecular sieve $AlPO_4$–11 has been synthesized by using additional templating agents such as n–dibutylamine and n–dipentylamine. The extended lengths of these molecules exceeds the unit cell c–dimension of the $AlPO_4$–11. Modelling and quantum chemical calculations results indicate conformational flexibility for the amine molecules due to rotational freedom along the N–C bond and the possibility to accommodate a terminal methyl group in the double 6–member side–pocket. Based

on MNDO calculations, the net charge on the nitrogen atom's in the amine molecules was found to be similar and independent of the dimension and nature of the alkyl group. Ammonia was chosen as a model amine molecule and its adsorption on bridging oxygen sites was studied. The results were extrapolated to understand the the nature of interaction of amine molecules with the $AlPO_4$–11 framework. In addition to the above studies, ^{13}C CP MASNMR results provided evidence for the dynamic movement of the amine molecules inside the one–dimensional tubular channels of $AlPO_4$–11.

X–ray diffraction pattern and NMR spectra showed different profiles on calcination and rehydration of $AlPO_4$–11. The extra peaks in the NMR spectra which correspond to 20% of the total area under the signals have been attributed to the interaction of the T–site of the framework with water molecules. The T3 site of the $AlPO_4$–11 framework corresponds to 20% of the total T–sites. The NMR results have been directly correlated to this ie. the T3 sites are affected by water molecules.

The results of modelling studies are consistent with the NMR results. The values of the adsorption energies calculated indicated that the Al3 and P3 are the preferred sites for adsorption of water molecules. Also the larger T3–O–T angle poses minimum steric hindrance to the approaching water molecules.

In addition to studies on $AlPO_4$–11, a cobalt substituted $AlPO_4$–11 has been successfully synthesized. Isolated redox centres have been detected based on catalytic test reactions. The CoAPO–11 has been compared with MnAPO–11.

Literature data show that both VPI–5, the largest pore molecular sieve and $AlPO_4$–8 crystallize from similar gel composition and hydrothermal treatment conditions. According to the present studies, VPI–5 transformed to $AlPO_4$–8 even at 388 K as studied by X–ray diffraction and MASNMR studies. The studies led to a precursor–product relationship between the two. The organic–free VPI–5, $AlPO_4$–H1 has been synthesized and its identity with VPI–5 re–established based on data from XRD and MASNMR spectral measurements. Transformation of H1 to $AlPO_4$–8 like that observed in the case of VPI–5 has been confirmed. The present studies show that $AlPO_4$–8 cannot be synthesized directly

without the thermal treatment of either VPI–5 or H1 and that no organic is needed for its synthesis.

An aluminophosphate probably having a layered structure has been crystallized by increasing the amine concentration in the synthesis system for VPI–5. Characterization by the different techniques indicates that it may have a layered structure.

PART-I

ALUMINOSILICATE MOLECULAR SIEVES

CHAPTER 1

HIGH SILICA ZSM-5 ZEOLITES

1 HIGH SILICA ZSM–5 ZEOLITES

1.1 INTRODUCTION

1.1.1 Zeolites

Zeolites are crystalline aluminosilicate molecular sieves, based on indefinitely extending 3D network of SiO_4 and AlO_4 units joined by sharing corner oxygen atoms. These framework structures contain channels and/or cages of specific dimensions, giving rise to sorption and molecular sieving properties of zeolites. A unit negative charge associated with every AlO_4 tetrahedron is balanced by cations in the channel or cavity of the zeolite. These charge–compensating cations can be freely interchanged, giving rise to ion–exchange properties in zeolites. If the cation is a proton, then the negatively charged Al is the source of Brönsted acidity.

Zeolites of interest to shape selective catalysis may be divided into three groups according to their pore/channel systems. Their classifications and structural properties are shown in Table 1.1. They differ from each other in their Si/Al ratio and/or ion–exchange capacity, pore size, shape selective behaviour, acidity and sorption, and find extensive commercial application in purification, separation and catalytic processes [1–5].

1.1.2 Pentasil Zeolites

These are medium pore zeolites. ZSM–5[6], ZSM–11[7], theta 1[8] (which is iso–structural with ZSM–22[9]), ZSM–23[10] and ZSM–48[11] are examples of this class. They are synthetic in origin. Their framework structure contains 5–member oxygen rings (hence the name Pentasil) and are more siliceous than previously known zeolites.

The configuration and linkage of the secondary building units (SBU) within the chains in ZSM–5 are shown in Fig. 1.1. The low energy complexes 5–1 SBU (which are thermodynamically stable) in the framework of pentasil zeolites are responsible for their high

Structure type	Ring size of channels	Largest channel (Å) dimensions
Linde Type A	8–8–8	4.1
Chabazite	8–8–8	3.6×3.7
Erionite	8–8	3.6×5.2
ZSM–22	10	4.5×5.5
ZSM–23	10	4.5×5.6
ZSM–48	10	5.3×5.6
Ferrierite	10–8	4.3×5.5
ZSM–5	10–10	5.4×5.6
ZSM–11	10–10	5.1×5.5
ZSM–12	12	5.7×6.1
Linde Type L	12	7.1
Modenite	12–8	6.7×7.4
Offertite	12–8–8	6.4
Faujasite	12–12–12	7.4

TABLE 1.1. **Classification of Zeolites According to the Size of Channels and Pores.**

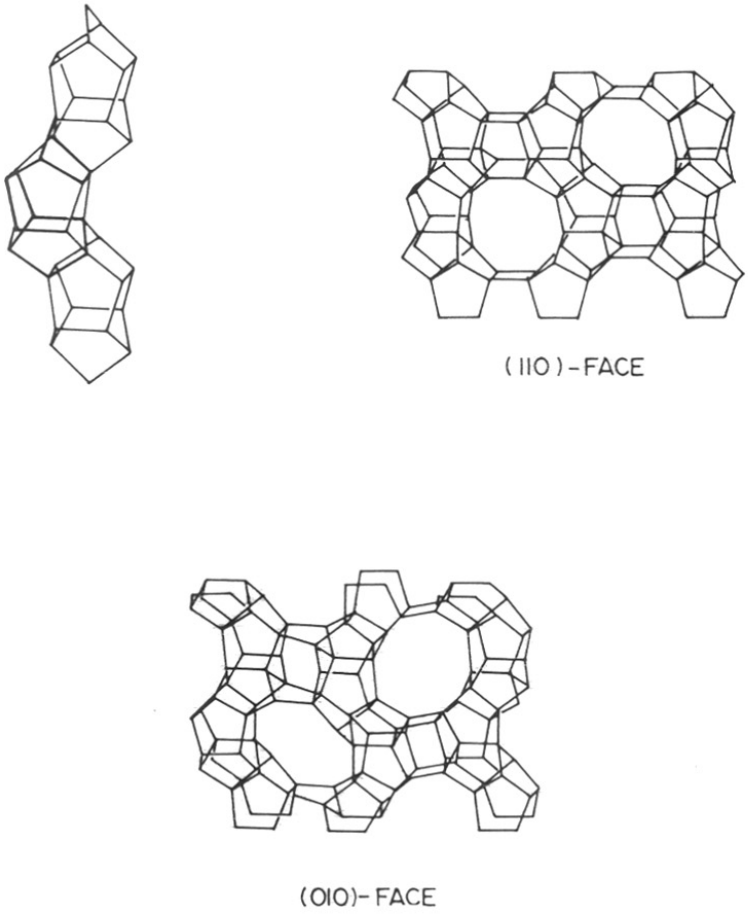

Fig. 1.1 ▷ **Framework model of ZSM–5.**

thermal and acid/base stability.

The pentasil zeolites are superior to the conventional ones like X,Y and mordenite because of their following unique properties:

1. High thermal and hydrothermal stability and inertness to most mineral acids (except HF).
2. Molecular shape selectivity arising from steric restrictions during sorption and catalytic reactions at active sites.
3. High resistance to deactivation by to coke formation and, hence, long life in catalytic conversion processes as compared to other zeolites.

1.2 ZSM–5 ZEOLITES

The discovery of the zeolite ZSM–5 by Mobil[12] has resulted in a number of high potential catalysts for obtaining synthetic fuels and hydrocarbons from methanol[3,4] as well as catalysts for other industrial conversion processes[3,5].

1.2.1 Structure of ZSM–5

The unit cell composition of the sodium form of ZSM–5 can be represented as follows:

$$Na_nAl_nSi_{96-n}O_{192} \approx 16H_2O(\text{where } n < 27)$$

The structure of ZSM–5 was reported by Mobil workers in 1978[6]. The framework of the zeolite (Fig. 1.1) consists of a 3D system of intersecting near circular zig–zag channels (0.54×0.56nm) defined by 10–ring of oxygen atoms in all three directions running parallel to (001) and cross linked by elliptical channels (0.51×0.55nm) parallel to the (010) plane. A large fraction of the crystal structure is made up of 5–member rings of silicon oxygen tetrahedra. Linkage of chains occurs through 4–, 5– and 6–member rings. The crystallographic data of ZSM–5 are presented in Table 1.2.

It has been shown that[13] the ZSM–5 can exist over a wide span of composition with the silica content approaching 100%. Silicalite 1 appears to be essentially the Al free end member of the iso–structural ZSM–5 series[14]. The X–ray and electron diffraction studies have shown that ZSM-5 and silicalite 1[14,15] have the same skeletal structure.

Secondary building units	Complex 5–1
Framework density	17.9 (Si+Al) per nm^3
Channels	10–member ring, intersecting, zig–zag, 0.54×0.56 nm parallel to [001] Straight, 0.51×0.55 nm parallel to [010]
Fault planes	100
Unit cell composition	$Na_n\ Al_n\ Si_{96-n}\ O_{192} \approx 16H_2O$ (where $n < 27$)
Crystal symmetry/Space group	Orhtorhombic/Pnma
Unit cell dimensions	a=2.01 nm, b=1.99 nm c=1.34 nm.

TABLE 1.2. **Crystallographic Parameters for ZSM–5**

1.2.2 Structural Stability of ZSM–5

ZSM–5 zeolite possesses high thermal (upto 1283 K) and steam stability, and is also stable to most mineral acids compared to other catalytically important zeolites[12,16–18]. It is stable even to heavy thermal shocks[17]. These properties permit reactions to be carried out in the presence of water vapour and regeneration of the deactivated catalyst at high temperature. Silicalite 1 possesses a very high thermal stability (up to 1573 K)[14] and converts only slowly to an amorphous glass at 1573 K. Like quartz it is stable to most mineral acids.

Wu et al.[19] have observed that the crystal symmetry of TPA–ZSM–5 is orthorhombic; However, it converts to an apparent monoclinic form when subjected to treatments such as calcination and ion–exchange. They have further observed that the change in the crystal symmetry is reversible and the displacive transformation between the two forms of the zeolite does not cause any basic change in the framework structure.

1.2.3 Acidic Properties

The acidic properties of ZSM–5 zeolites have been extensively investigated by temperature programmed desorption of ammonia[15,20–22] and pyridine[16,19,23,24], microcalorimetric measurements of the heat of ammonia sorption[25,26], and IR spectroscopy of adsorbed pyridine on the zeolite[21]. Haag and co-workers[13,27] have observed that the catalytic activity of HZSM–5 in cracking of n–hexane and in toluene disproportionation varies linearly with the tetrahedral Al content of the zeolite over a wide composition range and extrapolates to zero activity at zero Al content. Such a linear correlation has also been observed by Chen and Reagan[28] in the conversion of methanol to hydrocarbons.

1.2.4 Sorption Properties

Sorption measurements help in exploring specific interactions between sorbate molecules and framework structures in the intracrystalline channels[29].

In contrast to classical zeolites, ZSM–5 type zeolite are all hydrophobic with the degree of hydrophobicity increasing with the decrease in Al content[13]. Flanigen et al.[14] have

observed that silicalite has a low selectivity for the adsorption of water and a high preference for organic molecules. Anderson et al.[15] have studied the adsorption of hydrocarbons and heterogeneous bases on HZSM–5, NaHZSM–5 and silicalite at 293 K and assessed the ease of sorption in terms of the effective molecular size and channel size of the zeolite.

Isosteric heats of adsorption reflect the strength of interactions[29,30] between the sorbate molecules and the force field in the intracrystalline porous void. The void volume in zeolite can be measured by adsorption of molecules which have free access into the void. In the case of ZSM–5, the volume of hexane, heptane or p–xylene adsorbed gives an estimate of the void volume of the zeolite[30]. Derouane and Gabalica[31] and Valyon et al.[32] have evaluated the channel length per unit cell of ZSM–5 from a knowledge of sorbate molecules adsorbed per unit cell and their dimensions. Gabalica et al.[33] and Kim et al.[34] have studied the adsorption of hexane to investigate the influence of zeolite modification on sorption properties.

Dessau[35] has investigated the selective adsorption property of ZSM–5 by measuring sorption of hydrocarbons and alcohols from solutions. Competitive sorption, counter diffusion and selective sorption of binary alkane solutions were studied.

1.2.5 Shape Selectivity of ZSM–5 Zeolites

The principle of shape selective catalysis on zeolites has been discussed in a number of comprehensive reviews[36–39]. Recently, Chen and Garwood[40] presented data on the impact of shape selective catalysis on the petroleum industries with emphasis on medium pore zeolites. Molecular shape selectivities are distinguished in four main types: reactant selectivity, product selectivity, transition state shape selectivity, and molecular traffic control. These selectivities can be understood with the help of Fig. 1.2. Reactant shape selectivity results from a limited diffusivity of some of the reactants. Product selectivity occurs when some of the products cannot diffuse rapidly from the crystal and undergo secondary reactions. Restricted transition state selectivity arises from the local environment around the active site; the rate constant for a reaction via certain mechanisms is reduced if the mechanism needs a transition state too bulky to form readily[41] within the pore structure

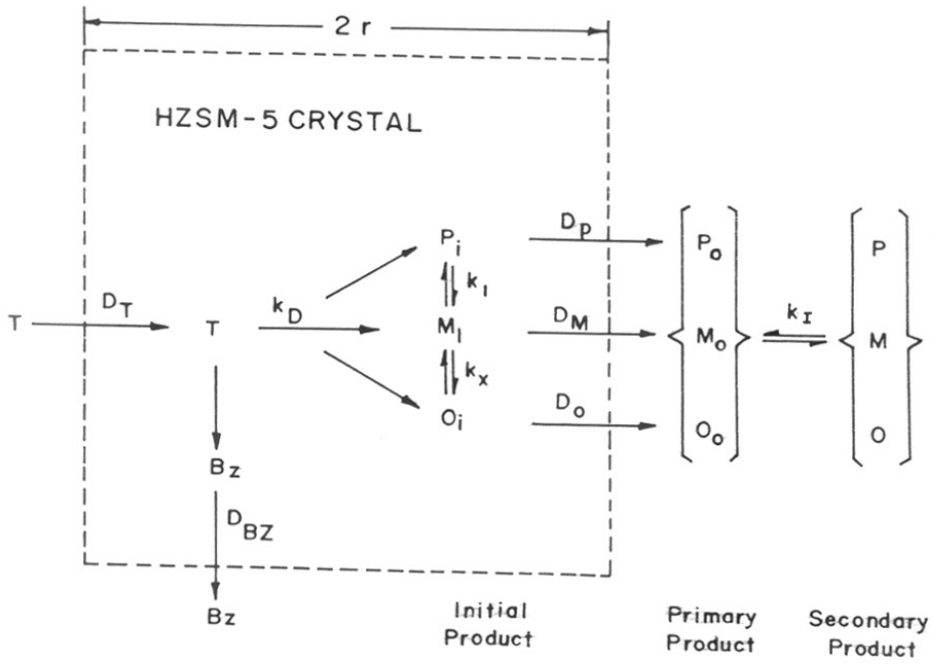

Fig. 1.2 ▷ Model for Toluene disproportionation. Bz = benzene, T = Toluene, P,M, O = para–, meta–, ortho–xylene

of the zeolite. In molecular traffic control, observed in the case of zeolites with more than one type of intersecting channel, reactants enter preferentially through one type of channels, whereas products diffuse out by the other thus minimizing counter diffusion. Evidence for[42] and against molecular traffic control[43] has been presented. According to Derouane[31,42,44], the product selectivity (in methanol conversion) is probably controlled by molecular shape selective constraints on the formation of the intermediate complex structures. Steric inhibition is attributed to the particular dimension of the channel intersection which restrain the oligomerization of iso–paraffin and precludes the accommodation of bimolecular complex of more than 10 atoms. The shape selective nature of ZSM–5 can also be utilized in the separation of hydrocarbons. Namba et al.[45] studied the relative sorption of 2–methyl pentane and 2–2–dimethyl butane and observed that only 2–methyl pentane was sorbed in the zeolite. This offers a process for complete separation of the normal from the branched hydrocarbons.

1.2.6 Para–selectivity

One of the unique shape selective properties of ZSM–5 is its para–selectivity[46] in reactions such as alkylation of alkyl aromatics. By adjusting the acid activity of the zeolite and controlling diffusion parameters, high para–selectivity can be achieved.

Olson and Haag[47] developed a model taking into account the interplay between diffusion and reaction (see Fig. 1.2) to explain the observed para–selectivity in toluene disproportionation. A necessary condition for para–selectivity[47] is $\frac{1}{k} \ll \frac{R^2}{D}$ Where k is the rate constant of reaction, R the crystal radius and D the diffusivity of the species with the slowest diffusion rate.

A mathematical analysis of the dimethylbenzenes system based on similar premises was reported by Wei[48], who showed that regardless of the intrinsic product selectivity, the observed isomer distribution is altered as a result of unequal diffusion rates of the various xylene isomers. The enrichment of p–xylene is made possible by the much greater diffusion coefficient of this isomer.

Without changing the intrinsic activity of the catalyst and the size of the crystal, the effective diffusion characteristic of the catalyst can be altered by a number of other techniques, including surface coking[49], surface poisoning[50], impregnation with MgO[51], Sb_2O_3[52] and compounds of phosphorous and boron[53,54]. The effect of some of these is examined in the present work for producing para–dialkylated products in alkylation and disproportionation reactions of aromatic compounds.

1.3 REFERENCES

1. D.W. Breck, *Zeolite Molecular Sieves*, Wiley and Sons, New York, 1974.
2. D.M. Ruthven, *Principles of Adsorption and Adsorption Processes*, Wiley and Sons, New York, 1984.
3. J. Scott (Ed) *Zeolite Technology and Applications. Recent Advances*, Noyes Data Corp., NJ, 1980.
4. a. C.D. Chang, *Catal. Rev. Sci. and Engg.*, **25**, 1, 1983.
   b. C.D. Chang, *Catal. Rev. Sci. and Engg.*, **26**, 323, 1984.
5. W.W. Kaeding, G.C. Barlie and M.M. Wu, *Catal. Rev. Sci. and Engg.*, **26**, 597, 1984.
6. G.T. Kokotailo, S.L. Lawton, D.H. Olson and W.M. Meier, *Nature*, **272**, 437, 1978.
7. G.T. Kokotailo, S.L. Lawton, P. Chu, and W.M. Meier, *Nature*, **275**, 119, 1978.
8. S.A. Barri, G.W. Smith, D. White and D. Young, *Nature*, **312**, 533, 1984.
9. G.T. Kokotailo, J.L. Schlenker, F.G. Dwyer amd E.W. Valyocsik, *Zeolites*, **5**, 349, 1985.
10. A.C. Rohrman Jr., R.B. La Pierre, J.L. Schlenker, J.D. Wood, E.W. Valyocsik, M.K. Rubin, J.B. Higgins and W.J. Rohrbaugh, *Zeolites*, **5**, 352, 1985.
11. J.L. Schlenker, W.J. Rohrbaugh, P. Chu, E.W. Valyocsik and G.T. Kokotailo, *Zeolites*, **5**, 355, 1985.
12. R.J. Argauer and G.R. Landolt, U.S. Pat. 3,702,886, 1972.
13. D.H. Olson, W.O. Hagg, R.M. Lago, *J. Catal.*, **61**, 390, 1980.
14. E.M. Flanigen, J.M. Bennet, R.W. Grose, J.P. Cohen, R.L. Patton, R.M. Kircher and J.V. Smith, *Nature*, **271**, 512, 1978.
15. J.R. Anderson, K. Foger, T. Mole, R.A. Rajadhyaksha and J.V. Sanders, *J. Catal.*, **58**, 114, 1979.
16. I. Wang, T.J. Chen, K.J. Chao and T.C. Tasai, *J. Catal.*, **60**, 140, 1979.
17. V.S. Nayak and V.R. Choudhary, *J. Catal.*, **81**, 26, 1983.
18. V.S. Nayak and V.R. Choudhary, *Appl. Catal.*, **10**, 137, 1984.
19. E.L. Wu, S.L. Lanton, D.H. Olson, A.C. Rohrman Jr. and G.T. Kokotailo, *J. Phys. Chem.*, **83**, 2777, 1979.
20. P.A. Jacobs, J.B. Uytterhoven, M. Steyns, G. Forment and J. Weitkamp, *Proc. 5th Int. Zeo. Conf.*, Naples, (Ed. L.V.C. Rees) ,Heydon, London, 1980, **p.607**.
21. N.Y. Topse, K. Pederson and E.G. Derouane, *J. Catal.*, **70**, 41, 1981.
22. G.P. Babu, S.G. Hegde, S.B. Kulkarni and P. Ratnasamy, *J. Catal.*, **81**, 471, 1983.

23. V.R. Choudhary and V.S. Nayak, *Materials Chem. Phy.*, **11**, 515, 1984.
24. V.R. Choudhary and V.S. Nayak, *Zeolites*, **5**, 15, 1985.
25. A. Auroux, V. Bolis, P. Wierzchowski, P.C. Gravelle and J.C. Vedrine, *J. Chem. Soc. Faraday Trans. 2*, **75**, 2544, 1979.
26. A. Auroux, P.C. Gravelle and J.C. Vedrine, *Proc. 5th Int. Zeo. Conf.*, Naples, (Ed. L.V.C. Rees, Heydon), London, 1980, **p.433**.
27. W.O. Hagg, *Proc. 6th Int. Zeo. Conf.*, Reno, USA, (Ed. D.H. Olson and A.Bisio), 1984, **p.466**.
28. N.Y. Chen and W.J. Reagan, *J. Catal.*, **59**, 123, 1979.
29. P.B. Venuto and P.S. Landis, *Adv. Catal.*, **18**, 269, 1968.
30. D.H. Olson, G.T. Kokotailo, S.L. Lawton and W.M. Meier, *J. Phys. Chem.*, **85**, 2238, 1981.
31. E.G. Derouane and Z. Gabalica, *J. Catal.*, **65**, 486, 1980.
32. J. Valyon, J. Michalyfi, H.K. Bayer and P.A. Jacobs, *Workshop on adsorption*, Berlin, 1979, **p.134.**
33. Z. Gabalica, J.P. Gibson and E.G. Derouane, *Proc. 2ndEuro. Symp. on Thermal Catal.*, (Ed. D. Dollimore), Heydon, 1981, **p.434**.
34. J.H. Kim, S. Namba and T. Yashima, *Bull. Chem. Soc. Japan.*, **61**, 1051, 1988.
35. R.M. Dessau, *ACS Symp. Ser.*, **135**, 123, 1980.
36. P.B. Weisz and V.J. Frilatte, *J. Phys. Chem.*, **64**, 382, 1960.
37. P.B. Weisz, *Chemtech.*, **3**, 498, 1973.
38. S. Csicsery, *Chem. Br.*, **21**, 473, 1985.
39. E.G. Derouane, *Zeolite Sci. Technol. (Eds. F.R. Reibeiro et al.), NATO ASI Ser.*, **80**, 347, 1984.
40. N.Y. Chen and W.E. Garwood, *Catal. Rev. Sci. and Engg.*, **28**, 1, 1986.
41. E.G. Derouane, *Stud. Surf. Sci. Catal.*, **19**, 1, 1984.
42. E.G. Derouane, P. Dejaifve, Z. Gabalica and J.C. Vedrine, *Faraday Discuss. Chem. Soc.*, **72**, 331, 1981.
43. C.G. Pope, *J. Catal.*, **72**, 174, 1981.
44. E.G. Derouane and J.C. Vedrine, *J. Mol. Catal.*, **8**, 479, 1980.
45. S. Namba, A. Yoshimura and T. Yashima, *Chem. Lett.*, 1979, **p.759**.
46. N.Y. Chen, W.W. Kaeding and F.G. Dwyer, *J. Am. Chem. Soc.*, **101**, 6783, 1979.
47. D.H. Olson and W.O. Hagg, *ACS Symp. Ser.*, **248**, 275, 1984.
48. J. Wei, *J. Catal.*, **76**, 433, 1982.

49. W.W. Kaeding, L.B. Young and C. Chu, *J. Catal.*, **89**, 267, 1984.
50. N.Y. Chen, *J. Catal.*, **114**, 17, 1988.
51. W.W. Kaeding, C. Chu, L.B. Young, B. Weinstein and S.A. Butter, *J. Catal.*, **67**,159, 1981.
52. S.A. Butter, U.S. pat. 4,007,231. 1977.
53. W.W. Kaeding, C. Chu, L.B. Young and S.A. Butter, *J. Catal.*, **69**, 392, 1981.
54. W.W. Kaeding, L.B. Young and C. Chu, *J. Catal.*, **89**, 267, 1984.

CHAPTER 2

PARA-SELECTIVE REACTIONS OVER CVD ZEOLITES

2 PARA–SELECTIVE REACTIONS OVER CVD ZEOLITES

2.1 INTRODUCTION

Chemical vapour deposition (CVD) is a technique for the deposition of inorganic/organic substances with the aid of thermal reactions[1] at high temperature. In contrast, physical vapour deposition uses physical energy such as heat or plasma for this purpose. The technique when applied to catalytic systems enables modification of catalytic properties.

Silica[2,3] is one of the compounds used to coat the external surface of a catalyst. Silynation is usually achieved by step wise addition of silicon compounds such as silicon tetrachloride[4,5] silicon alkoxides[6,7], silicon hydride[2,3] etc. Compounds of phosphorous[8,9], germanium[10] and boron[2,3] have also been deposited to modify the catalytic properties. Silynation is specifically applied to zeolite systems. The modified zeolites act by affecting acidic and diffusional properties. By selectively poisoning the external surface acid sites and reducing the pore diameter in a controlled manner, the reaction is favoured to take place in the desired direction and in the process, catalyst life is also enhanced.

2.1.1 Modification of Zeolites by Chemical Vapour Deposition (CVD)

Conventional adsorption units[5,6,11] or continuous flow reactors[12] are used for deposition. The deposition temperature is usually 473–573 K. Traces of carbonaceous residue remaining after the deposition are removed by calcination in air.

Modification by the following reagents has been reported:

(a) **Disilane**[13–15]: At low temperature (253–303 K) implantation of disilane occurs throughout the zeolite (ie. both external and internal sites), while at high temperature (373–473 K) a preferential reaction occurs resulting in modification of external zeolite surface.

(b) **Alkoxides of silicon**[5,12]: There are two possibilities for the deposition of silica when silicon alkoxides are used; hydrolysis of alkoxide by water to generate –OH groups

on surface on which deposition continues or direct condensation of alkoxide. The water molecules formed from the dehydration of solvent methanol compete with the alkoxide for adsorption on the active site resulting in uniform deposition throughout the catalyst bed.

2.1.2 Characterization of CVD Zeolites

Conservation of the internal pore structure of zeolite (after deposition of silica) has been shown by sorption experiments using small molecules such as water, nitrogen, ammonia etc. while the reduction of the pore opening sizes has been determined by sorption of large molecules such as hexane and o–xylene[5]. The rate of o–xylene sorption was found to be suppressed significantly by deposition. TPD of ammonia has shown that CVD zeolite possesses acidity comparable to that of the parent zeolite[16]. On chemisorption of alkoxide, the –CH stretching frequencies at 2900 cm^{-1} and 1600, 1480, and 3135 cm^{-1} could be observed in the IR spectrum[6] . On chemisorption of hydride, the characteristic stretching vibration of Si–H appear in the 2313–2213 cm^{-1} [15]. The thickness of the silica layers formed has been as determined by estimating Si/Al ratio by the XPS method[6].

2.1.3 CVD Zeolites and Shape Selective Properties

Selectivity enhancement by CVD on HZSM–5 (Si–HZSM–5) has reduced the yield of large aromatics in the methanol to hydrocarbon reaction[16]. Large hydrocarbons are isomerized or cracked to smaller ones due to diffusional resistance imposed by reduction in pore/channel size. External acid sites are blocked by deposition of silica and hence these are not available for non–shape selective reactions. Some of the reactions studied over silynated zeolites are hydrocarbon cracking[6,15] and para–selective aromatic reactions[12,17].

The present investigation was taken up as a part of a larger project on the production of p–substituted dialkylbenzenes. The aim of the work was to prepare ZSM–5 having different Si/Al ratio and to study the effect of silynation on para–selective aromatic reactions.

2.2 EXPERIMENTAL

2.2.1 Chemicals

The following chemicals were used for chemical vapour deposition and reactions:

- Ethylbenzene (HP 99.7%)
- Ortho–xylene (Fluka > 99%)
- Para–xylene (Fluka > 99%)
- Toluene (Glaxo, Excelar, 99.5%)
- Tetraethyl orthosilicate (TEOS) (Fluka > 99%)
- Methanol (Glaxo, Excelar, 99. 5%)
- Ethanol (Rectified spirit, 93–95%)

2.2.2 Catalysts

ZSM–5 zeolite having different SiO_2/Al_2O_3 mole ratio (R) were prepared following method described in the patent[18]. Their conversions to NH_4^+ and H^+ forms were carried out following the usual procedures.

2.2.3 CVD–Modified ZSM–5 Zeolites

Silynation feed was prepared by mixing 5 g of TEOS, 45 g of methanol and 50 g toluene.

The ZSM–5 zeolite (R=300, crystal size= 2μ) was pelleted and crushed to 10–20 mesh. About two gram of the catalyst was loaded in a down–flow silica reactor. The catalyst was activated in air at 723 K and cooled under nitrogen to the silynation temperature of 473 K. A procedure first suggested by Wang et al.[12,17] was modified to deposit varying amounts of silica. In this procedure, silynation feed was passed at a rate of 10 ml/hr.$^{-1}$ for two hours to deposit 0.0625 g of SiO_2 /g of catalyst (Si1). By extending the time of silynation to 4–, 6–, and 8– hours it was possible to deposit 0.125, 0.186, and 0.23 g of SiO_2/g of catalyst (Si2, Si3, and Si4). The change in weight after silynation and calcination was monitored to calculate the amount of SiO_2 deposited. The efficiency of silynation was $\approx$ 50% in all the cases.

2.2.4 Sorption

Sorption measurements were carried out on a calibrated Cahn balance. About 50 mg of the sample was weighed into an aluminium bucket, suspended from a calibrated silica spring. The system was evacuated to about 10^{-6} torr, isolated and cooled to room temperature and the weight of the sample noted. Sorbate vapours were admitted to the samples. The amount sorbed was measured as a function of time using a pre–calibrated strip chart recorder (Fig. 2.1).

All measurements were carried out at 298 K and a relative pressure P/P_0 of 0.5 where P_0 is the saturation vapour pressure of the sorbate at 298 K and P the equilibrium pressure at the temperature of sorption.

The sorption of nitrogen was carried out in a Omnisorb—100 CX instrument. About 100 mg of the sample was weighed into a sample holder. It was activated at 673 K, cooled and placed in liquid nitrogen Dewar and connected to sample port. The system was evacuated to 10^{-6} torr. The sorbate was introduced through a mass flow controller. The volume adsorbed was calculated by integrating the flow over time, and substracting the dead volume. All the measurements were carried out at liquid nitrogen temperature and a relative pressure P/P_0 of 0.6.

2.2.5 Activity Measurements

About two gram of the catalyst was loaded in a down flow silica reactor, activated in air overnight at 773 K and brought to reaction temperature in a flow of nitrogen. The feed was passed at a desired WHSV (weight hourly space velocity) using a Sage feed pump. The products were cooled in an ice trap collected and analyzed using Shimadzu GC 16A with R4A integrator fitted with Bentone 34 (5%) + DIDP (5%) on chromosorb W and Apiezon L on Anachrom columns.

Activity was tested as a function of SiO_2/Al_2O_3, temperature, WHSV, and extent of silynation.

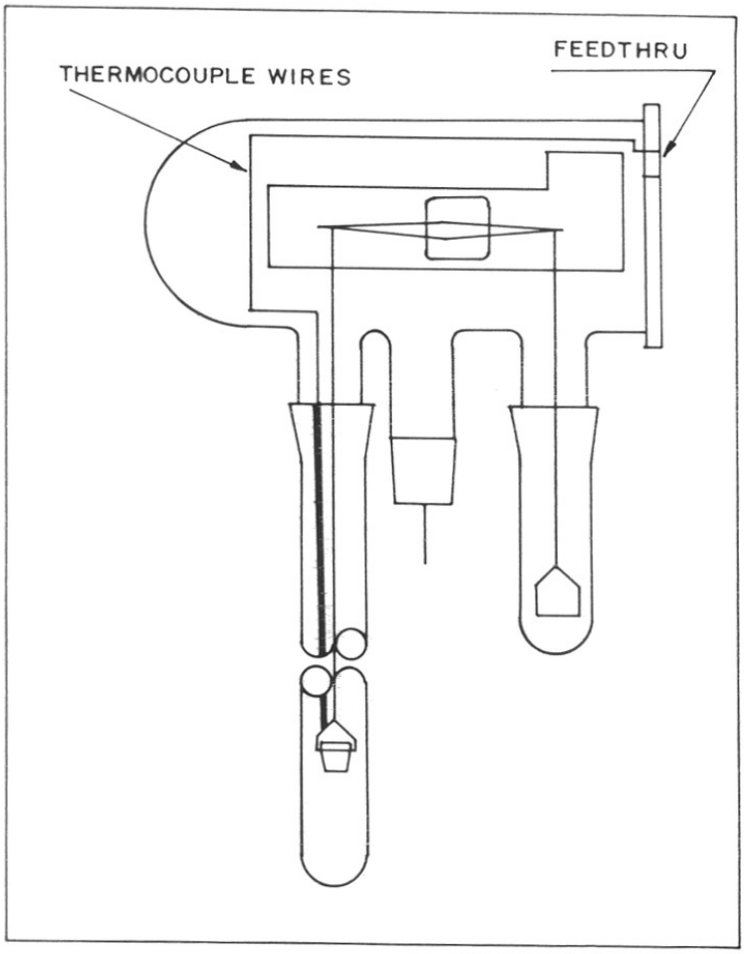

Fig. 2.1 ▷ **Automatic recording Electro–microbalance (Cahn 2000 C)**

2.3 RESULTS AND DISCUSSION

Table 2.1 gives the effect of SiO_2/Al_2O_3 on ethylbenzene disproportionation (EBDP). HZSM–5(90) shows high activity but the selectivity to diethylbenzenes (DEB's) is poor due to competing dealkylation reactions indicated by the high B/DEB ratio. This may be attributed to the high acidity of the sample. The PDEB selectivity remains almost the same for all the three samples. Due to high yield of DEB's obtained with HZSM–5 (300), this catalyst was investigated in detail. Almost clean disproportionation occurs (B/DEB≈1) with this catalyst at low temperatures of 598–623 K (Table 2.2). At high temperature dealkylation is favoured while at high WHSV, a marginal increase in para–selectivity is observed[19].

2.3.1 Sorption and Catalytic Properties of Silynated HZSM–5

2.3.1.a. Sorption

Table 2.3 and Fig. 2.2 & 2.3 present sorption data for p– and o–xylenes for HZSM–5 and samples silynated to different extents.

With progressive increase in the amount of silica deposited, the following changes in the sorption and surface area may be noted:

1. The surface area and the volume of nitrogen adsorbed remains essentially constant.
2. Sorption rate for p–xylene is significantly affected only with larger quantities of silica deposited.
3. The influence of silynation is reflected on the sorption rate of o–xylene even at low levels of deposition.

These results would mean that:

1. Silynation of only the external sites has taken place which is in agreement with the inability of TEOS molecules to go into the channels
2. The size of p–xylene molecule being smaller, its diffusion into the zeolite channels is hindered only at severe silynation
3. The small reduction in pore size at low levels of silica deposition is sufficient to affect the sorption rate of o-xylene.

Sample Si4 which contained a maximum of 23% silica must have considerable

R	90.0	200.0	300.0
Temp. (K)	623.0	628.0	623.0
WHSV	2.6	2.6	2.6
Benzene	27.4	18.2	14.9
Diethylbenzenes	14.5	17.6	20.6
B/DEB	3.3	1.7	1.2
% PDEB	37.4	43.5	38.6
Conversion of Ethylbenzene	57.6	52.4	37.6

TABLE 2.1. **Effect of SiO_2/Al_2O_3 (R) Ratio on Product Distribution in Ethylbenzene Disproportionation.**

Temp.(K)	598	623	657	678	623	623
WHSV	←———		3.5	———→	9	17
Product Distribution						
Non–Aromatics	0.01	0.17	0.47	1.23	0.03	0.03
Benzene	7.77	14.90	18.00	23.00	8.53	5.30
Toluene	0.07	0.51	0.77	1.45	0.03	0.04
Ethylbenzene	79.55	62.33	58.50	54.90	78.20	86.80
Ethyltoluenes	0.10	0.62	0.90	1.50	0.12	0.05
Other C8, C9	0.01	0.12	0.24	0.44	0.01	—
M DEB	7.09	12.65	11.50	9.44	6.53	3.55
P DEB	5.31	7.95	8.16	6.54	5.92	4.19
Total DEB's	12.40	20.60	19.66	15.98	12.45	7.74
Higher Aromatics	0.08	0.72	1.40	1.50	0.55	0.03
B/DEB	1.07	1.24	1.60	2.50	1.17	1.17
% PDEB	42.84	38.60	41.50	40.90	47.50	54.10
Conversion of Ethylbenzene	20.5	37.60	41.50	45.20	21.80	13.20

TABLE 2.2. **Effect of Temperature and WHSV on Product Distribution: Catalyst HZSM–5 (300).**

Sample	p–xylene (wt. %)	o–xylene (wt. %)	Surface area m^2g	Vol.adsorbed ml/g
Si0	14.04	1.06	534.8	144.3
Si1	13.47	0.56	531.0	143.3
Si2	12.61	0.48	469.0	126.6
Si3	9.59	0.38	565.3	129.9
Si4	6.36	0.27	459.9	124.1

TABLE 2.3. **Sorption Data for HZSM–5 (300) and Silynated HZSM–5 (300).**

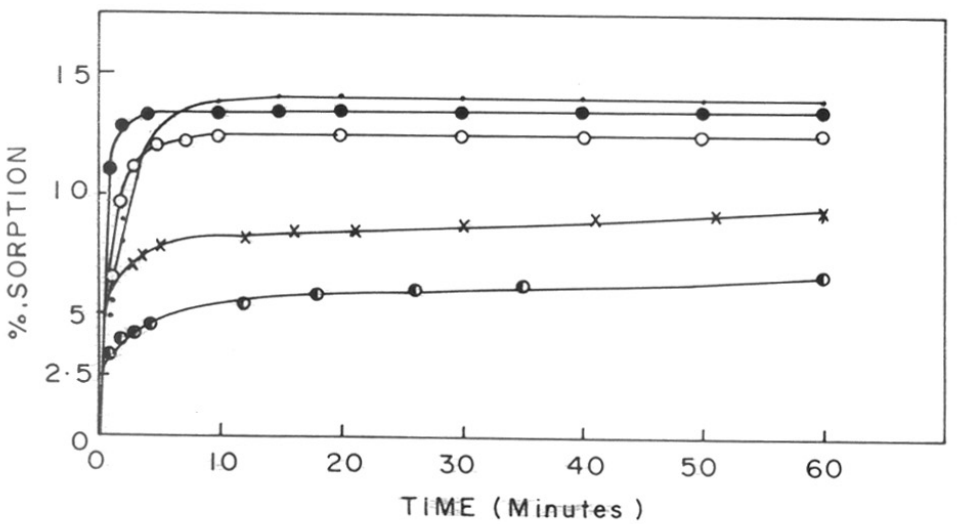

Fig. 2.2 ▷ Kinetics of p–xylene sorption for ZSM–5 silynated to different extends. (.) Si0, (○) Si1, (●) Si2, (x) Si3, (⊙)Si4.

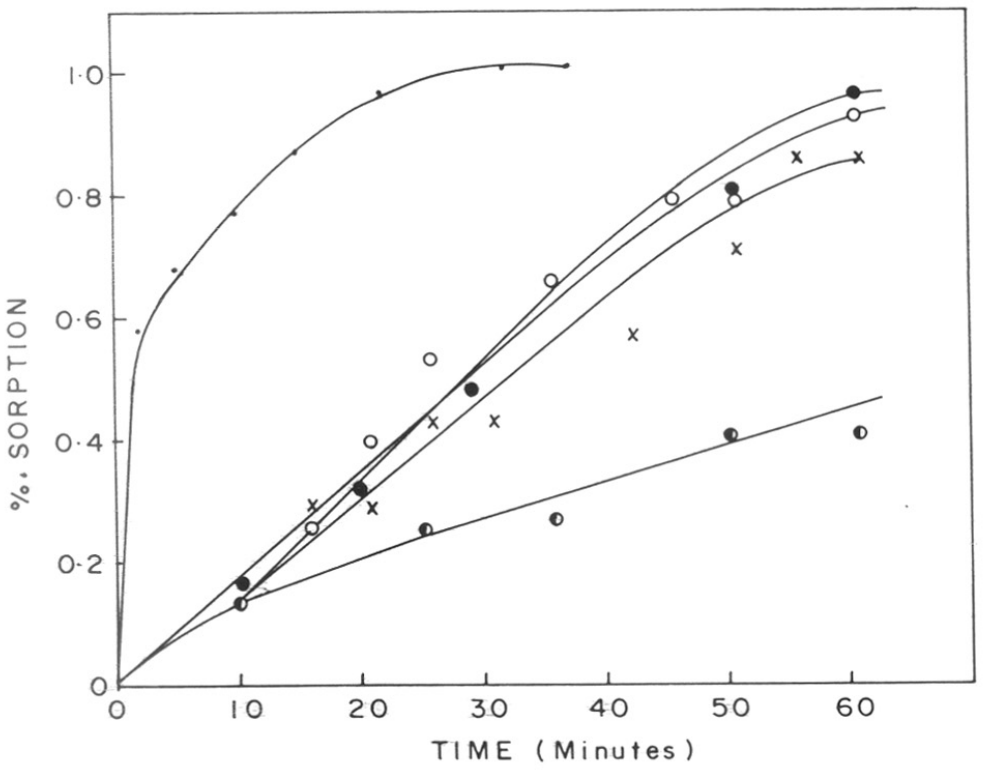

Fig. 2.3 ▷ Kinetics of o–xylene sorption for ZSM–5 silynated to different extends. (.)Si0, (○) Si1, (•) Si2, (x) Si3, (◐) Si4.

number of Si–O–Si linkages caused by silynation and calcination. These may have been formed by any of the mechanisms suggested by Vansant and co–workers[13–15].

2.3.1.b. Disproportionation of Ethylbenzene

Since silicon alkoxides have a molecular size larger than the pore size of ZSM–5, it cannot have affected the zeolite internal acidity[5] or internal pore volume. This was confirmed by TPD of ammonia and sorption measurements.

Disproportionation of ethylbenzene over silynated zeolites give results conforming to this interpretation. Table 2.4 and Fig. 2.4 show the effect of silynation on this reaction. They further show that both activity and selectivity depend on the extent of silynation.

Conversion of ethylbenzene, is related to the ease of its diffusion into the channels. As there is a gradual reduction in the rate of sorption, there is a corresponding drop in activity for ethylbenzene disproportionation as both these are related. There is also a further reduction in activity caused by removal of external acid sites.

On the other hand there is an increase in selectivity to PDEB. In the ethylbenzene disproportionation, the primary product, PDEB, isomerizes to m– and o–isomers. This isomerization is subject to diffusional restrictions. The rapid diffusion of the p–isomer out of the pores and its subsequent isomerization at the external surface results in low para–selectivity in a two step mechanism[20] suggested for the unmodified zeolite. Non–shape selective reactions on the external surface is a major factor in determining the extent of this isomerization. Since these are blocked by silynation. In addition, there is a controlled reduction of the pore diameter which reduces the diffusivity of the bulkier isomers, the increase in PDEB selectivity is caused by both these factors. Table 2.5 compares the catalysts at similar conversion levels. The similar B/DEB ratio indicates that the intracrystalline active sites are unaffected by silynation.

Catalyst	Si0	Si1	Si2	Si3	Si4
Temp.(K)	623	623	623	623	623
WHSV	←3.5→				
Product Distribution					
Non–Aromatics	0.17	0.05	0.06	0.04	0.06
Benzene	14.85	8.34	6.23	4.63	2.85
Toluene	0.51	0.35	0.70	0.34	0.20
Ethylbenzene	62.33	78.89	82.61	88.09	92.00
Ethyltoluenes	0.62	0.24	0.18	0.19	0.08
Other C8, C9	0.12	0.11	0.12	0.11	0.05
M DEB	12.65	3.72	0.70	0.08	—
P DEB	7.95	8.24	8.90	6.32	3.70
Total DEB's	20.60	11.96	9.16	6.40	3.70
Higher Aromatics	0.72	0.18	0.14	0.13	0.02
B/DEB	1.24	1.20	1.17	1.24	1.32
% PDEB	38.60	69.00	97.00	98.70	100.00
Conversion of Ethylbenzene	37.67	21.11	17.39	11.91	8.00

TABLE 2.4. **Effect of Silynation on Product Distribution in Ethylbenzene Disproportionation.**

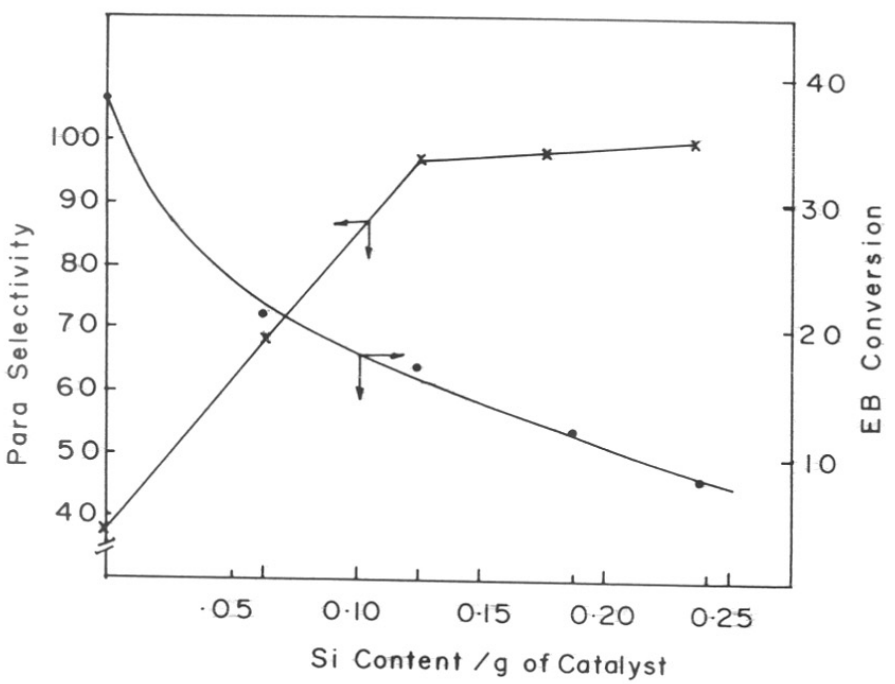

Fig. 2.4 ▷ Effect of silynation on ethylbenzene conversion and para–selectivity.

Catalyst	HZSM–5(300)	Si4 HZSM–5(300)
Temp. (K)	598	598
WHSV	7.0	3.0
Product Distribution		
Non–Aromatics	—	—
Benzene	2.98	2.93
Toluene	0.02	0.02
Ethylbenzene	92.40	92.70
Ethyltoluenes	0.05	0.05
Other C8, C9	0.07	0.07
M DEB	1.91	0.06
P DEB	2.51	4.21
Total DEB's	4.42	4.27
Higher Aromatics	0.05	0.02
B/DEB	1.16	1.18
% PDEB	56.80	98.50
Conversion of Ethylbenzene	7.60	7.30

TABLE 2.5. **Comparison of HZSM–5 (300) and Si4 HZSM–5 (300) at Comparable Conversion Levels.**

2.3.1.c. Comparison of Para–selectivity for Different Dialkylbenzenes

Si4 was also tested for para–selectivity in other reactions such as toluene disproportionation, toluene–methanol alkylation, toluene–ethanol alkylation, EB ethylation. Table 2.6 gives a comparison of para–selectivity for different alkylbenzenes.

The order of selectivity of the p–dialkylbenzenes are:

$$\text{PDEB} > \text{PET} > \text{PX}$$

Thus a direct relationship exists between para–selectivity and molecular dimensions. The constrain on diffusion of bulkier substituent may be expected to be larger than that on diffusion of a smaller molecule[21]. The results obtained are different from those of Wang et al.[17] who obtained an order of PET>PDEB>PX.

2.4 CONCLUSIONS

The increase in para–selectivity by silynation may be understood in terms of:

1. The formation of para–compounds as the primary products.
2. The restricted diffusion of m– and o–isomers out of the zeolite pores due to gradual reduction of the pore size.
3. Prevention of isomerization of the p–isomer over the external sites which are blocked by silynation.

In this way a high selectivity to PDEB (compared to the thermodynamic equilibrium distribution of isomers) is obtained. By controlling the extent of silynation, it is possible to direct the reaction to produce PDEB exclusively.

Feed	Toluene	Toluene/ C_1OH $\frac{3}{1}$	Toluene/ C_2OH $\frac{8}{1}$	EB	EB/C_2OH $\frac{8}{1}$
Temp.(K)	823	623	623	623	623
WHSV	←		3.5		→
Product Distribution					
Aliphatics	—	0.04	0.04	0.06	0.20
Benzene	3.67	0.29	0.14	2.85	0.34
Toluene	92.29	89.97	90.50	0.20	0.03
Ethylbenzene	0.01	1.53	0.15	92.00	90.10
P–Xylene	3.50	5.38	0.18	—	—
M–Xylene	0.35	0.45	0.10	—	—
O–Xylene	0.10	0.35	—	—	—
Xylenes	3.95	6.18	0.20	—	—
P–Ethyltoluene	—	2.62	7.44	0.05	0.19
M–Ethyltoluene	—	0.11	0.40	—	0.01
Ethyltoluenes	—	2.72	7.84	0.05	0.20
TMB's	0.05	—	—	—	—
M DEB	—	—	—	—	0.08
P DEB	—	—	—	3.70	9.60
DEB's	—	—	—	3.70	9.68
Higher Aromatics	—	—	0.10	—	0.17
% P–Xylene	88.60	86.90	—	—	—
% PET	—	95.80	94.80	—	—
% PDEB	—	—	—	100.00	99.00
Conversion of Aromatics	7.61	10.03	9.50	8.00	9.90

TABLE 2.6. **Para–selectivity Towards Different Dialkylbenzenes Over Si4 HZSM–5 (300).**

2.5 REFERENCES

1. J. Bloem, *Reactivity of solids, Vol.1*, (Eds. . Dyrek, J. Hayber and J. Nowotony) Elseveir, Amsterdam, **p.301**.
2. R.M. Barrer, E.F. Vansant and G. Peeters, *J. Chem. Soc. Fararday Trans. 1*, **74**, 1871, 1978.
3. A. Thijis, G. Peeters, E.F. Vansant and L. Verhaert, *J. Chem. Soc. Fararday Trans. 1*, **79**, 2821, 1983.
4. J. Klinowski, J.M. Thomas, M.W. Anderson, C.A. Fyfe and C. Gobbi, *Zeolites*, **3**, 5, 1983.
5. M. Niwa, S. Kato, T. Hattori and Y. Murakami, *J. Chem. Soc. Fararday Trans. 1*, **80**, 3135, 1984.
6. M. Niwa, Y. Kawashima and Y. Murakami, *J. Chem. Soc. Fararday Trans. 1*, **81**, 2757, 1985.
7. M. Niwa, S. Morimoto, M. Kato and T. Hattori, *Proc. Int. Congr. Catal.*, **4**, 701, 1984.
8. W.W. Kaeding, C. Chu, L.B. Young, B. Weinstein and S.A. Butter, *J. Catal.*, **67**, 159, 1981.
9. W.W. Kaeding and S.A. Butter, *J. Catal.*, **61**, 155, 1980.
10. C.V. Hidealgo, M. Kato, T. Hattori, M. Niwa and Y. Murakami, *Zeolites*, **4**, 175, 1984.
11. Y.F. Chu, C.F. Keweshan and E.F. Vansant, *Stud. Surf. Sci. Catal.*, **46**, 749, 1989.
12. I. Wang, C.L. Ay, B.J. Lee and M.H. Chen, *Proc. 9th Int. Congr. Catal.*, Calgary, 1988, **p. 324**.
13. Y. Yan, J. Verbiest, P. De Hulsters and E.F. Vansant, *J. Chem. Soc. Faraday Trans. 1*, **85**, 3087, 1989.
14. Y. Yan, J. Verbiest, P. De Hulsters and E.F. Vansant, *J. Chem. Soc. Faraday Trans. 1*, **85**, 3095, 1989.
15. Y. Yan and E.F. Vansant, *J. Phys. Chem.*, **94**, 2582, 1990.
16. M. Niwa, M. Kato, T. Hattori and Y. Murakami, *J. Phys. Chem.*, **90**, 6233, 1986.
17. I. Wang, C.L. Ay, B.J. Lee and M.H. Chen, *Appl. Catal.*, **54**, 257, 1989.
18. R.J. Argauer and G.R. Landolt, U.S. Pat. 3,702, 886, 1972.
19. J. Wei, *J. Catal.*, **76**, 433, 1982.
20. G. Paparatto, E. Moretti, G. Leofanti and F. Gatti, *J. Catal.*, **105**, 227, 1987.
21. D.H. Olson, G.T. Kokotailo and S.L. Lawton, *J. Phys. Chem.*, **81**, 2238, 1985.

CHAPTER 3

ALKYLATION OVER ALUMINO-LANTHANO-SILICATE CATALYSTS

3 ALKYLATION OVER ALUMINO-LANTHANOSILICATE CATALYSTS

3.1 INTRODUCTION

The advantage of using ZSM–5 type zeolites as catalysts for aromatic reactions has been brought out in a number of publications[1–6]. This can be attributed to the shape selective properties of these zeolites and the scope for further modification to obtain highly shape selective catalysts.

In addition to silynation, other methods of modification have been used to enhance para–selectivity in aromatic reactions. These are synthesizing larger crystallites[6], incorporation of other inorganic oxides into the pores/ channels[1–6] and pre–treatment of the zeolite by coking[7,8]. Aluminolanthanosilicate (MFI) (La–ZSM–5) has been known to be a good catalyst for conversion of methanol to olefins[9]. The present chapter reports the activity and selectivity of La–ZSM–5 and its modification in the alkylation of ethylbenzene.

3.2 EXPERIMENTAL

3.2.1 Chemicals

- Aluminium sulphate (SD Chemicals)
- Sodium silicate (SiO_2 27.2%, Na_2O 8.4%, Water 64.4%)
- Lanthanum chloride (Indian Rare Earths)
- Sulphuric acid (98%, BDH AR)
- Triethyl n–butylammonium bromide

3.2.2 Catalysts

Aluminolanthanosilicate (La–ZSM–5) was prepared by adding $LaCl_3$ in the ZSM–5 synthesis reported in the patent[10]. Tetrapropylammonium hydroxide was replaced by triethyl n–butylammonium hydroxide in the synthesis. A gel composition of 4.4 TEABr 89 Na_2O_3

Al_2O_3 300 SiO_2 2.67 La_2O_3 32 H_2O was heated in an autoclave at 453 K for 36 hours. The reaction was quenched to ambient and the product filtered and dried. The conversion to NH_4^+ and H^+ forms was carried out following the procedure reported[11].

La–ZSM–5 modified by magnesium (Mg/La–ZSM–5) was prepared by impregnating five grams of the catalyst with 20 g aqueous magnesium nitrate solution containing 2% of magnesium. The slurry was slowly evaporated at 363 K with stirring, dried at 393 K and finally calcined at 773 K. The catalyst contained 8% magnesium by weight. A sample of Si/La–ZSM–5 was prepared following the CVD technique described in Chapter 2 to coat the surface with 0.23 g of silica per gram of La–ZSM–5.

3.2.3 Sorption

Sorption measurements were carried out in a conventional McBain balance at a P/P_0 of 0.5 and a temperature of 298 K.

3.2.4 IR Spectroscopy

The zeolite samples were placed in a thin–walled quartz ampoule and evacuated at 673 K for four hours under 10^{-6} torr. Diffuse reflectance IR spectra were recorded at room temperature on Perkin–Elmer spectrometer.

3.2.5 Activity Measurements

Catalytic activity for ethylbenzene ethylation were carried out in a conventional down–flow silica reactor. The liquid and gaseous products were analyzed by GC 16 A (Shimadzu) using Apiezon L on Anachrom (Analabs) and Porapak Q columns, respectively.

3.3 RESULTS AND DISCUSSION

Based on the chemical analysis, the catalyst had a SiO_2/Al_2O_3 ratio of $\approx$ 240 and SiO_2/La_2O_3 of $\approx$90.

3.3.1 Sorption

Table 3.1 shows the sorption data and Fig. 3.1 the adsorption isotherm for n–hexane for the samples La–ZSM–5 and La–ZSM–5 modified by MgO. Both La–ZSM–5 and Mg/La–ZSM–5 exhibit lower adsorption capacity for cyclohexane.

The probability of isomorphous substitution of Si^{4+} by other metal ions M^{n+} and the stability of M^{n+} in tetrahedral oxygen surrounding has been predicted by Ione et al.[12] using Pauling's criterion[13]. The tetrahedral surrounding should be stable for cations at $0.414 > r_c/r_o > 0.225$ where r_c is the cation radius and r_o the radius of oxygen ion. This group of cations include only Al^{3+}, Mn^{4+}, Ge^{4+}, V^{4+}, Cr^{6+}, Si^{4+}, P^{5+}, and Be^{2+}. In La–ZSM–5, the radius ratio falls outside the above limit. Therefore, most of the La in La–ZSM–5 may be present in occluded form as oxides in the channels and a part in exchangeable position. This causes diffusional restriction and the reduction in sorption (Table 3.1). In Mg/La–ZSM–5, part of the MgO may be even blocking the pore mouth reducing the rate of sorption and sorption capacity. Thus, the effect of La and MgO incorporation is to restrict the diffusion of bulkier molecules (like cyclohexane) in the channels.

3.3.2 Acidity by IR Spectroscopy

The IR spectra of –OH groups of La–ZSM–5 and Mg/La–ZSM–5 are shown in Fig. 3.2 and the data presented in Table 3.2. Both the spectra contains bands at 3740 cm^{-1} attributed to silanol groups[15]. However, the intensity of the band is reduced for Mg/La–ZSM–5. Probably part of MgO is located at the outer surface of the crystallites where silanol groups are located.

The narrow band at 3610 cm^{-1} corresponds to bridged hydroxyls (–Si–O(H)–Al–)[15]. The intensity of this band is also decreased on impregnation of magnesium. Taking into account that the -OH groups are situated inside the channels of the zeolite structure, it may be concluded that MgO is distributed both in the internal and the external surface of the zeolite. The 3670 cm^{-1} band may be due to LaOH species or H–bonded silanols. The new line at 3500 cm^{-1} for the Mg/La–ZSM–5 is probably due to H–bonded Mg–OH groups. The activity of La–ZSM–5 and MgO modified sample can be attributed to

Catalyst	Sorption(wt. %)		
	Water	n–Hexane	Cyclohexane
ZSM–5 (300)	3.50	12.80	2.76
La–ZSM–5	1.90	11.50	2.50
Mg/La–ZSM–5	2.00	8.39	1.81

TABLE 3.1. **Sorption Capacity for Aluminolanthanosilicate Catalysts.**

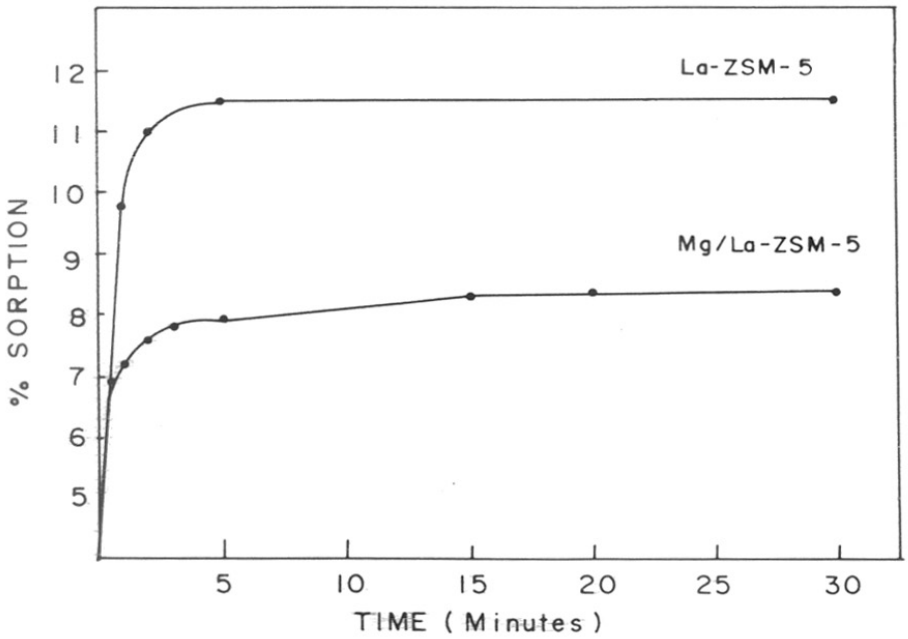

Fig. 3.1 ▷ Kinetics of n–hexane sorption for La–ZSM–5 and Mg/La–ZSM–5.

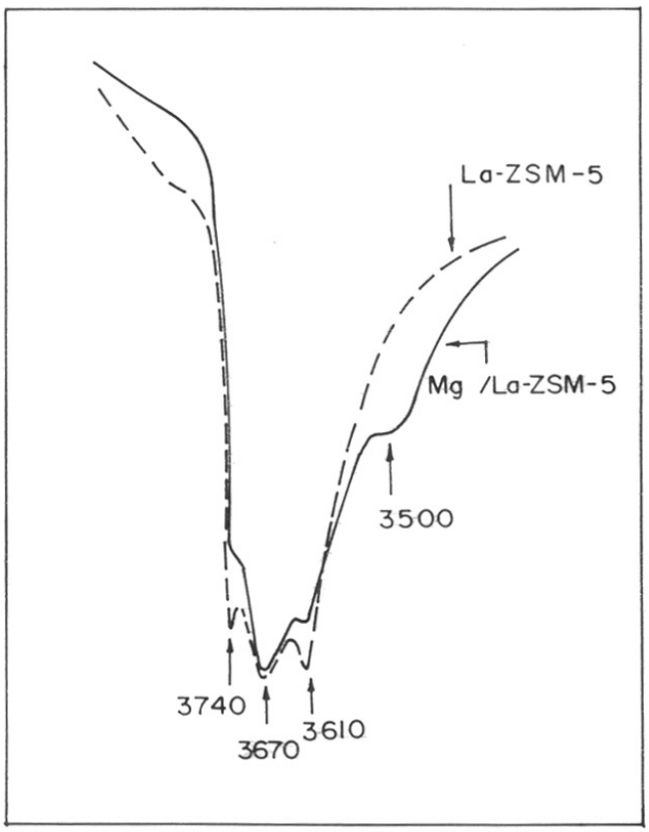

Fig. 3.2 ▷ IR spectra of –OH groups of La–ZSM–5 and Mg/La–ZSM–5.

Catalyst	–OH Frequency (cm^{-1})
ZSM–5*	3610
	3740
La–ZSM–5	3610
	3670
	3740
Mg/La–ZSM–5	3500 (broad)
	3610
	3670
	3740

⋆ from ref. 14

TABLE 3.2. **Hydroxyl Frequency Data for Aluminolanthanosilicate Catalysts.**

Brönsted acidity arising from the acidic hydroxyl band at 3610 cm^{-1}.

3.3.3 Activity and Para–selectivity of La–ZSM–5 and its Modifications for the Alkylation of Ethylbenzene

With the system studied here the two starting agents, ethylbenzene and ethanol, readily enter the pores of the catalyst. Under conditions used for alkylation, protonation of the ethanol to form the corresponding oxonium ion is the initial step (Scheme 1). This is followed by the transfer of the ethyl group to the aromatic ring and proton elimination. Less steric hindrance for alkylation at the para position within the confines of the catalyst pores is predicted by comparison with meta and ortho positions.

Ethylation of ethylbenzene was carried out over La–ZSM–5 as a function of WHSV and temperature. The reactant feed used had a mole ratio of 4:1 for ethylbenzene : alcohol.

The effect of WHSV on conversion of ethylbenzene and para–selectivity at 723 K is shown in Fig. 3.3. Increase in para–selectivity with increase in WHSV is in agreement with para isomer being the primary product in the reaction[16].

When temperature is increased (Fig. 3.4), benzene is produced in large amount, an indication of the increased contribution of the disproportionation reaction of ethylbenzene (Scheme 2). The proton form of the zeolite attacks the aromatic nucleus. The alkyl group is then transferred to another aromatic ring in the transalkylation step. The catalyst aging is faster at low reaction temperature, probably due to slow desorption of products. At 648–673 K, steady state performance was observed.

The catalyst activity of La–ZSM–5 may be attributed to the bridging –OH groups connected with Al as evidenced by the 3610 cm^{-1} band in IR spectrum. Higher para–selectivity observed may be due to presence of occluded La species inside the channels which impose diffusional restrictions on the meta and ortho isomers favouring their isomerization to para.

Modification by impregnation with MgO has resulted in lower activity and high para–selectivity (Table 3.3). The lower activity may be due blocking of some of the acid sites

SCHEME - 1

ALKYLATION

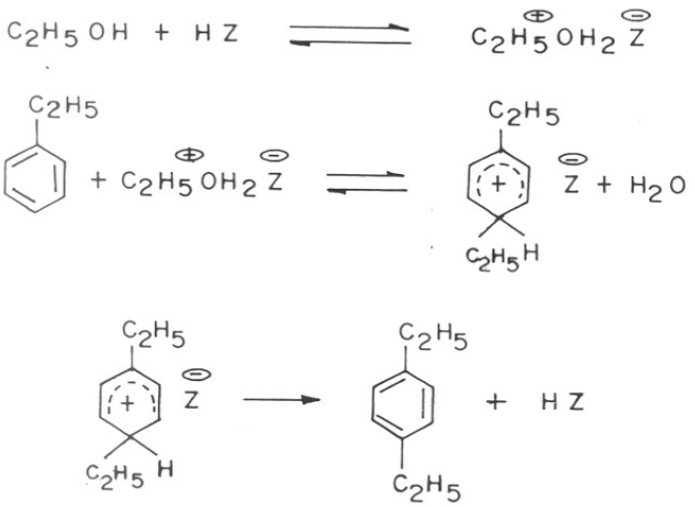

SCHEME - 2

DISPROPORTIONATION

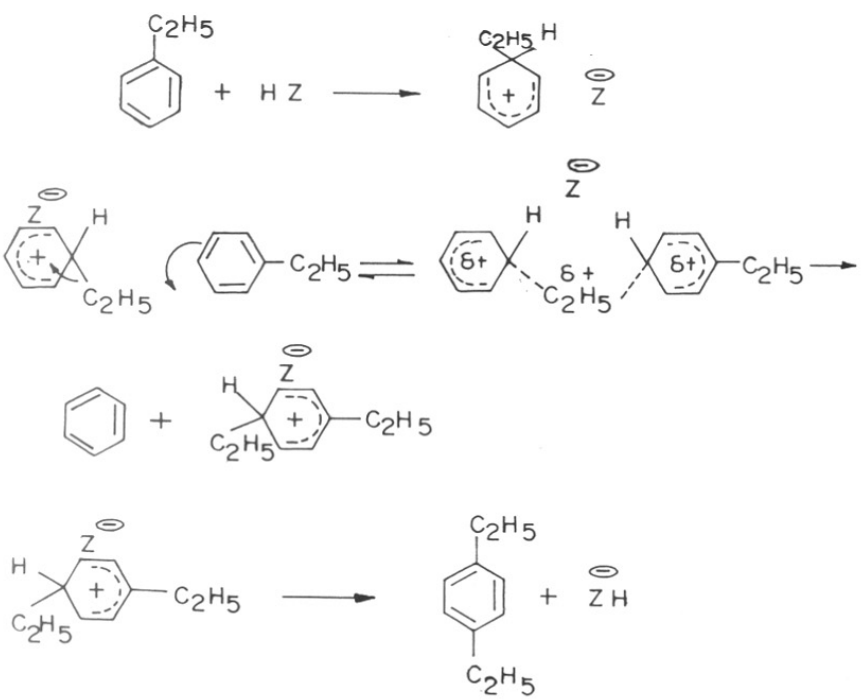

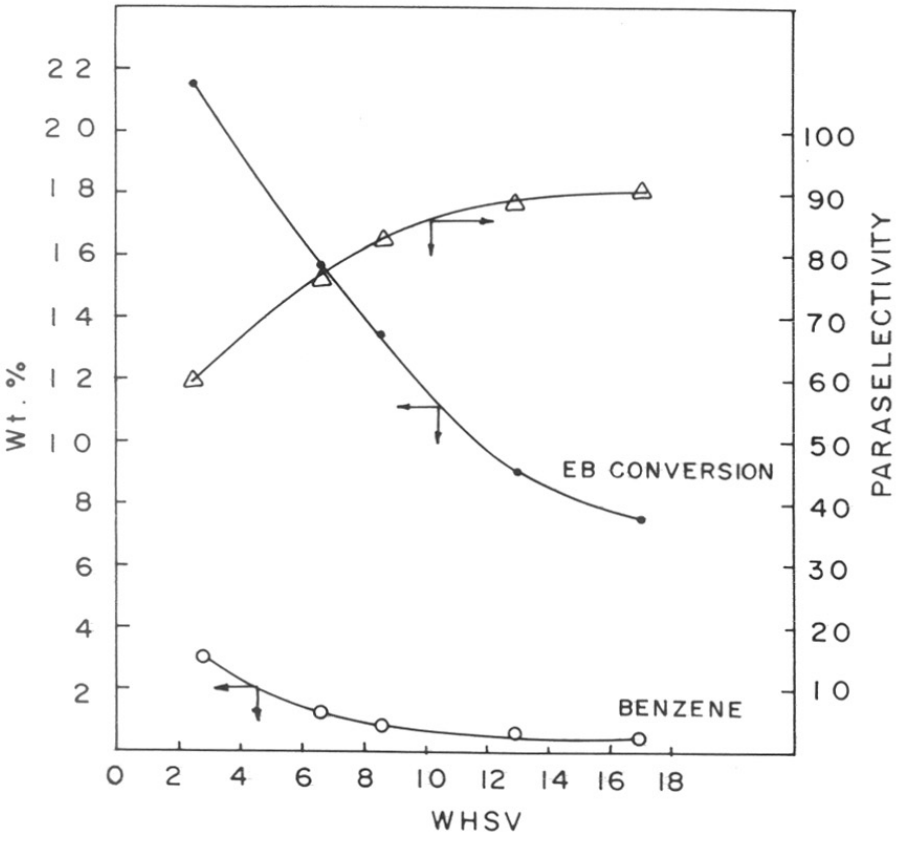

Fig. 3.3 ▷ Effect of WHSV on conversion of ethylbenzene and para–selectivity.

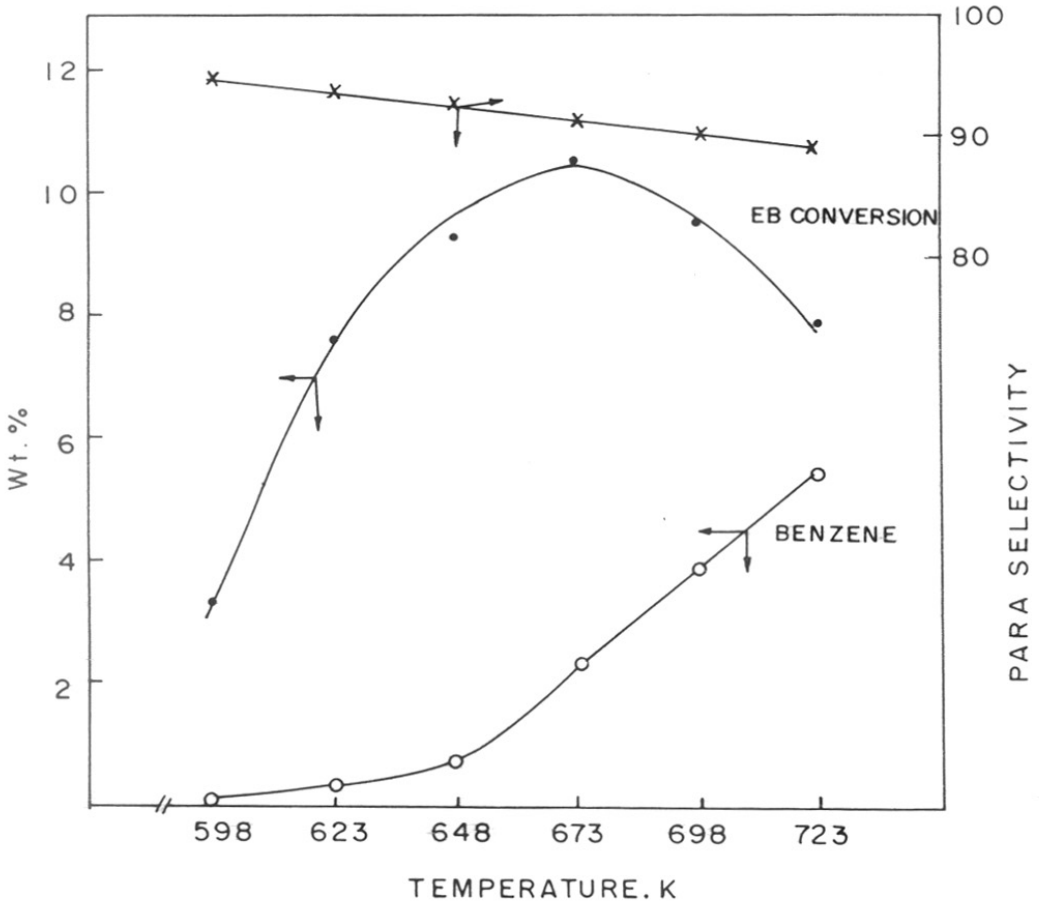

Fig. 3.4 ▷ Effect of temperature on conversion of ethylbenzene and para–selectivity.

Catalyst	ZSM-5(300)	La-ZSM-5	Mg/La-ZSM-5	Si/La-ZSM-5
Temp.(K)	623	623	648	648
WHSV	12.50	12.50	12.50	3.50
Product Distribution				
Non–Aromatics	0.14	0.01	0.02	0.03
Benzene	0.64	0.57	0.22	0.25
Toluene	0.10	0.10	—	—
Ethylbenzene	87.10	89.40	93.69	93.50
Ethyltoluenes	0.35	0.38	0.14	0.08
Other C8, C9	0.11	0.02	0.01	—
M DEB	1.54	1.10	0.09	0.31
P DEB	10.13	8.37	5.40	5.87
Total DEB's	11.67	9.47	5.49	6.18
Higher Aromatics	0.12	0.18	0.02	0.01
% PDEB	87.00	90.00	98.40	95.10
Conversion of Ethylbenzene	12.90	10.60	6.21	6.50

Diethylbenzene Equilibrium Composition at 673 K: para 28.5%; meta 52%; ortho 19.5%.

TABLE 3.3. **Para–selectivity in Aluminolanthanosilicate Catalysts.**

by MgO. This is indicated by reduction in intensity of the 3610 cm^{-1} band representing acidic OH groups in the IR study. Higher para- selectivity can be explained on the basis of Wei's[17] explanation or Olson and Haag's diffusion model[18] for increased para–selectivity on the modified zeolites.

Table 3.3 also compares catalytic properties of La–ZSM–5 with the silynated La–ZSM–5 for alkylation of ethylbenzene. Upon silynation,the external acid sites are blocked and there is narrowing of pores caused by controlled deposition of silica as shown in Chapter 2. This results in reduced activity for ethylbenzene conversion as well as increased para–selectivity in the reaction by decreasing the rate of sorption, hindering diffusion of the less favoured ortho and meta isomers and, eliminating external acid sites responsible for isomerization of PDEB.

3.4 CONCLUSIONS

In La–ZSM–5, the presence of La species inside the channels creates tortuosity effects on diffusion of bulky isomer molecules, which are converted to the para isomer. Thus there is an increased selectivity to para isomer.

Modification by imprenation or deposition of silica by CVD also also results in higher para–selectivity. Impregnation method affects acidity, channel pore–mouth blocking, where as CVD acts by passivating the surface active sites and narrows the pore opening.

3.5 REFERENCES

1. N.Y. Chen, W.W. Kaeding and F.G. Dwyer, *J. Am. Chem. Soc.*, **76**, 418, 1976.
2. W.W. Kaeding, C. Chu, L.B. Young, B. Weinstein and S.A. Butter, *J. Catal.*, **67**, 159, 1981.
3. W.W. Kaeding, C. Chu, L.B. Young and S.A. Butter, *J. Catal.*, **69**, 392, 1981.
4. L.B. Young, S.A. Butter and W.W. Kaeding, *J. Catal.*, **76**, 418, 1982.
5. W.W. Kaeding, L.B. Young and C. Chu, *J. Catal.*, **89**, 267, 1981.
6. W.W. Kaeding, *J. Catal.*, **95**, 512, 1985.
7. L.D. Rollman, *J. Catal.*, **47**, 113, 1977.
8. L.D. Rollman and D.E. Walsh, *J. Catal.*, **56**, 139, 1979.
9. I. Balakrishnan, Ph.D thesis, University of Poona, 1985.
10. R.J. Argauer and G.R. Landolt, U.S. Pat. 3,702,886, 1972.
11. T. Hibino, M. Niwa and Y. Murakami, *J. Catal.*, **128**, 551, 1991.
12. K.G. Ione L.A. Vostrikova and V.M. Mastikhin, *J. Mol. Catal.*, **31**, 355, 1985.
13. L. Pauling, *The Nature of Chemical Bond*, Cornell, 1960.
14. V.L. Zholobenko, L.M. Kustov, V. Yu Borovkov and V.B. Kazansky, *Zeolites*, **8**, 175, 1988.
15. O.V. Bragin, L.M. Kustov, V. Yu Borovkov, T.V. Vasina, N.V. Palishkina and V.B. Kazansky, *Kinet. Catal.*, **26**, 337, 1985.
16. G. Paparatto, E. Moretti, G. Loefanti and F. Gatti, *J. Catal.*, **105**, 227, 1987.
17. J. Wei, *J. Catal.*, **76**, 432, 1982.
18. D.H. Olson and W.O. Haag, *ACS. Symp. Ser.*, **248**, 275, 1984.

PART - II

ALUMINOPHOSPHATE MOLECULAR SIEVES

CHAPTER 1

GENERAL INTRODUCTION

1 GENERAL INTRODUCTION

1.1 ALUMINOPHOSPHATE MOLECULAR SIEVES

1.1.1 Introduction

In 1982, workers at the Union Carbide reported synthesis of a large number of new microporous molecular sieves based on an aluminophosphate framework ($AlPO_4$)[1,2]. In these materials the framework positions are occupied by Al^{3+} or P^{5+}. VPI–5 is an $AlPO_4$ containing unique 18–membered oxygen ring openings[3]. Jones et al.[4] have reported a novel chain $AlPO_4$ macroanion which has little or no catalytic activity[5]. Novel crystalline microporous metal sulphides[6,7] have also been reported recently. Pillard clays (PILC) are yet another class of catalytically active microporous materials[8].

1.1.2 Natural Aluminophosphates

A number of phosphates of aluminium exist in the natural mineral state and feature in early studies of phosphate[9].

There are 9 naturally occurring neutral $AlPO_4$ materials[10]. The dense phase structures, 3 forms of tridymite and 2 phases of crystobalite have been synthesised in $AlPO_4$ systems[11]. Varicite and metavaricite contain 6–coordinated Al bonded to 4–coordinate P[12]. Loss of water in these materials results in structural collapse.

1.1.3 Synthetic Aluminophosphates

Synthesis of aluminophosphates was reported in 1961 by D'Yvoire[13]. Several of these appeared to be thermally unstable.

About 20 structure types of thermally stable, microcrystalline aluminophosphates, $AlPO_4$-n (where n stands for structure type) have been synthesised in aqueous media using structure directing agents[1]. A notable feature of $AlPO_4$ composition is the invariant

Al_2O_3/P_2O_5 ratio which is in direct contrast with the variable ratio found in zeolite frameworks. Unlike the zeolite framework which contains Al^{3+} and Si^{4+} in tetrahedral positions and exhibit a negative charge, the $AlPO_4$ framework may contain Al in a coordination other than tetrahedral and is neutral. The overall anhydrous formula is $(Al_{0.5}\ P_{0.5})O_2$. Just as zeolites, the $AlPO_4$'s also obey the Lowenstein's rule[14] for the avoidance of –Al–O–Al– bonds. The $AlPO_4$ molecular sieves exhibits 4–, 6–, 8–, 12–, and 18– membered rings. Some are zeolite structural analogs, but many are microporous structures with no known zeolite analogs. Some of the structures have been determined for eg. $AlPO_4$–5[15], $AlPO_4$–11[16], $AlPO_4$–14[17], $AlPO_4$–46[18], $AlPO_4$–8[19], and VPI–5[20] (Table 1.1).

1.1.4 Synthesis

Like the zeolites, the $AlPO_4$ materials are synthesised hydrothermally with a preferred temperature range of 398–473 K. Reactive $AlPO_4$ gels are used. The preferred source of aluminium is pseudoboehmite, and phosphorus is added as phosphoric acid. Instead of highly caustic conditions, employed in synthesis of zeolites, the $AlPO_4$ gel exhibits an initial acidic pH of ≈ 3.

Numerous synthesis parameters contribute to the crystalline phase(s). At low temperatures (373–398 K) crystallization of condensed phases occur.

Addition of an organic structure directing agent seems to be a necessary step in $AlPO_4$ synthesis[3]. Organic additives appear to promote crystallization of specific structures as in zeolite systems. However, not all organics added to the reaction mixture are so specific. The novel $AlPO_4$–5 crystallizes in presence of a wide range of organic additives. There appears to be no correlation between size, solubility or pKb, yet, all promote crystallization of $AlPO_4$–5. In addition to several organics promoting specific structures, one organic may promote crystallization of several molecular sieve structure depending on temperature, crystallization aging, time, gel composition etc.[21] just as in zeolite systems[22]. Recently, however, it has been found that addition of organic additive is not always necessary for synthesis of microporous crystalline $AlPO_4$[23].

Name	Structure	Ring size	Pore size(Å)
VPI–5	Novel	18	12
$AlPO_4$–8	Novel	14	9
$AlPO_4$–5	Novel	12	8
$AlPO_4$–37	Fau	12	8
$AlPO_4$–46	Novel	12	8
$AlPO_4$–11	Novel	10	6
$AlPO_4$–31	Novel	10	6.5
$AlPO_4$–14	Novel	8	4.3
$AlPO_4$–17	Erio	8	4.3
$AlPO_4$–18	Novel	8	4.3
$AlPO_4$–44	Cha	8	4.3
$AlPO_4$–20	Sod	6	3
$AlPO_4$–25	Novel	6	3

TABLE 1.1. **Aluminophosphate–based Molecular Sieves (Ref. 10).**

1.1.5 Element Substituted Aluminophosphates

Incorporation of Si source in $AlPO_4$ gel is the method used to form silicoaluminophosphate SAPO–n[24,25]. The SAPO materials crystallize from an aqueous medium in presence of organics[24]. The anhydrous chemical composition of SAPO–n is $(Si_x\ Al_y\ P_z)O_2$. A SAPO material can be considered to originate from silicon substitution in $AlPO_4$ framework[24,26]. The predominant substitution mechanisms are Si for P (Mechanism 2) and two Si atoms for a pair of Al and P (Mechanism 3). Si substitution for Al (Mechanism 1) does not occur. Recently, contributions of aluminosilicate (SA) and silicoaluminophosphate (SAPO) domains have been identified in SAPO materials[27]. *Ab initio* calculations have predicted that Si substitutes for P preferentially in $AlPO_4$[28] in agreement with the experimental results[24]. The negative charge in SAPO is therefore, proportional to mol fraction of Si incorporated via mechanism 2. SAPO's are cation exchangers and Brönsted acid catalysts.

Crystalline microporous silicoaluminophosphates have been patented as Mobil Crystalline Materials (MCM–n) also[29]. The MCM's crystallizes from a biphasic medium by use of similar organic additives as in the case of SAPO's. The general anhydrous formula for MCM is[29]:

$$R\ M_{\frac{x}{m}}^{m+}\ (AlO_2)_{1-y}^{-}\ (PO_2)_{1-x}^{+}\ (SiO_2)_{x+y}\ N_{\frac{y}{n}}^{n-}$$

where x and y are the mole fraction of Al and P, respectively; M and N are metal cation and anion with charges m^+ and n^-, respectively.

The MCM formula precludes isomorphous substitution via mechanism 3. MCM's are potential Brönsted acid, Brönsted base or acid/base catalysts.

In metal substituted $AlPO_4$ (MeAPO) family, the framework composition contains metals in addition to Al and P. The metal species include divalent forms of Co, Fe, Mg, Zn, Mn, and trivalent Fe[30]. The anhydrous chemical composition is $(Me_xAl_yP_z)O_2$. In MeAPO's, metal appears to substitute exclusively for Al[31].

The MeAPSO family[32] further extends the structural diversity and composition variation found in SAPO's and MeAPO's. These quaternary frameworks have metal, Si, Al,and

P framework species. In ElAPO[33] and ElAPSO[33,34] compositions, additional elements such as Li, Be, B, Ga, As, and Ti are incorporated into framework structures.

Some of the properties, and measurements used for characterization and catalytic properties of $AlPO_4$ based materials are given below.

1.1.6 Adsorption Properties

The adsorption properties of $AlPO_4$ molecular sieves exhibit features characteristic of zeolite like nature. Adsorption pore volume for water ranges from 0.04 to 0.35 cm^3/g, similar to those of known zeolites. The adsorption properties of VPI–5 are typical of adsorption in a very large pore system. Triisopropylbenzene (TIPB) is readily adsorbed into the large 18 ring channels[35]. $AlPO_4$–5 readily adsorbs neopentane into 12 ring channels[21]. Both $AlPO_4$–11 and $AlPO_4$–31 exhibit similar adsorption properties; neither adsorbs neopentane, consistent with medium pore ring channels[21]. $AlPO_4$–18 has a novel structure, but its adsorption properties are similar to those of erionite[21].

1.1.7 Nuclear Magnetic Resonance

The aluminium species in an oxide matrix having tetrahedral coordination are found about 35–45 ppm from $Al(H_2O)_6^{3+}$ [36] and for octahedral coordination the signal is found between -7 to -29 ppm[37]. The ^{31}P MASNMR spectrum of aluminophosphate exhibit symmetrical line with chemical shift ranging from -19 to -30 ppm relative to external H_3PO_4[38].

In varicite and metavaricite, the observed symmetrical peaks at -13.2 and -12.5 ppm, respectively[39,40], is consistent with reported structure of alternating PO_4 and $(AlO_4)(H_2O)_2$ octahedra[12]. By (^1H–^{27}Al) CP MAS experiments the Al was strongly cross polarized and this produced a strong signal at -13 ppm, thus demonstrating that CP can locate H_2O coordinated strongly to Al. The molecular sieves $AlPO_4$–H3[13] and VPI–5[3] showed peaks due to 4– and 6–coordinated Al[41,42] in the ratio 1:1 and 2:1 respectively. These match with the reported crystal structure[43,20]. Double rotation (DOR) spectrum of VPI–5[44] distinguishes 8 non–equivalent Al atoms in the structure. Some of the $AlPO_4$ molecular sieves showed 6–coordinated Al on calcination and rehydration, for e.g. $AlPO_4$–11[45],

$AlPO_4$–5[46], $AlPO_4$–17[47], and SAPO–31[48].

Multiple resonance maxima are observed in ^{31}P spectra of $AlPO_4$–H3[41] VPI–5[35,42] and $AlPO_4$–21[47]. These results are consistent with the reported crystal structure[43,20,49] indicating different phosphorus environments in these materials.

MASNMR technique can be used in phase identification also. Grobet et al. using ^{31}P, ^{27}Al and ^{29}Si MASNMR technique have recently shown that a member of MCM family, MCM–1 is similar to $AlPO_4$–H3[41] and MCM–9 is a mixture of SiVPI–5 and SAPO–11[50]. In the same way, VPI–5 has been found to be similar to H1(GTRI)[51].

Barrie and Klinowski[52] have assigned the ^{31}P spectral signals to different coordinated sites of P in MAPO–20.

Montes et al.[53], Goldfarb[54] and Shiralkar et al.[55] have observed intense spinning side bands in NMR spectra of transition metal substituted $AlPO_4$–5. These bands have been attributed to strong dipolar interactions of Al and P with the paramagnetic nuclei.

1.1.8 Other Techniques

Some of the other techniques used for the characterization of substituted $AlPO_4$'s are Mossbaüer[56,57], ESR[54,58] and UV[58,59].

1.1.9 Acidity Concepts

The Brönsted acidity of $AlPO_4$ based materials depend on both framework composition and structure type. Incorporation of heterovalent elements in general generates weak to strong acidity. The acidity may be determined by measurement of pseudo-first order rate constant for the cracking of n–butane[60]. However, no simple relationship between the rate constant and concentration of a specific metal incorporated into the framework has been observed.

Peaks at 3675 and 3790 cm^{-1} in the IR spectrum of $AlPO_4$–5 have been attributed to P–OH and Al–OH defect groups[61]. Weak absorption are observed in IR spectrum between 3520 and 3630 cm^{-1} in SAPO's[21]. Halick et al.[62] have interpreted the bands at 3745, 3678, 3626, and 3515 cm^{-1} as due to Si–OH, P–OH and two types of Si–O–

Al groups in SAPO–5. These results are consistent with the predictions of Derouane et al.[28]; that bridging OH groups in $AlPO_4$'s originating from non–stochiometry, defects or Si incorporation should show acidic property. Brönsted and Lewis acid sites have been detected and distinguished by the presence of specific adsorption bands at 1545 and 1450 cm^{-1}, respectively, in $AlPO_4$–5[61] and SAPO–5[62] upon pyridine sorption. Brönsted acid sites are generated by cobalt substitution also, but in this case considerable enhancement in Lewis acidity has also been observed[63].

Acidity in $AlPO_4$–5 has been determined by TPD of ammonia[62] and pyridine[64]. Only one peak of desorption at $\approx$ 473K indicates the involvement of one type of acid site. SAPO–5[62] exhibited three maxima indicative of the presence of both Brönsted and Lewis sites. Two maxima have been observed in CoAPO–11 also[31,65].

1.1.10 Catalysis

$AlPO_4$ lattice, though electrically neutral and not expected to exhibit acidity, does show acidic sites[64,66]. These acid sites are shown to bring about reactions such as cracking[64,66], isomerization[64] and methanol conversion[67].

Chemical modification enhances the catalytic activity in $AlPO_4$ molecular sieves[68,69]. SAPO–5 has been the most widely studied among the $AlPO_4$ based materials. Catalytic activity of SAPO–5 in n–butane cracking[26], cumene cracking[70], xylene isomerization[70,71], alkylation[72], conversion of decane[73], and ethylbenzene hydrogenation[74] has been reported. Pyke et al.[69] have presented evidence for isomorphous substitution of di, tri and tetravalent metals in $AlPO_4$-5. $AlPO_4$ molecular sieves can be used as supports in Fisher–Tropsch reaction[75].

Pellet et al.[72,76] have shown that the Brönsted acidity of $AlPO_4$ molecular sieves depend both on framework composition and structure type. The enhanced selectivity observed with medium pore SAPO's and MeAPO's has been attributed to unique combination of mild acidity and shape selectivity. The lack of hydride shift and cracking activity in olefin mediated reactions are suggestive of mild acidity. Transition metal framework constituents appear to exert a special chemical effect on the catalytic performance.

Anderson et al.[77] have monitored the shape selective conversion of methanol to low molecular weight hydrocarbons over SAPO–34 by ^{13}C and ^{1}H MASNMR in tandem with gas chromatography. The intracrystalline formation of branched C_4 and C_5 hydrocarbons imposes an additional steric requirement on the diffusion of linear hydrocarbons. This favours the diffusion of C_1 and C_2 species out of the crystallite and is responsible for the apparent overall selectivity for ethylene.

1.2 VERY LARGE PORE ALUMINO-PHOSPHATE MOLECULAR SIEVES

1.2.1 Introduction

Until recently the largest channel molecular sieves were based on 12 membered rings of tetrahedral atoms and these rings were invariably less than 10Å wide, though large ring sizes are known, for e.g. Cacoxenite mineral among natural phosphates[78]. Cacoxenite contains rings of $\approx$ 15 Å free diameter. It possesses Fe^{3-} oxygen tetrahedron[79]. Hypothetical large ring structures have been predicted by Barrer and Villiger[80], Smith and Dytrych[81] and Meier[82].

Smith and Dytrych[81] labeled the $AlPO_4$–5 topology as net 81. They also developed the concept of inserting 4–membered rings into net 81 to produce an infinite series nets, net 81(n). As n, the number of rings, increases, the limiting ring of the channel expands from 12 nodes for 4–ring to 18($n = 1$), to 24($n = 2$) and 6($n + 2$) in general. Davis et al.[3] described the preparation of a crystalline $AlPO_4$, VPI–5, using organic additives with the precise structure (net 81(1)) as envisaged by Smith.

$AlPO_4$–8 is an aluminophosphate reported in the patent by Wilson et al.[1]. An appropriate structural model for $AlPO_4$–8 was obtained recently[19] by modifying the topology of net 81(1) framework of Smith[81].

$AlPO_4$–H1 is an aluminophosphate hydrate first reported by D'Yvoire[13]. It crystallizes from an organic free $AlPO_4$ gel as a minor component along with another phase $AlPO_4$–H2. $AlPO_4$–H1 reportedly transforms to tridymite upon mild heating[13].

1.2.2 The Molecular Sieve VPI–5

VPI–5 is prepared from reactive $AlPO_4$ gel in presence of organic additives at a hydrothermal treatment temperature of 413–423 K under autogenous pressure. N–dipropylamine[83,84], tetrabutylammonium hydroxide[83] as well as another secondary amine[42] are known to encourage crystallization of the material.

1.2.2.a. Structure

The elemental composition of VPI–5 can be expressed as $(Al_{0.5}P_{0.5})O_2$. The structure is composed of AlO_4 and PO_4 tetrahedra. Each tetrahedron is linked to form sheets containing 4–, 6–, and 18– rings. The 18– ring channel corresponds to 12Å in size (Fig. 1.1). The crystallographc details are shown in Table 1.2.

1.2.2.b. Structural Stability

Davis et al.[85] have claimed the structure to be stable upto 1073 K. However, facile transformation of VPI–5 to $AlPO_4$–8 on thermal treatment has been reported[86–88].

1.2.2.c. Physico–chemical Properties

Thermal analysis[35] and ^{13}C MASNMR[42] studies showed absence of occluded organic additives in the structure. The ^{27}Al NMR spectrum showed 4– and 6–coordinated Al and the ^{31}P NMR showed three peaks indicating three different environment for P[35,42]. The water adsorption isotherm for VPI–5 appears to be similar to that of $AlPO_4$–5 with an adsorption capacity of 0.32 cm^3/g. VPI–5 adsorbs triisopropylbenzene (kinetic diameter 8.5Å) suggesting presence of extra large pores in the structure[35].

1.2.3 The Molecular Sieve $AlPO_4$–8

$AlPO_4$–8 crystallizes at 423 K with the aid of organic additives[1].

1.2.3.a. Structure

The structural model was obtained recently[19]. $AlPO_4$–8 is found to contain one–dimensional elliptical pores, with a free diameter of 7.5×9.5Å circumscribed by tetrahedral atoms (Fig. 1.2). The Al–O–P linkages in four of the double 4–rings in VPI–5 are broken

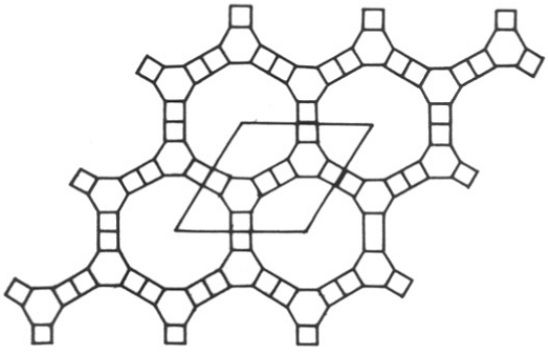

Fig. 1.1 ▷ **[001] Projection of a layer of the VPI–5 framework.**

	$AlPO_4$–11 (Ref.16)	VPI–5 (Ref.20)	$AlPO_4$–8 (Ref.19)
Channel size	10 ring 7.0×4.1Å elliptical	18 ring 12.1Å circular	14 ring 8.7×7.9Å elliptical
Crystal structure	orthorhombic	hexagonal	orthorhombic
Space group	Icm2	$P6_3Cm$	$CmC2_1$
a(Å)	13.53	18.99	33.29
b(Å)	18.48	–	14.76
c(Å)	8.37	8.11	8.26
Density g/cc		1.42	1.8

TABLE 1.2. **Crystallographic Details of $AlPO_4$–11, VPI–5 and $AlPO_4$–8.**

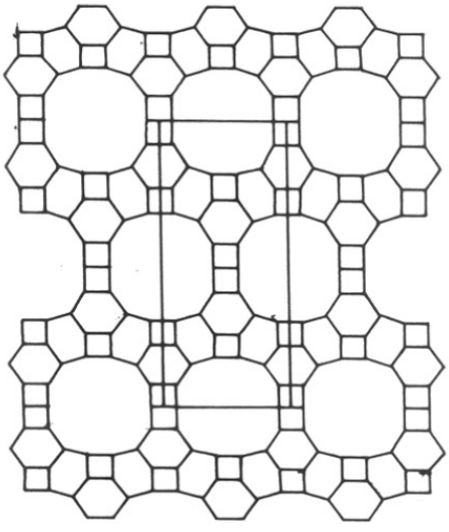

Fig. 1.2 ▷ [001] Projection of a layer of the $AlPO_4$–8 framework.

and recombined to form 6–rings in $AlPO_4$–8[86]. The crystallographic details are presented in Table 1.2.

1.2.4 Comparison of VPI–5, $AlPO_4$–8 and $AlPO_4$–H1

Davis et al.[89] have recently compared VPI–5 with $AlPO_4$–8 and concluded that the former is thermally stable and different from the latter which is a distinct phase containing no extra–large pores. However, subsequent studies show that VPI–5 converts to $AlPO_4$–8[86–88] by thermal treatment and both can be crystallized from similar gel compositions under identical hydrothermal treatment conditions[87].

Similarity between the X–ray diffraction patterns of VPI–5 and $AlPO_4$–H1 raises question of the role of organic additive in VPI–5 synthesis. Duncan et al.[23] reproduced the $AlPO_4$–H1 in pure form, H1(GTRI), using a modified procedure of D'Yvoire[13]. The XRD, IR, NMR, and water sorption of H1(GTRI) match with that of VPI–5 and, the sorption of organics with that of small pore VPI–5[88]. On thermal treatment H1(GTRI) converts to $AlPO_4$–8[23,51] an observation similar to that found with VPI–5[86–88]. For samples containing small amounts of H1(GTRI) (H1$\ll$H2), only tridymite lines could be observed in XRD[23]. Thus, low concentration of $AlPO_4$–H1 in D'Yvoire's mixture explains the possible mis–assignment of $AlPO_4$–H1 thermal product as tridymite. These results indicate that VPI–5 does not represent a new microporous phase but, rather, $AlPO_4$–H1 prepared in the presence of organic additives.

1.3 THE ALUMINOPHOSPHATE MOLECULAR SIEVE $AlPO_4$–11

$AlPO_4$–11 is synthesised from $AlPO_4$ gel by using n–dipropylamine or diisopropylamine as typical organic additives. Other secondary amines are also found to promote crystallization of the structure[90]. The electronic property of the amines doesnot differ much[91] suggesting a role as pH modifier rather than structure directing species for the amines.

1.3.1 Structure

The structure of $AlPO_4$–11 is composed of AlO_4 and PO_4 tetrahedra. Three vertices of each tetrahedron are linked to form sheets containing 4–, 6–, and 10–membered rings[16]. The 3D network(Fig. 1.3) is produced by linking the remaining vertices. The one–dimensional channel is elliptical and has a pore opening of 7.0×4.1Å. The crystallographic data are given in Table 1.2.

1.3.2 Physico–chemical Properties

TG/MS studies[92] of $AlPO_4$–11 precursors show that the organics desorbed at a temperature range of 573–623 K. A Single signal for ^{31}P and ^{27}Al atoms at -30 ppm and 34 ppm, respectively, in the MASNMR spectral signals suggests environment for both Al and P atoms in the structure. $AlPO_4$–11 shows type 1 adsorption isotherm with an adsorption capacity of 0.13 cm^3/g[21] for water. Sorption measurements with organics yield data consistent with a medium pore structure.

The as–synthesized and calcined hydrated forms of $AlPO_4$–11/SAPO–11 correspond to different XRD pattern[93,94] and NMR signals[45,93–95]. A phase transition is found to occur resulting in space group change[45,93–95].

1.3.3 Element Substituted $AlPO_4$–11

Flanigen et al.[60] have reported a large number of element substituted $AlPO_4$–11. But only few (cobalt, silicon) have appeared in the open literature[63,65,93]. TPD measurements have confirmed the presence of acid sites in CoAPO–11[31,65] implying substitution of Co^{2+} for Al^{3+}. CoAPO–11 is found to catalyse reactions such as methanol conversion[63], propene oligomerization[76] etc.

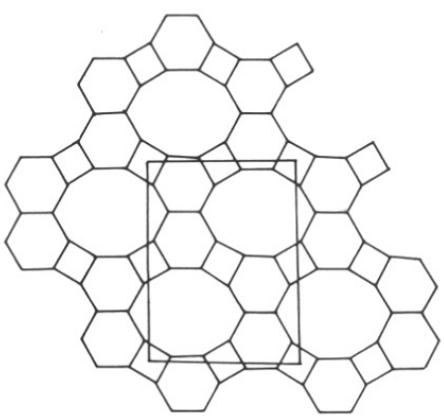

Fig. 1.3 ▷ [001] Projection of a layer of the $AlPO_4$–11 framework.

1.4 REFERENCES

1. S.T. Wilson, B.M. Lok and E.M. Flanigen, U.S. Pat. 4,310,440, 1982.
2. S.T. Wilson, B.M. Lok, C.A. Messina, T.R. Cannan and E.M. Flanigen, *J. Am. Chem. Soc.*, **104**, 1146, 1982.
3. M.E. Davis, C. Saldarriaga, C. Montes, J.M. Garces and C. Crowder, *Nature*, **331**, 698, 1988.
4. R.H. Jones, J.M. Thomas, R. Xu, A.K. Cheetham and D. Bieber, *J. Chem. Soc. Chem. Comm.*, 1990, **p.1170**.
5. Y. Xu, J.M. Thomas, C.P. Grey and A.K. Cheetham, *Catal. Lett.*, **4**, 251, 1990.
6. R.L. Bernard, S.T. Wilson, L.D. Vail, J.M. Bennet and E.M. Flanigen, *Stud. Surf. Sci. Catal.*, **49A**, 199, 1989.
7. J.B. Parise, *J. Chem. Soc. Chem. Comm.*, 1990, **p.1553**.
8. D.E.W. Vaughan, *ACS. Symp. Ser.*, **368**, 308, 1988.
9. C. Ramelsberg, *Pogg. Ann.*, **64**, 251, 1845,
   G.C. Wittnstein, *Pogg. Ann.*, **97**, 258, 1856.
10. R. Szostak, *Molecular Sieves: Principle of Synthesis and Identification*, van Nostrand, 1988.
11. K. Kosten and H. Arnold, *Z. Kristallogr.*, **152**, 119, 1980.,
    J.H. Morris, P.G. Perkins, A.E.A. Rose and W.E. Smith, *Chem. Soc. Rev.*, **6**, 173, 1977.
12. R. Kniep and D. Mortz, *Acta. Crystallogr.*, **B29**, 2292, 1972.,
    R. Kniep, D. Mortz and A. Vegas, *Acta. Crystallogr.*, **B33**, 263, 1977.
13. F. D'Yvoire, *Bull. Soc. Chim. Fr.*, 1961, **p. 1762.**
14. W. Lowenstein, *Am. Mineral.*, **39**, 92, 1954.
15. S.T. Wilson, B.M. Lok, T.R. Cannan and E.M. Flanigen, *ACS. Symp. Ser.*, **218**, 79, 1983.
16. J.W. Richardson. Jr., J.J. Pluth and J.V. Smith, *Acta. Crystallogr.*, **B44**, 367, 1988.
17. J.J. Pluth and J.V. Smith, *Acta. Crystallogr.*, **C43**, 866, 1987.
18. J.M. Bennet and B.K. Markus, *Stud. Surf. Sci. Catal.*, **37**, 269, 1988.
19. R.M. Dessau, J.L. Schlenker and J.B. Higgins, *Zeolites*, **10**, 1522, 1990.
20. C.E. Crowder, J.M. Garces and M.E. Davis, *Adv. X-ray. Anal.*, **32**, 503, 1989.
21. S.T. Wilson, B.M. Lok, C.A. Messina and E.M. Flanigen, *Proc. 6th Int. Zeo. Conf.*, Reno, USA (Eds: D. Olson and A. Bisio), 1983, **p. 97**.
22. L.D. Rollman, *Adv. Chem. Ser.*, **173**, 387, 1977.

23. B. Duncan, R. Szostak, K. Sorby and J.G. Ulan, *Catal Lett.*, **7**, 367, 1990.
24. B.M. Lok, C.A. Messina, R.L. Patton, R.T. Gajek, T.R. Cannan and E.M. Flanigen, *J. Am. Chem. Soc.*, **106**, 6092, 1984.
25. B.M. Lok, C.A. Messina, R.L. Patton, R.T. Gajek, T.R. Cannan and E.M. Flanigen, U.S. Pat., 4,440,871, 1984.
26. E.M. Flanigen, R.L. Patton and S.T. Wilson, *Stud. Surf. Sci. Catal.*, **37**, 13, 1988.
27. J.A. Martens, P.J. Grobet and P.A. Jacobs, *J. Catal.*, **126**, 299, 1990.
28. E.G. Derouane, J.G. Fripiat and R. von Ballmoos, *J. Phys. Chem.*, **94**, 1687, 1990.
29. E.G. Derouane, E.W. Valyocsik and R. von Ballmoos, Eur. Pat. App., 146,384, 1984.
30. S.T. Wilson and E.M. Flanigen, Eur.Pat. App., 132,708, 1985, U.S. Pat. 4,567,029, 1985.
31. N.J. Tapp, N.B. Milestone and J.M. Wright, *J. Chem. Soc. Chem. Comm.*, 1985, **p. 1801**.
32. B.M. Lok, B.K. Markus and E.M. Flanigen, Eur. Pat. App., 161,489, 161,190, 1985., B.M. Lok, L.D. Vail and E.M. Flanigen, Eur. Pat. App., 158,348, 158,975, 161,491, 1985.
33. B.M. Lok, B.K. Markus and E.M. Flanigen, U.S. Pat., 4,500,651, 1985., E.M. Flanigen, B.M. Lok, R.L. Patton and S.T. Wilson, Eur. Pat. App., 158,976, 1985.
34. B.M. Lok, B.K. Markus, L.D. Vail, E.M. Flanigen, R.L. Patton and S.T. Wilson, Eur. Pat. App., 159,624, 1985.
35. M.E. Davis, C.E. Montes, P.E. Hathaway, J.P. Arahncet, D.L. Hasha and J.M. Garces, *J. Am. Chem. Soc.*, **111**, 3919, 1989.
36. D. Muller, E. Jahn, G. Ladwig and U. Haubenreisser, *Chem. Phys. Lett.*, **109**, 382, 1984.
37. D. Muller, I. Grunge, E. Hallas, and G. Ladwig, *Z. Anorg. Allog. Chem.*, **500**, 80, 1983.
38. R.P.J. Williams, R.G.F. Giles and A.M. Posner, *J. Chem. Soc. Chem. Comm.*, 1981, **p. 105**.
39. C.S. Blackwell and R.L. Patton, *J. Phys. Chem.*, **88**, 6134, 1984.
40. N.S. Kotsarenko, V.M. Mastikin, I.L. Mudrakovskii and V.P. Shmachkova, *Reac. Kinet. Catal. Lett.*, **30**, 375, 1989.
41. J.A. Martens, B. Verlinden, M. Mertens, P.J Grobet and P.A. Jacobs, *ACS. Symp. Ser.*, **398**, 305, 1989.

42. P.J. Grobet, J.A. Martens, I. Balakrishnan, M. Mertens and P.A. Jacobs, *Appl. Catal.*, 1989, **56**, L21.

43. J.J. Pluth and J.V. Smith, *Nature*, **318**, 165, 1985.

44. Y. Wu, B.F. Chmelka, A. Pines, M.E. Davis, P.J. Grobet and P.A. Jacobs, *Nature*, **346**, 550, 1990.

45. M. Goepper, F. Guth, L. Delmotte, J.L. Guth and H. Kessler, *Stud. Surf. Sci. Catal.*, **49B**, 857, 1989.

46. R. Meinhold and N.J. Tapp, *J. Chem. Soc. Chem. Comm.*, 1990, **p. 219**.

47. C.S. Blackwell and R.L. Patton, *J. Phys. Chem.*, **92**, 3965, 1988.

48. H.L. Zubowa, E. Alsdorf, R. Fricke, F. Neissendorfer, J.R. Menden, E. Scheier, D. Zeigan and B. Zibrowius, *J. Chem. Soc. Faraday Trans 1*, **86**, 2307, 1990.

49. J.M. Bennet, J.M. Cohen, G. Artioli, J.J. Pluth and J.V. Smith, *Inorg. Chem.*, **24**, 188, 1985.

50. P.J. Grobet, H. Greets, J.A. Martens, and P.A. Jacobs, *Stud. Surf. Sci. Catal.*, **52**, 193, 1989.

51. S. Prasad, Ph.D Thesis, Part 2, Chapter 2.

52. P.J. Barrie and J. Klinowski, *J. Phys. Chem.*, **93**, 5972, 1989.

53. C. Montes, M.E. Davis, B. Murray and M. Narayana, *J. Phys. Chem.*, **94**, 6425, 1990.

54. D. Goldfarb, *Zeolites*, **9**, 509, 1989.

55. V.P. Shiralkar, C.H. Saldarriaga, J.O. Perez, A. Clearfield, M. Chen, R.G. Antony and J.A. Donohue, *Zeolites*, **9**, 474, 1989.

56. C.M. Cardile, N.J. Tapp and N.B. Milestone, *Zeolites*, **10**, 90, 1990.

57. H.X. Li, J.A. Martens, P.A. Jacobs, S. Schubert, F. Schmidt, H.M. Zeithen and A.X. Trantwein, *Stud. Surf. Sci. Catal.*, **37**, 75, 1988.

58. L.E. Iton, I. Choi, J.A. Desjardines and V.A. Moroni, *Zeolites*, **9**, 535, 1990.

59. R.A. Schoondeydt, R. De Vos, J. Pilgrims and H. Leeman, *Stud. Surf. Sci. Catal.*, **49A**, 559, 1989.

60. E.M. Flanigen, B.M. Lok, R.L. Patton and S.T. Wilson, *Proc. 7th Int. Zeo. Conf.*, Tokyo, Japan, (Eds: Y. Murakami et al.), 1986, **p. 103**.

61. O.V. Kikhtyanin, E.A. Paushtis, K.G. Ione and V.M. Mastikhin, *J. Catal.*, **126**, 1, 1990.

62. C. Halick, J.A. Lercher and H. Meyer, *J. Chem. Soc.Faraday Trans 1*, **84**, 4457, 1988.

63. N.J. Tapp, N.B. Milestone and D.M. Bibby, *Stud. Surf. Sci. Catal.*, **37**, 393, 1988.

64. V.R. Choudhary and D.B. Akolekar, *J. Catal.*, **103**, 115, 1987.
65. S. Ernst, L. Puppe and J. Weitkamp, *Stud. Surf. Sci. Catal.*, **49A**, 447, 1989.
66. S.G. Hegde, P. Ratnasamy, L.M. Kustov and V.B. Kazansky, *Zeolites*, **8**, 137, 1988.
67. O.V. Kikhtyanin, V.M. Mastikhin and K.G. Ione, *Appl. Catal.*, **42**, 1, 1988.
68. N.B. Milestone and N.J. Tapp, *Stud. Surf. Sci. Catal.*, **36**, 553, 1987.
69. D.R. Pyke, P. Whitney and H. Houghton, *Appl. Catal.*, **18**, 175, 1985.
70. X. Quinhua, Y. Aizhen, B. Shulin and X. Kaijun, *Proc. 7th Int. Zeo. Conf.*, Tokyo, Japan, (Eds: Y. Murakami et al.), 1986, **p. 835**.
71. C.H. MInchev, V. Kanazierev, V. Mardoninova, V.P. Penchev and H. Lerchert, *Stud. Surf. Sci. Catal.*, **46**, 29, 1989.
72. P.J. Pellet, G.N. Long and J.A. Rabo, *Proc. 7th Int. Zeo. Conf.*, Tokyo, Japan, (Eds: Y. Murakami et al.), 1986, **p. 843**.
73. J.A. Martens, M. Mertens, P.J. Grobet and P.A. Jacobs, *Stud. Surf. Sci. Catal.*, **37**, 97, 1988.
74. K.J. Chao and L.J. Leu, *Stud. Surf. Sci. Catal.*, **46**, 19, 1989.
75. P.K. Coughlin and J.A. Rabo, U.S. Pat., 4,556,645, 1985.
76. P.J. Pellet, P.K. Coughlin, E.S. Shamshoun and J.A. Rabo, *ACS. Symp. Ser.*, **398**, 512, 1989.
77. M.W. Anderson, B. Sulikowski, P.J. Barrie and J. Klinowski, *J. Phys. Chem.*, **94**, 2730, 1990.
78. P.B. Moore and J. Shen, *Nature*, **306**, 356, 1983.
79. R. Szostak, R. Kuvadia, J. Brown and T.L. Thomas, *Stud. Surf. Sci. Catal.*, **49A**, 439, 1989.
80. R.M. Barrer and H. Villiger, *Z. Kristallogr.*, **128**, 352, 1969.
81. J.V. Smith and W.J. Dytrych, *Nature*, **309**, 607, 1984.
82. W.M. Meier, *Proc. 7th Int. Zeo. Conf.*, Tokyo, Japan, (Eds: Y. Murakami et al.), 1986, **p. 13**.
83. M.E. Davis, C. Montes, P.E. Hathaway and J.M. Garces, *Stud. Surf. Sci. Catal.*, **49A**, 199, 1989.
84. M.E. Davis, C. Montes, J.M. Garces and C. Crowder, *ACS. Symp. Ser.*, **398**, 291, 1989.
85. M.E. Davis, C. Saldarriaga, C. Montes, J.M. Garces and C.E. Crowder, *Zeolites*, **8**, 362, 1989.

    M.J. Annen, D. Young, M.E. Davis, O.B. Cavin and C.R. Hubbard, *J. Phys. Chem.*, **95**, 1380, 1991.

86. E.T.C. Vogt and J.W. Richardson Jr., *J. Solid State Chem.*, **87**, 409, 1990.
87. S. Prasad and I. Balakrishnan, *Inorg. Chem.*, **29**, 4830, 1990.
88. K. Sorby, R. Szostak, J.G. Ulan and R. Gronsky, *Catal. Lett.*, **6**, 209, 1990.
89. M.E. Davis, P.E. Hathaway and C. Montes, *Zeolites*, **9**, 436, 1989.
90. I. Balakrishnan and S. Prasad, *Appl. Catal.*, **62**, L7, 1990.
91. S. Prasad and R. Vetrivel, Proc. 10th Natl. Symp. Catal., (Eds: B. Viswanathan and C.N. Pillai), Madras, 1990, **p. 175**.
92. N.J. Tapp and N.B. Milestone, *Stud. Surf. Sci. Catal.*, **36**, 639, 1987.
93. J.C. Vedrine, G. Coudurier and B.F. Mentzen, *ACS. Sypm. Ser.*, **368**, 66, 1988.
94. N.J. Tapp, N.B. Milestone, M.E. Bowden and R.H. Meinhold, *Zeolites*, **10**, 105, 1990.
95. R. Khouzami, G. Coudurier, F. Lefebvre, J.C. Vedrine and B.F. Mentzen, *Zeolites*, **10**, 183, 1990.

CHAPTER 2

SYNTHESIS AND CHARACTERIZATION OF SOME $AlPO_4$ MOLECULAR SIEVES

2 SYNTHESIS AND CHARACTERIZATION OF SOME $AlPO_4$ MOLECULAR SIEVES

2.1 INTRODUCTION

There are similarities and differences between the synthesis of zeolite and aluminophosphate molecular sieves ($AlPO_4$). The former are synthesized from reactive aluminosilicate gels and the latter from aluminophosphate gels. Synthesis of both in majority of the cases involves the use of organic additives. Synthesis without additives leads to amorphous or condensed phases. The gel systems in the former case are highly alkaline while in the latter they are slightly acidic. The acidity allows the use of amines besides quaternary ammonium salts as additives for the synthesis of $AlPO_4$'s. These additives also facilitate the successful incorporation of hydrolyzable metal cation forms of the elements into the framework to synthesize metal substituted $AlPO_4$'s (MeAPO's). Both zeolites and $AlPO_4$'s are synthesized by hydrothermal treatment of the respective gels in the temperature range of 398–423 K.

The work of D'Yvoire[1], Martens et al.[2] and recently of Duncan et al.[3] have shown that some of the microporous crystalline $AlPO_4$'s can be synthesized in the absence of organic additives.

The synthesis materials for $AlPO_4$ molecular sieves are an Al source, usually pseudoboehmite, a reactive hydrate alumina, phosphoric acid, an organic additive and water. Synthesis of $AlPO_4$ molecular sieves takes place in the following steps:

1. Neutralization of aluminium hydroxide suspended in water with nearly equimolar amount of dilute phosphoric acid to obtain a reactive aluminophosphate gel.
2. Addition of the particular amine or quaternary ammonium salt to the gel before or after its aging usually in the same mole ratio as the hydroxide and the acid. This mixture is referred to as the precursor gel.
3. Aging of the precursor gel, if necessary, and
4. Hydrothermal treatment of the precursor gel.

The order of addition of the reagent and the agitation/non agitation of the system are some of the important synthesis parameters in steps 1–4. Hydrothermal treatment temperature and duration of the treatment are also parameters which affect synthesis.

N–dipropylamine(DPA) and diisopropylamine(DIPA) are the typical organic additives used in the synthesis of $AlPO_4$–11[4,5], though others have been reported in the patent literature[5].

Tapp et al.[4] in the context of their studies in the synthesis of $AlPO_4$–11 have noticed metavaricite as the intermediate. The poorly crystalline metavaricite gave rise to microporous crystalline $AlPO_4$–11, $AlPO_4$–5 and $AlPO_4$–20 by subsequent addition of appropriate structure directing agents. They have also identified layered aluminophosphate materials capable of intercalating various amines.

Tetrabutylammonium hydroxide (TBAOH) and DPA were used as organic additives in the original work of Davis et al.[6,7] in the synthesis of VPI–5. VPI–5 obtained with DPA was reportedly unstable in the mother liquor after 24 hours of heating. The procedure adopted by Grobet et al.[8] reports the use of n–dibutylamine(DBA) as organic additive to yield VPI–5 in shorter crystallization period. Instead of pseudoboehmite, aluminium isopropoxide was used as the source of Al in this work.

In the present chapter, successful synthesis of $AlPO_4$–11 by using DBA and n–dipentylamine (DPENTA) in place of DPA is described. The amines could also be used for synthesis of substituted $AlPO_4$–11 described in Chapter 4.

Synthesis of VPI–5 using two different Al source, aluminium isopropoxide and pseudoboehmite as Al source is reported. DBA was used as the organic additive. The synthesis of what appears to be a layered phase $AlPO_4$ (LP), is also reported.

The effect of Al source, temperature and period of crystallization, and concentration of the amines in the synthesis have been studied. H1(GTRI), the $AlPO_4$–H1 first reported by D'Yvoire[1] and synthesized in pure form by Duncan et al.[3], has been synthesized following their procedure and its identity verified.

The samples prepared have been characterized by XRD, SEM, MASNMR and thermal measurements.

2.2 EXPERIMENTAL

2.2.1 Chemicals

The following chemicals have been used in the synthesis.

- Pseudoboehmite (Catapal B. Vista, 71% Al_2O_3)
- Aluminium isopropoxide (Fluka, 99%)
- Phosphoric acid (SD Chemicals, 85%)
- N–dipropylamine (DPA) (Fluka, 99%)
- N–dibutylamine (DBA) (Merck, 99%)
- N–dipentylamine (DPENTA) (Merck, 99%)
- Water (Distilled)

2.2.2 Experimental Procedure for the Synthesis of $AlPO_4$ Molecular Sieves

2.2.2.a. Synthesis of $AlPO_4$–11

To 24.2 g of aluminium isopropoxide was added 22.5 g of distilled water. Dilute solution of H_3PO_4(13.8 g in 12.0 g) was added to the above Al source and mixed thoroughly. Organic additive (6.0 g DPA, 7.6 g DBA or 9.1 g DPENTA) was added and the contents stirred. The precursor gel was transferred in to a steel autoclaves (id=5cm^3, capacity=200 cm^3) which were heated in a uniform temperature air oven at 428 K under autogenous pressure. After 24 hours, the autoclaves were cooled to room temperature and the product filtered off. Residue was washed thoroughly with distilled water and air dried.

The synthesis conditions are given in Table 2.1.

2.2.2.b Synthesis of VPI–5

24.2 g of aluminium isopropoxide was converted to $Al(OH)_3$ by mixing with 22.5 g of water and letting the mixture stand for several hours. Alternatively, 8.4 g of pseudoboehmite was added to the same quantity of water to form a slurry. A Dilute solution of H_3PO_4(13.4

Synthesis system : nR. $Al_2O_3.P_2O_5$. 40 H_2O

Aluminium source	Amine, amine conc. (molar)	Hydrothermal treatment		Crystal(s) obtained
		Temp.(K)	Time	
I	DPA, 1.0	428	24	$AlPO_4$–11
I	DPENTA, 1.0	428	24	$AlPO_4$–11
I	DBA, 1.0	428	24–65	$AlPO_4$–11
I	DBA, 1.0	423	24	VPI–5†
I	DBA, 1.0	423	8–24 (agitation)	VPI–5
I	DBA, 1.0	473	24	Condensed phase
I	—	423	4 (agitation)	H1(GTRI)‡
B	DBA, 1.0	423	24	VPI–5
B	DBA, 1.5	423	24	VPI–5+LP
B	DBA, 2.0	423	8–24	LP
B	DBA, 0.5	473	24	$AlPO_4$–11†
B	DBA, 1–1.5	473	24	$AlPO_4$–11

† Impure phase

‡ Synthesis system: Al_2O_3. $0.8P_2O_5$.HCl.50 H_2O

- I = Aluminium isopropoxide
- B = Pseudoboehmite
- DPA = n–dipropylamine
- DBA = n–dibutylamine
- DPENTA = n–dipentylamine
- LP = Layered Phase

TABLE 2.1. **Synthesis Parameters and Products Obtained in $AlPO_4$ Systems.**

g in 12.0 g H_2O) was added slowly to the Al–containing slurry and mixed thoroughly for 5 minutes. 7.6 g of DBA was then added and again mixed for 5 to 10 minutes. The crystallization was carried out at 423 K (under agitation in the case of aluminium isopropoxide as Al source) in stainless steel autoclaves. The reaction mixture was quenched to ambient after 8–72 hours. The crystals were washed with water and air dried.

2.2.2.c. Synthesis of H1(GTRI)

16.1 g of aluminium isopropoxide was aged overnight in 17 g water. Addition of 7.1 g H_3PO_4 resulted in thick gel. To this $AlPO_4$ gel was added 3.4 g (35%) HCl. Finally 12 g of water was added to obtain a gel having a pH of 2. The gel was subjected to hydrothermal treatment at 423 K for 4 hours. The reaction mixture was quenched to ambient and the crystals obtained washed with water and air dried.

2.2.3 Characterization

2.2.3.a. X–ray Diffraction

X–ray diffraction patterns were recorded with a PW/1730 Philips instrument using nickel–filtered Cu k_α radiation.

2.2.3.b. Solid State MASNMR

MASNMR spectra were recorded in the solid state with a Bruker MSL 300 spectrometer operating at a field of 7 Tesla. ^{27}Al spectra were run at a frequency of 78.2 kHz, with a pulse length of 2μ s and a spinning speed of 3–5 kHz. ^{31}P spectra were run at 121.4 kHz with a pulse length of 4μ s and a spinning speed of 2–3 kHz. The chemical shifts were measured relative to aqueous $AlCl_3$ solution and 85% H_3PO_4 solutions, respectively.

2.2.3.c. Scanning Electron Microscopy

The size and morphology of the crystals were determined by using Cambridge steroscan model 150 Scanning Electron Microscope.

2.2.3.d. Thermal Analysis

A Netz'ch STA 409 Differential Thermal Analyzer was used to study the thermal behaviour at the following conditions: Sample size, 30mg; reference compound, alumina; sample holder, Pt crucible; temperature, 303—873 K; heating rate, 10 K minutes^{-1}.

2.3 RESULTS AND DISCUSSION

2.3.1 $AlPO_4$–11

In addition to DPA the typical tamplate, DBA and DPENTA have been found to aid the synthesis of $AlPO_4$–11. Low temperature aging of the precursor gel at 363 K gave rise to better purity. Samples synthesized by using all three amines gave the same XRD pattern (Fig. 2.1a).

The SEM image photograph of $AlPO_4$–11 crystallized using DBA is shown in Fig. 2.2. Crystalline aggregates are revealed.

Fig. 2.1b and 1c. show the ^{27}Al and ^{31}P MASNMR of the samples prepared by using DBA as organic additive. The single resonance line for both the spectra shows that P and Al atoms in the structure are located at sites of identical environments[9]. This shows that there is a strict Al–P ordering of alternating AlO_4 and PO_4 tetrahedra in the crystal structure of $AlPO_4$–11. The Al–P ordering follows the avoidance of Al–O–Al bonds analogous to the Lowenstein's rule[10] valid for the aluminosilicates. A shoulder in ^{31}P spectra at -22 ppm may be assigned to framework P adjacent to occluded organic template molecules[11].

Thermoanalytical curves for the samples synthesized by using the three amines are shown in Fig. 2.3. Strong exothermic peak occurs in the temperature range of 553–623 K due to combustion of the amines. This indicates that calcination at 723 K should effectively remove the occluded organic additive. TG trace of a calcined rehydrated sample (Fig. 2.3, inset) of $AlPO_4$–11 showed desorption of water upto 13%, in agreement with the water sorption capacity reported in the literature[5].

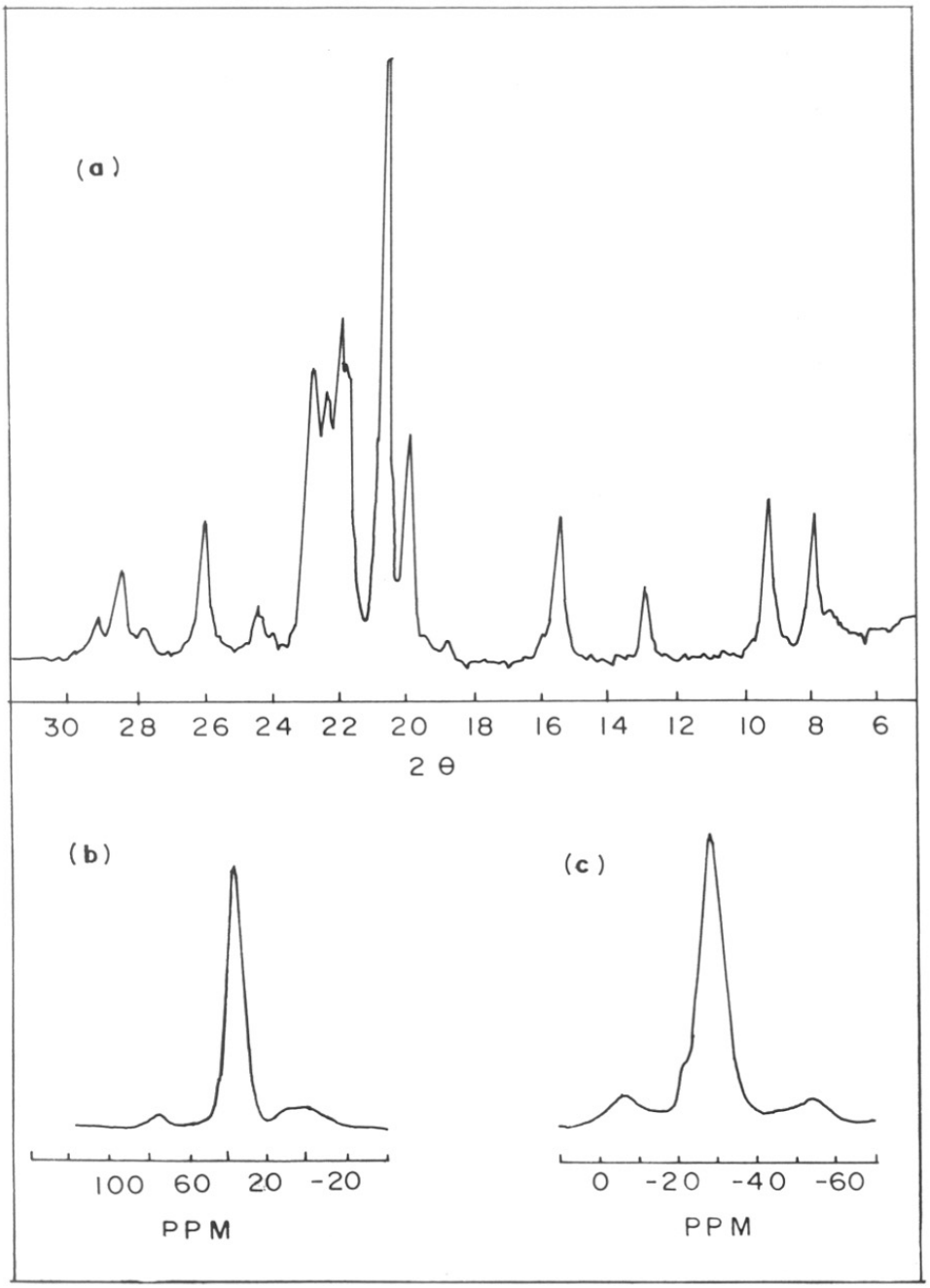

Fig. 2.1 ▷ (a) XRD pattern; (b) ^{27}MASNMR spectrum; (c) ^{31}P MASNMR spectrum for $AlPO_4$–11 synthesized using n–dibutylamine.

Fig. 2.2 ▷ SEM photograph for $AlPO_4$–11 synthesized using n–dibutylamine.

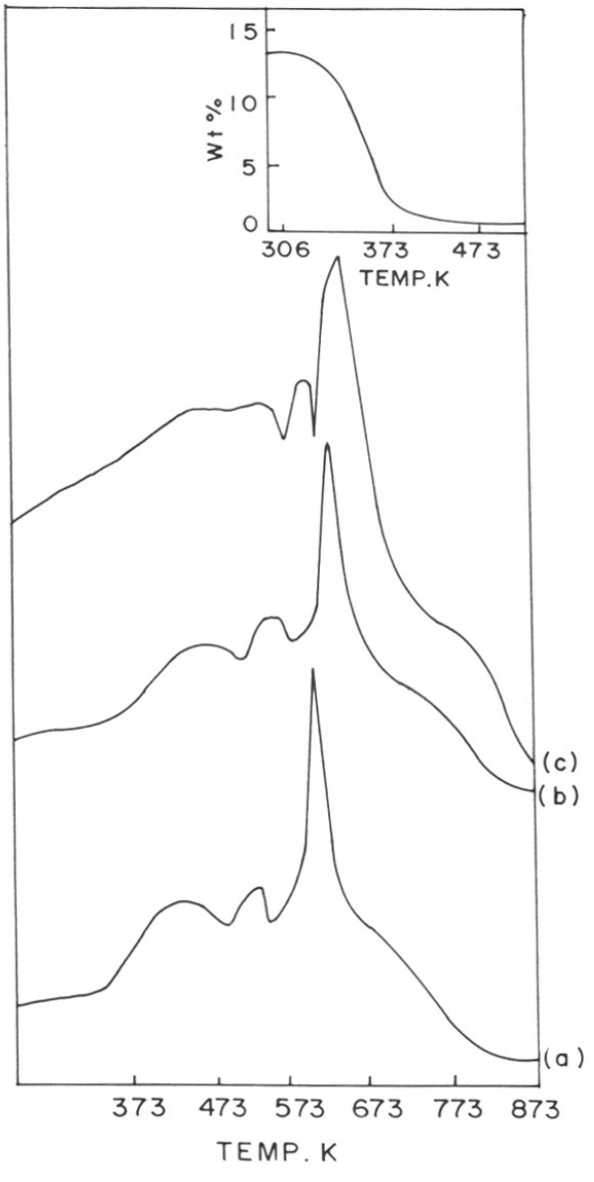

Fig. 2.3 ▷ DTA traces for $AlPO_4$–11 synthesized using (a) n–dipropylamine; (b) n–dibutylamine; (c) n–dipentylamine. Inset shows TG curve for a fully hydrated $AlPO_4$–11.

Calcination–induced structural changes in $AlPO_4$–11 produce changes in XRD pattern and MASNMR spectra. Chapter 3 reports these results.

2.3.2 VPI–5

VPI–5 crystallized from the gel at about 8 hours time and the product is stable in the mother liquor atleast upto 72 hours at the hydrothermal temperature. This is unlike the VPI–5 synthesized using DPA[6,7].

The X–ray pattern of VPI–5 is given in Fig. 2.4a. The pattern matches closely with that reported in the literature[6,7]. There is no impurity phase due to $AlPO_4$–H3 or $AlPO_4$–11 usually co-crystallizing with VPI–5[7].

The ^{27}Al MASNMR spectrum shows the presence of 2 lines (Fig. 2.4b.): One sharp line at 40ppm in the range ascribed to tetrahedrally co-ordinated framework Al and an additional high field signal at −19 ppm in the range of octahedral Al. The ratio of the intensities of the two signals is close to 2:1. The Al(Vl) line at −19 ppm representing one third of the total Al is due to distorted framework Al linked to four lattice oxygen atoms and to two water molecules. Thus, the as–synthesized VPI–5 is an aluminophosphate hydrate[8].

VPI–5 displays three distinct resonances at −23.7, −27.5 and −33.2 ppm in an approximate ratio of 1:1:1 in the ^{31}P spectrum (Fig. 2.4c). The peak intensity and and chemical shifts match closely with that reported by Grobet et al.[8] and Davis et al.[12]. The former ascribe these peaks to 3 different coordinated P with Al(IV) and /or Al (VI). On the other hand, the latter attributes the peaks at −27.2 and −33.2 ppm to P located in Site S1 (6–MR) and S2 (4–MR). The peak at −23.3 ppm was postulated to arise from the influence of relatively immobile occluded water molecules in the 6–MR on the P environment in Site S1. A more recent work[13] assigns the peaks at −23 and −27 ppm to P–atoms in 6–MR and the one at −33 ppm to the P–atom in between the fused 4–MR. This assignment is based on the lowered symmetry of $P6_3$ space group suggested by McCusker et al.[14].

Thermoanalytical curves of VPI–5 are shown in Fig. 2.5. TG curve shows loss of weight upto 393 K corresponding to desorbed water of 22%. Weight loss beyond 398 K is

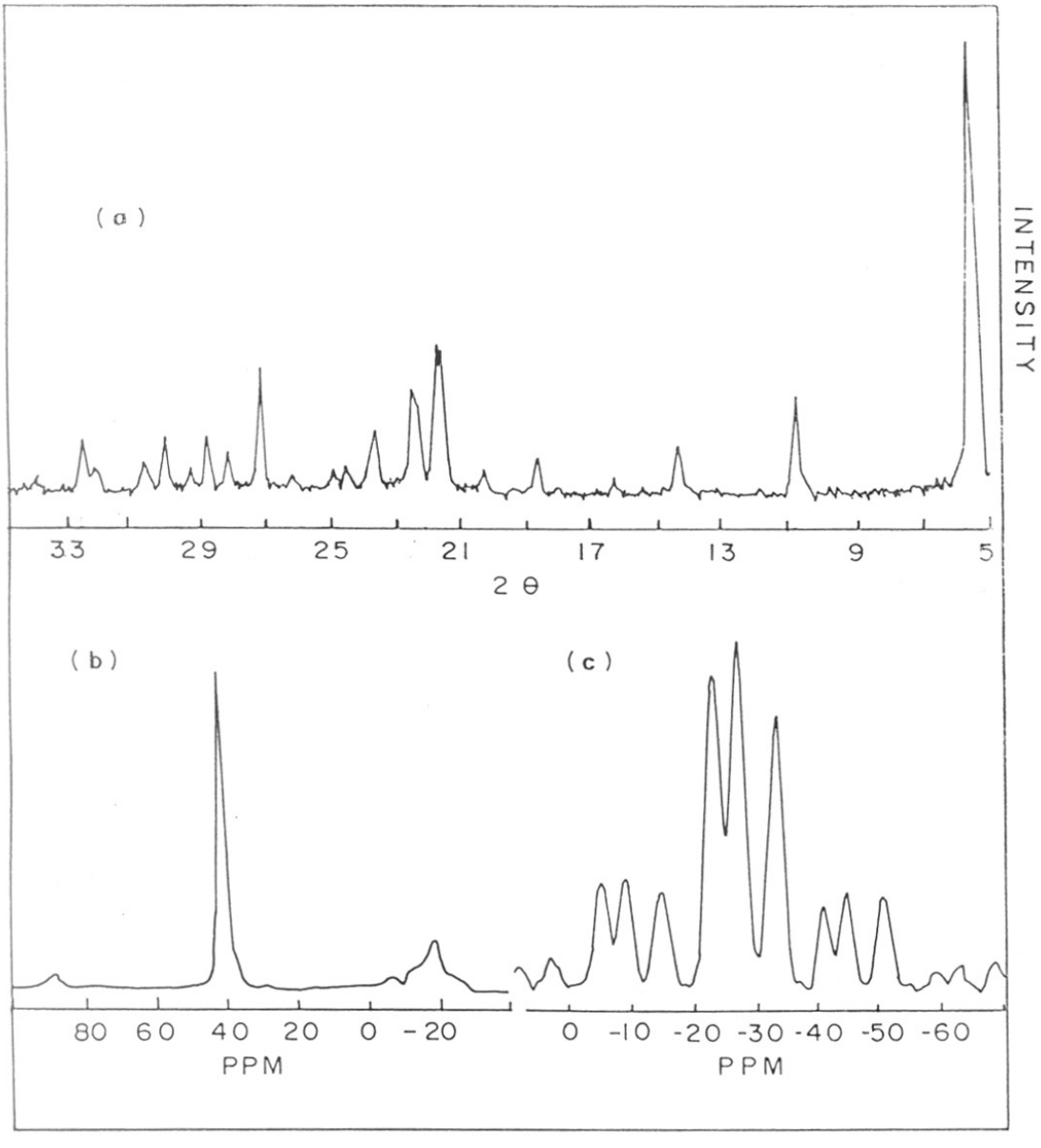

Fig. 2.4 ▷ (a) XRD pattern; (b) ^{27}Al MASNMR spectrum; (c) ^{31}P MASNMR spectrum for VPI–5.

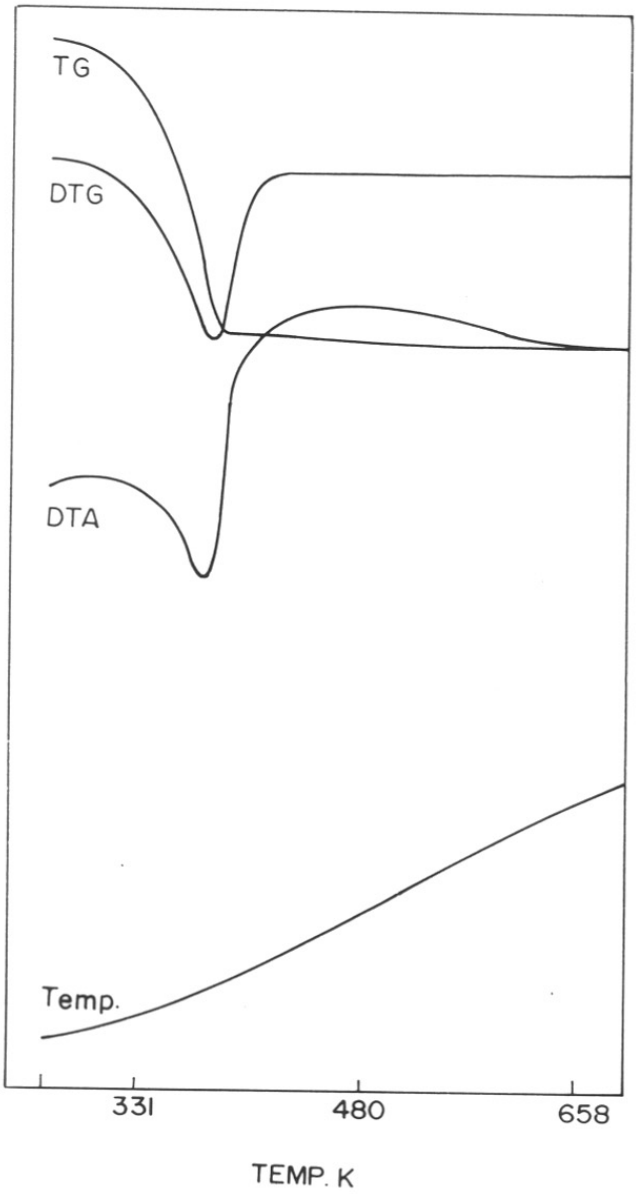

Fig. 2.5 ▷ Themoanalytical traces for VPI–5.

negligible. This and the absence of strong exothermic peak at high temperature in DTA curve characteristic of removal of occluded organic additive are in agreement with the reported role of the organic agents in the synthesis of VPI–5[6,7].

On thermal treatment VPI–5 transformed itself to another aluminophosphate, $AlPO_4$–8. This transformation which led to the identification of VPI–5 as a precursor to $AlPO_4$–8 is discussed in Chapter 3.

2.3.3 H1 (GTRI)

X–ray diffraction pattern of H1(GTRI) is shown in Fig. 2.6a. Comparison of the pattern and relative intensity values with VPI–5(Fig. 2.4a) indicates identical crystalline phases in the two samples in accordance with earlier findings[3]. It also demonstrates the suitability of aluminium isopropoxide for syntheses of both.

Fig. 2.6b shows the ^{27}Al spectrum of H1(GTRI). The sharp peak at 40 ppm and a high field signal at -19 ppm are due to 4– coordinated and 6–coordinated Al. Further, the ratio of the two peaks at 40 ppm and -19 ppm are in the ratio of 2:1 in both H1(GTRI) and VPI–5(Fig. 2.4b). In ^{31}P spectrum, H1 (GTRI) displays 3 distinct resonances at -23.1, -27.0 and -33.0 ppm in the approximate intensity ratio of 1:1:1 (Fig. 2.6c) similar to that observed in VPI–5(Fig. 2.4c). These peaks are, therefore, assigned to the same species as for VPI–5. H1(GTRI) also transforms to $AlPO_4$–8 on thermal treatment above 373 K[3,15]. The finding of Duncan et al.[3] that VPI–5 does not represent a distinct phase is corroborated from the above NMR results.

2.3.4 Effect of the Source of Aluminium

The nature of the Al source (polymeric pseudoboehmite or monomeric aluminium isopropoxide) and the use of agitation/ non agitation during hydrothermal treatment play a crucial role in the synthesis of the final product. Lok et al.[16] and Mertens et al.[17] have obtained amorphous, dense phase and microporous materials by proper choice of these.

Pure VPI–5 crystallized with pseudoboehmite (B) as the source of Al under static hydrothermal treatment conditions. The isopropoxide (I) required agitation for better pu-

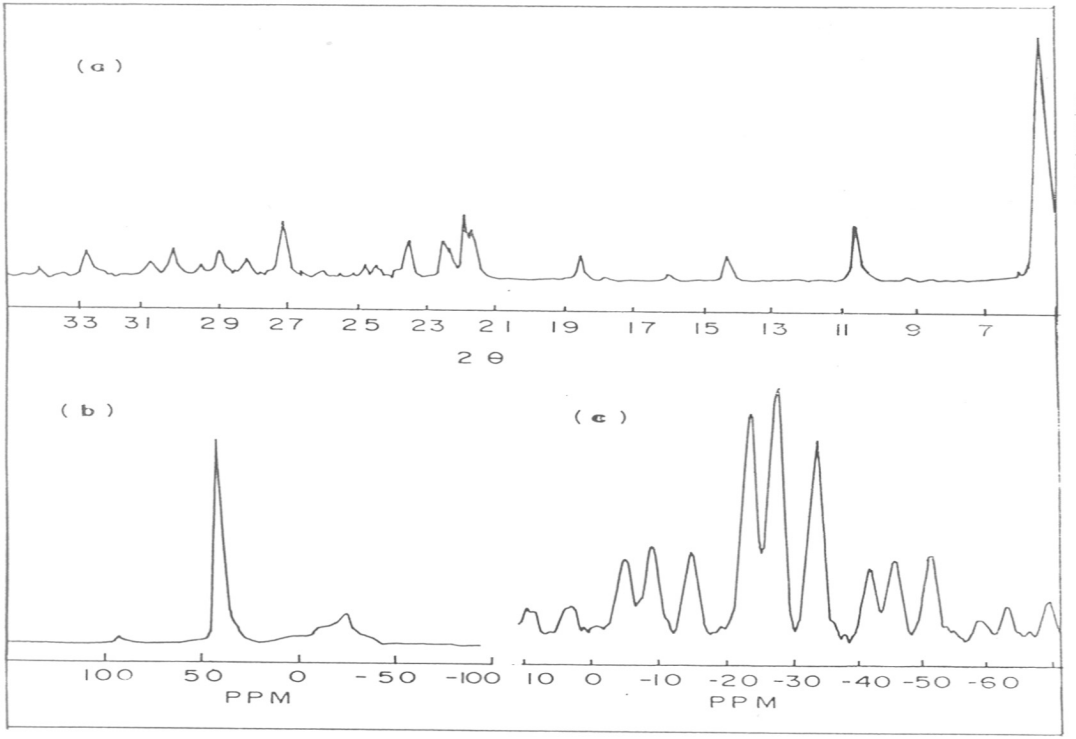

Fig. 2.6 ▷ **(a) XRD pattern; (b) ^{27}Al MASNMR spectrum; (c) ^{31}P MASNMR spectrum for H1(GTRI).**

rity. At higher temperature of 428 K with static conditions, isopropoxide yielded $AlPO_4$–11 while pseudoboehmite at a higher temperature gave $AlPO_4$–11. Table 2.1 shows the influence of the synthetic parameters on the end product.

2.3.5 Effect of Crystallization Time and Temperature

At 423 and 428 K, with pseudoboehmite and aluminium isopropoxide as aluminium source, VPI–5 and $AlPO_4$–11 crystallized, respectively. At 473 K, the same gel system gives $AlPO_4$–11 and condensed phase, respectively (Table 2.1). Formation of a condensed phase has been reported on increasing temperature in the case of $AlPO_4$–5 synthesis. This observation has been attributed to the presence of a low concentration of amine in the pores at high temperature[18].

The $AlPO_4$–11 crystals obtained in the present work seems to be stable upto 72 hours unlike $AlPO_4$–5[19].

2.3.6 Effect of Concentration of the Amine

By varying the concentration of the amine in the synthesis system, different crystalline phases result. $AlPO_4$–11, MCM–9 and VPI–5 have been synthesized from the same gel system following this procedure[20].

Davis et al.[6] have indicated an intermediate formation of a layered phase aluminophosphate in the solid phase re–ordering mechanism proposed for the formation of VPI–5. The solid isolated after 45 minutes during the synthesis showed one sharp line at $d \approx 16$. At this stage of crystallization, the sample showed VPI–5 morphology but had no argon adsorption capacity. On heating in vacuum the sharp line in the XRD pattern vanished.

The present work shows that increasing the concentration of amine in the system for VPI–5 does not have any effect if the crystallization temperature is higher (473 K) ; the end product is always $AlPO_4$–11. If, however, the crystallization temperature is lower (423), increasing the amine concentration 1.5–2.0 times results in synthesis of what appears to be a layered phosphate (LP). The conclusion was arrived at on the basis of the following considerations.

X–ray powder diffraction pattern of LP is shown in Fig. 2.7. By comparison with patterns of aluminophosphates known so far, it was found that LP may have a unique structure. The 2θ values, especially the major peak ($2\theta = 5.6$) falls slightly outside the limit of VPI–5 ($2\theta = 5.38$).

The SEM photograph (Fig. 2.8.) shows that the product crystallizes in flakes with no amorphous impurity (VPI–5 crystallizes in needle form). The morphology indicates a layered structure for the aluminophosphate. The ^{27}Al MASNMR spectrum showed a single peak at 37 ppm attributable to 4–coordinated Al, characteristic of all $AlPO_4$ materials. VPI–5, in contrast, has 4–coordinated and 6–coordinated Al. So, the product is different from VPI–5 with respect to aluminium environment.

TG measurements showed that a carefully air dried sample displays a weight loss in two stages to an extent of 42% (Fig. 2.9). The weight loss in the first stage (upto 393 K) is due to water which amounts to 10% of the total loss. During the second stage, 32% weight loss is observed which may be attributed to the loss of the amine. Based on the weight loss at different stages, the calculated formula for LP corresponds to DBA. $AlPO_4$. 20 H_2O, a ratio similar to the gel composition. The synthesis of LP required the presence of a secondary amine, DBA. DTA trace shows an endothermic peak with a minimum at 517 K.

The sample was dried at 393 K (sample 1) and 520 K (sample 2) and the evolved gases analyzed by gas chromatography. The sample 2 gave a peak due to DBA whereas sample 1 gave only trace quantity of DBA. This provides evidence for the hypothesis that DBA is only desorbed at high temperature. Thus, the endotherm at 517 K in the DTA curve corresponds to the slow desorption of the organic from between the layers of the aluminophosphate.

LP did not transform to VPI–5 in aqueous medium or in presence of organic additive. This treatment did not affect the stability of the phase.

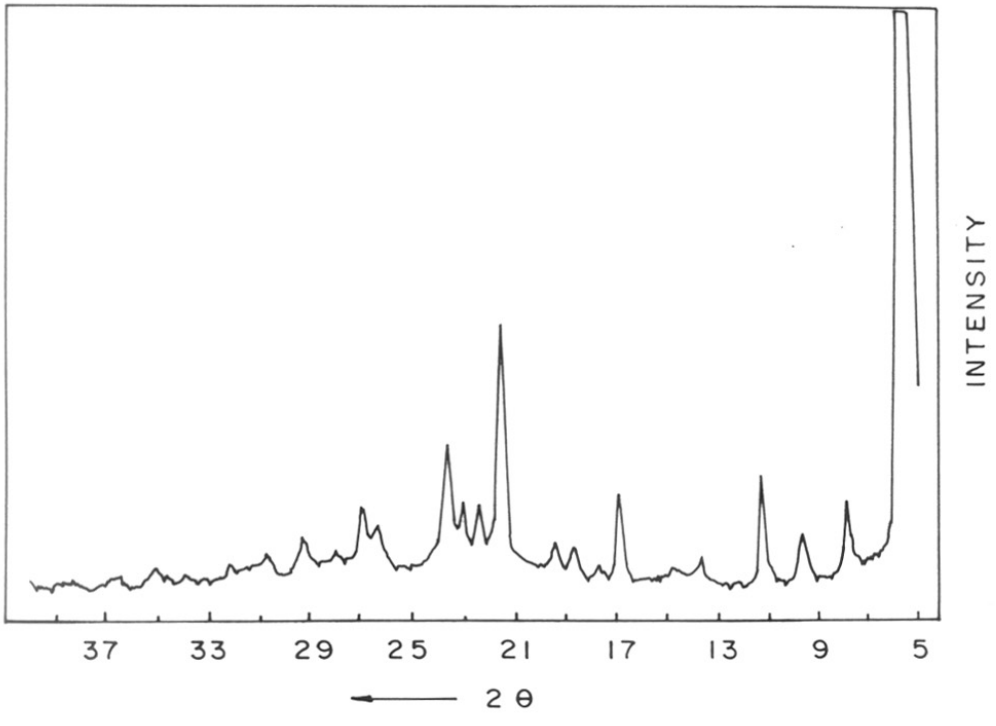

Fig. 2.7 ▷ XRD pattern for layered $AlPO_4$.

Fig. 2.8 ▷ SEM photograph for layered $AlPO_4$.

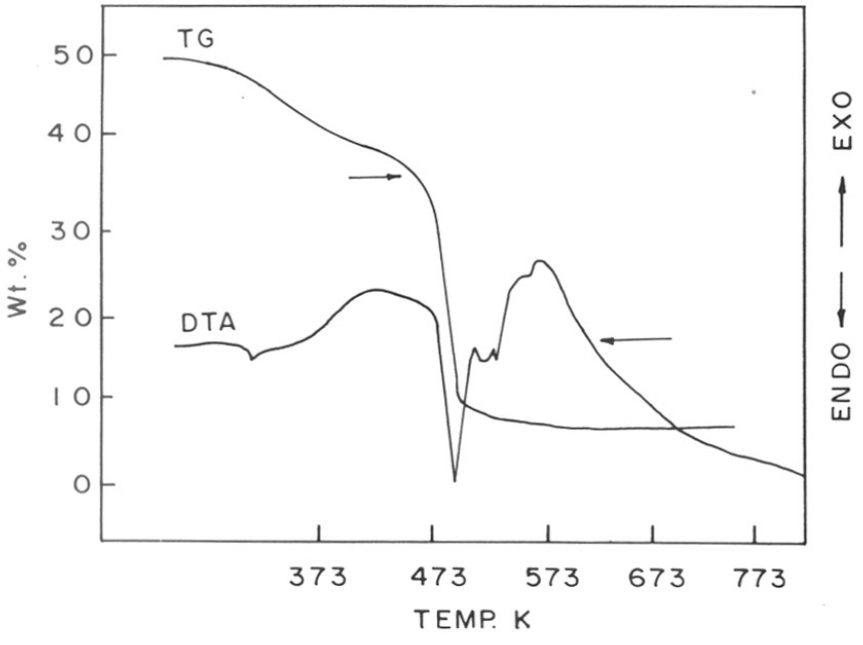

Fig. 2.9 ▷ Thermoanalytical curves for layered $AlPO_4$.

2.4 CONCLUSIONS

1. Successful synthesis of $AlPO_4$–11 is possible with n–dibutylamine and n–dipentylamine as organic additives.
2. The largest pore molecular sieve VPI–5 can be synthesized using DBA as organic additive and, polymeric pseudoboehmite as well as monomeric aluminium isopropoxide as Al source.
3. The organic free $AlPO_4$, H1(GTRI) has been synthesized by using aluminium isopropoxide in acid medium. The XRD and MASNMR results for this and VPI–5 indicate that the two materials represent the same crystalline phase.
4. In the course of a study of the influence of the Al source, crystallization temperature and period, and the concentration of amine, a new phase, probably a layered $AlPO_4$, has been synthesized.

2.5 REFERENCES

1. F. D'Yvoire, *Bull. Soc. Chim. Fr.*, 1961, **p. 1762.**
2. J.A. Martens, B. Verlinden, M. Mertens, P.J. Grobet and P.A. Jacobs, *ACS. Symp. Ser.*, **398**, 305, 1989.
3. B. Duncan, R. Szostak, K. Sorby and J.G. Ulan, *Catal. Lett.*, **7**, 367, 1990.
4. N. Tapp, N.B. Milestone and D.M. Bibby, *Zeolites*, **8**, 183, 1988.
5. S.T. Wilson, B.M. Lok and E.M. Flanigen, U.S. Pat. 4310440, 1982.
6. M.E. Davis, C. Montes, P.E. Hathaway and J.M. Garces, *Stud. Surf. Sci. Catal.*, **49A**, 199, 1989.
7. M.E. Davis, C. Montes, J.M. Garces and C. Crowder, *ACS. Symp. Ser.*, **398**, 291, 1989.
8. P.J. Grobet, J.A. Martens, I. Balakrishnan, M. Mertens, P.J. Grobet and P.A. Jacobs, *Appl. Catal.*, **56**, L21, 1989.
9. D. Muller, E. Jahn, B. Fahlke, G. Ladwig and U. Hanbenreisser, *Zeolites*, **5**, 53, 1985.
10. W. Lowenstein, *Am. Mineral.*, **39**, 92, 1954.
11. I.P. Appleyard, R.K. Harris and F.R. Fitch, *Chem. Lett.*, 1985, **p. 1747.**
12. M.E. Davis, C. Montes, P.E. Hathaway, J.P. Arhancet, D.L. Hasha and J.M. Garces, *J. Am. Chem. Soc.*, **111**, 3919, 1989.
13. J.P.V.B. Hockgeest, B–K. Czarnetski, R.J. Dogterom and A. de Groot, *J. Chem. Soc. Chem. Comm.*, 1991, **p. 666.**
14. L.B. McCusker, Ch Baerlocher, E. Jahn and M. Bülow, *Zeolites*, **11**, 308, 1991.
15. S. Prasad, Ph.D thesis, Part 2, Chapter 3.
16. B.M. Lok, T.R. Cannan and C.A. Messina, *Zeolites*, **3**, 283, 1983.
17. M. Mertens, J.A. Martens, P.J. Grobet and P.A. Jacobs, *Guidelines for mastering the properties of molecular sieves* (Eds: Barthmauef et al.), Plenum Press, 1990, **p. 1.**
18. S.T. Wilson, B.M. Lok, C.A. Messina and E.M. Flanigen, *Proc. 6th Int. Zeo. Conf.*, Reno, USA (Eds: D. Olson and A. Bisio), Butterworths, 1983, **p. 97.**
19. D.B. Akolekar, Ph.D thesis, University of Poona, 1987.
20. K. Sorby, R. Szostak, J.G. Ulan and R. Gronsky, *Catal. Lett.*, **6**, 209, 1990.

CHAPTER 3

THERMAL BEHAVIOUR OF VPI-5 H1(GTRI) AND $AlPO_4$-11

3 THERMAL BEHAVIOUR OF VPI–5, H1(GTRI) AND $AlPO_4$–11

3.1 INTRODUCTION

$AlPO_4$ molecular sieves are hydrophillic materials having high water sorption capacity. The dehydration–hydration behaviour studies of these molecular sieves are of interest. They give information on the nature of structural transformations following calcination. Most of the $AlPO_4$ materials have occluded templating agents in their as-synthesized form reflecting participation of these during the synthesis. In the case of others, the added organic additives serve as pH modifying agents, for e.g. VPI–5, facilitating synthesis. A characteristic common to this class of $AlPO_4$'s is that they contain coordinated water molecules whose removal by thermal treatment brings about irreversible structural transformation and in some cases structural collapse. Table 3.1 gives a summary of the thermal treatment conditions and observations in respect of $AlPO_4$'s which contain structural water in the as–synthesized form. Table 3.2 presents similar data for $AlPO_4$ molecular sieves which contain occluded templating agents in the as–synthesized form. Removal of templating agents takes place in the temperature range indicated and subsequent exposure to water results in chemisorption and generation of coordinated water molecules in the structure. Here, dehydration–rehydration brings about only reversible changes.

X–ray diffraction[5,6,13,14], MASNMR[6,8,9,11,13–15], IR[13] and thermal analysis[16] have been used to study the dehydration–rehydration behaviour. In this chapter, results on dehydration–rehydration behaviour of VPI–5 and H1(GTRI) which belong to the first group and $AlPO_4$–11 that belong to the second group are discussed. They indicate that VPI–5 and H1(GTRI) represent the same structure type and both act as precursors to $AlPO_4$–8. MASNMR spectral data on $AlPO_4$–11 show that part of the water sorbed is present as chemisorbed water in $AlPO_4$–11. These spectral studies along with the molecular modelling and quantum chemical calculations have been used to predict the nature

$AlPO_4$	Thermal treatment (K)	Product of transformation	Reference
$AlPO_4$–H1	>383	Tridymite	1
$AlPO_4$–H3	673	Tridymite	1
Varisite, Metavariste	673	Tridymite	1
$AlPO_4$–21	523	$AlPO_4$–25	2
$AlPO_4$–23	523	$AlPO_4$–25	3
$AlPO_4$–15	673	Breakdown, Tridymite	4
VPI–5	>373	$AlPO_4$–8	5,6
H1(GTRI)	>373	$AlPO_4$–8	7,†

† Present work

TABLE 3.1. **$AlPO_4$'s Having 6–coordinated Al in the as–synthesised Form.**

$AlPO_4$ precursor†	Thermal treatment (K)	Product type‡	Reference
R–$AlPO_4$–5	>673	AFI, $AlPO_4$–5	8,9
R–SAPO–34	"	CHA, SAPO–34	9
R–$AlPO_4$–17	"	Erio, $AlPO_4$–17	10
R–SAPO–31	"	SAPO–31	11
R–$AlPO_4$–20	"	Sod, $AlPO_4$–20	12
R–$AlPO_4$–11	"	AEL, $AlPO_4$–11	9

† R stands for template molecule

‡ upon hydration, Al(VI) peaks are observed in addition to Al(IV) peaks

TABLE 3.2. **$AlPO_4$ Molecular Sieves Having Occluded Organic Additives in as–synthesised Form.**

of adsorption and identify adsorption sites of water molecules in hydrated $AlPO_4$–11.

3.2 EXPERIMENTAL

Synthesis details reported in a patent[3] for $AlPO_4$–8 (example 28 in the patent) were followed for the synthesis of sample A. N–dibutylamine (DBA) was used as the organic additive. A shorter crystallization period of 72 hours was used instead of 150 hours (cf. Chapter 2, synthesis of VPI–5, for details). Samples of H1(GTRI) and $AlPO_4$–11 whose syntheses details are presented in the previous chapter were also used for the study.

Part of sample A, denoted as A(AS) after air drying was calcined in a flow of dry air or nitrogen in a closed tube in a temperature range of 388–773 K to give A(CD) (calcined dehydrated). Another part of the sample after calcination was stored over saturated ammonium nitrate solution in a desiccator for 72 hours to get A(FH) fully hydrated. The samples were studied by XRD, MASNMR and thermal analysis.

A sample of H1(GTRI) was also subjected to thermal treatment in a similar manner as above.

As–synthesized $AlPO_4$–11, was calcined in air at 723 K to remove occluded organic amine. The calcined sample was divided into two portions; One part was dehydrated at 473 K and cooled in a desiccator containing P_2O_5 and packed under nitrogen atmosphere, sample CD. Another part was stored over saturated ammonium nitrate in a desiccator for 72 hours, sample FH. These samples were studied by XRD and MASNMR measurements.

Details of the instrumental set up and measurements carried out have been described in Chapter 2.

Molecular orbital calculations using MNDO (modified neglect of differential overlap) technique[17] was used to study the electronic structure of tetrahedral cluster models of $AlPO_4$–11 and their water adsorption complexes. The geometry and structure of each tetrahedral unit (either AlO_4 or PO_4) is obtained from the crystal structure reported[18]. The unsaturated valency of the oxygen atoms in the tetrahedra is balanced by bonding a hydrogen atom to them and the position of these hydrogen atoms are the adjacent

T–atoms in the $AlPO_4$–11 structure. The values of net charge density on various atoms of the clusters are calculated using the Mulliken population analysis method[19]. The value of total energy are used to decide the favourable adsorption site. The partial charges calculated on the framework oxygen atoms are used to elucidate the nature of interaction between the water molecule and the $AlPO_4$–11 framework.

3.3 RESULTS AND DISCUSSION

3.3.1 Identification of Sample A(AS) as VPI–5 and its Transformation to $AlPO_4$–8

Following the synthesis of $AlPO_4$–8, the sample obtained A(AS) was characterized by XRD, MASNMR and thermal analysis. The data obtained from these analysis were identical with those obtained for VPI–5. This led to the identification of sample A(AS) as VPI–5 (cf. Chapter 2 for characterization of VPI–5). A re–examination of the patent[3] indicated $AlPO_4$–8 being described as 'the major phase' obtained by drying the as–synthesized sample at 388 K and hence the possibility that $AlPO_4$–8 is a thermal product of VPI–5 came to be considered. The following considerations contributed to the identification of VPI–5 as a precursor to $AlPO_4$–8.

Both VPI–5 and $AlPO_4$–8 are synthesized from identical gel compositions by using tetrabutylammonium hydroxide, DBA as organic additives at 423 K. In addition, VPI–5 can be synthesized by using n–dipropylamine also.

The reported difference between the synthesis of VPI–5 and $AlPO_4$–8 are only with respect to aging and longer crystallization period required, respectively, in the two cases. However, the procedure adopted by Grobet et al.[20] eliminates the steps involving aging and yields VPI–5 in shorter crystallization period. Also, the only role of organic additives appears to be to provide the optimum pH conditions[3,21]. Thus, all synthesis factors are common for both synthesis.

A(AS) identified as VPI–5 was calcined in the temperature range 388–773 K to get A(CD). The XRD of A(CD) match with that reported for $AlPO_4$–8[3] (Fig. 3.1a). On hydration, A(FH), the XRD peaks showed shift in d values and reduction in peak intensities (Fig. 3.1b). The effect on calcination and hydration can be schematically represented as:

$$\underset{(A\,(AS))}{VPI-5} \xrightarrow{heat} \underset{(A(CD))}{AlPO_4-8} \overset{H_2O}{\rightleftharpoons} \underset{(A(FH))}{AlPO_4-8\ (hydrated)}$$

The transformation has been studied by ^{27}Al MASNMR also[6].

Thermoanalytical curves of VPI–5 (A(AS)) and $AlPO_4$–8 (A(FH)) are shown in Fig. 3.2 and data presented in Table 3.3. Comparison of the curves brings out the following features:

Both samples show weight loss upto 393 K corresponding to desorbed water. These are respectively 22% and 16%. In VPI–5 most of the desorbed water is known to be structural water. This is reflected in DTA endothermic peak maximum of VPI–5 being at a temperature (393–398 K) higher than $AlPO_4$–8 (363–368 K) obtained by calcination and rehydration. Lower percent of desorbed water in $AlPO_4$–8 is probably consistent with its structure which contains reduced void space[22].

Weight loss beyond 398 K is negligible for both the samples. This and the absence of exothermic peak in A(AS) at higher temperature characteristic of occluded organic additive are in agreement with reported role of the additive in the synthesis of VPI–5[21].

Identical DTA curves for both samples beyond 398 K suggests that the transformation VPI–5 to $AlPO_4$–8 takes place below this temperature, possibly at the drying temperature used by Wilson et al.[3] in the synthesis of $AlPO_4$–8 ie. at 388 K.

3.3.2 Transformation of H1(GTRI)

It was indicated in the previous chapter that H1(GTRI) and VPI–5 represent the same crystalline phase.

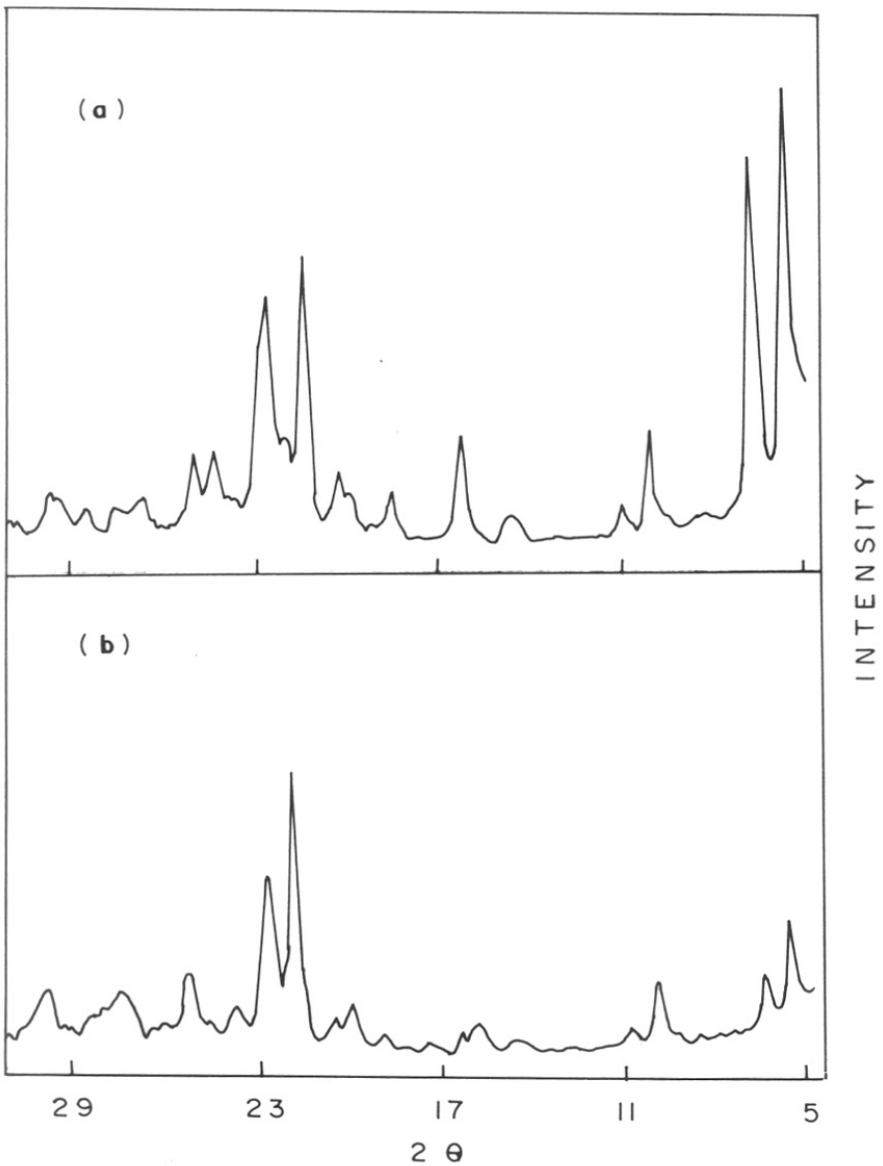

Fig. 3.1 ▷ (a) XRD pattern for A(CD), $AlPO_4$–8; (b) XRD pattern for A(FH), hydrated $AlPO_4$–8.

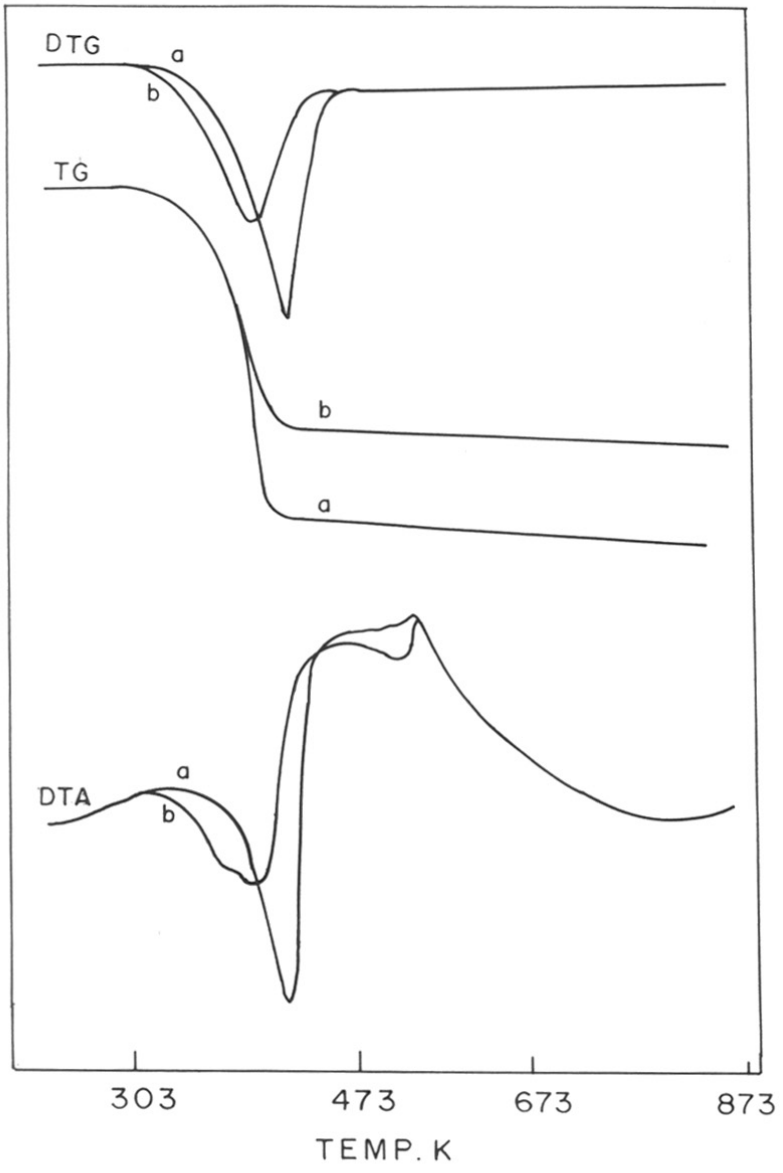

Fig. 3.2 ▷ Thermoanalytical curves for (a) VPI–5; (b) $AlPO_4$–8.

Sample No	Temp (K) of DTG peak	Thermal nature of transformation	Temp range (K) DTA peak	Temp (K) of DTA peak	Wt. loss (%)
1	398	Endo	303–458	393	22
		Exo	413–553	541	–
2	371	Endo	576–651	363	16
		Exo	523–573	276	–

TABLE 3.3. **Thermal Analysis Data for Samples A(CD) and A(FH).**

Further evidence for the identity of these phases phases comes from the thermal studies. H1(GTRI) too transforms to $AlPO_4$–8 upon thermal treatment as reported earlier[7]. This transformation could also be confirmed by MASNMR spectral studies.

The ^{27}Al MASNMR spectrum of $AlPO_4$–8 is devoid of the signal attributed to Al(VI) and shows only Al(IV) signal at ≈40 ppm characteristic of all $AlPO_4$ materials[23] (Fig. 3.3a). The ^{31}P MASNMR spectrum (Fig. 3.3b) shows peaks at −30 and −26.7 ppm and a shoulder at −23.3 ppm. The available data on ^{31}P spectra of VPI–5 treated by different methods is given in Table 3.4. The peak at −23.3 ppm reported by Grobet et al.[20] comes as a shoulder in the present study. From the near complete identity between the spectra in the present work and those given in the table, it is suggested that the changes observed by Grobet et al.[20] and Davis et al.[24] may be associated with the transformation of VPI–5 to $AlPO_4$–8. Transformation of both H1(GTRI) and VPI–5 to $AlPO_4$–8 provides evidence to show that the former two represent same crystalline phase. $AlPO_4$–H1 and $AlPO_4$–8 besides $AlPO_4$–H3[25], are examples of synthesis of microporous $AlPO_4$'s without the use of organic additives.

In a recent work, Perez et al.[26] have reported that VPI–5 has a phase distinct from H1 based on the following considerations:

1. High resolution X–ray measurements show that doublets at $d = 4.10$ and 3.97 which are absent in VPI–5.
2. H1 exhibits 6–coordinated Al atom in the 4–rings and contain excess Al over P where as VPI–5 has a Al:P ratio of one and prefers a 6–coordinated Al in alternate 6–rings.

However, in a more recent work, McCusker et al.[27] have shown that VPI–5 too has Al in 4–rings. Evidence presented by Perez et al.[26] is therefore not conclusive enough to show a distinct phase for VPI–5.

3.3.3 Calcination Studies on $AlPO_4$–11

Precursor $AlPO_4$–11, DBA–$AlPO_4$–11 and DPENTA–$AlPO_4$–11 were used to study the effect of calcination and rehydration behaviour. Data presented are for DBA–$AlPO_4$–11. Similar results were obtained for DPENTA–$AlPO_4$–11.

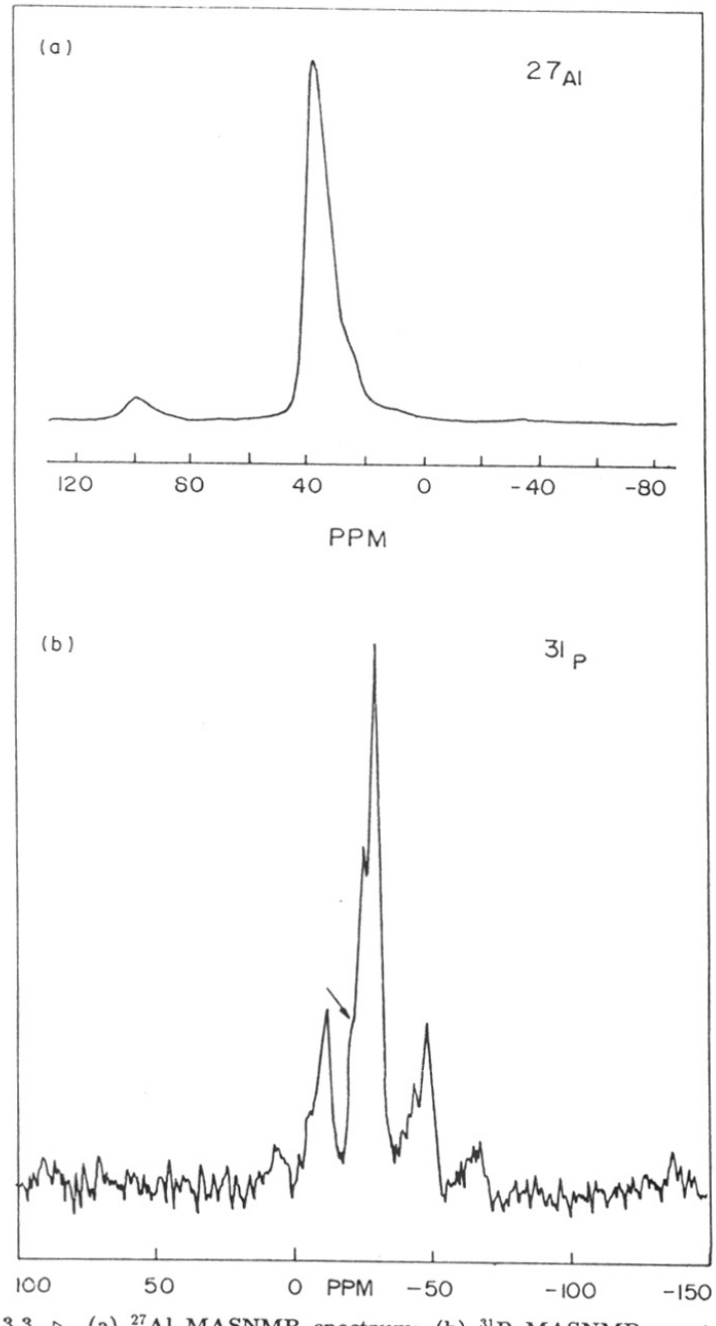

Fig. 3.3. ▷ (a) ^{27}Al MASNMR spectrum; (b) ^{31}P MASNMR spectrum for $AlPO_4$–8.

$AlPO_4$–8 Present work	VPI–5† Evac. room temp./ Calcination 823 K	VPI–5‡ Evac.293 /723 K
−22.4(Sh.)	–	−23.0(0.5)
−26.7(1)	−27.0(1)	−26.0(1)
−31.0(2)	−32.0(2)	−30.0(2)

† From a description of ^{31}P spectrum in ref. 24

‡ Approximate values derivable from Fig. 2., ref. 20.

TABLE 3.4. **^{31}P Chemical Shifts (in ppm) for $AlPO_4$–8, and VPI–5 Treated by Different Methods. Intensity Ratios are Given in Brackets.**

3.3.3.a. X–ray Diffraction

X–ray diffraction profiles recorded for $AlPO_4$–11 under different conditions—as–synthesized (AS), calcined and dehydrated (CD), and fully hydrated (FH) are shown in Fig. 3.4. The XRD profiles for AS and CD samples correspond to orthorhombic Icm2 space group as reported earlier[3,28]. However, the XRD pattern of FH sample showed a different profile. The peaks at $2\theta = 9.5, 13.0$ and 15.75 were shifted to $9.80, 12.75$ and 16.10, respectively. There were additional peaks at $2\theta = 13.65, 14.6$ and 17.5, and the peaks in the range of $2\theta = 20$ to 30 show splittings. Similar results have been reported by Tapp et al.[13] for $AlPO_4$–11 and Khouzami et al.[14] for SAPO–11 The changes in the XRD pattern are attributed to a change in the crystal structure with lower symmetry, namely $Pna2_1$ space group. The reduction in the intensity of the peaks at $2\theta = 8 - 10$ may be an indication of the interaction of water molecules with the framework T–sites. A similar reduction in peak heights in XRD pattern at $2\theta = 8 - 10$ with simultaneous appearance of peaks due to Al(VI) in ^{27}Al MASNMR have been observed in related materials such as SAPO–31[11] and $AlPO_4$–8[6] upon hydration.

The amount of water in FH sample is 13%. This amounts to the presence of approximately 20 water molecules in a unit cell ($Al_{20}P_{20}O_{80}$) of $AlPO_4$–11. Assuming that each T–site is adsorbing two water molecules, ≈25% of the T–sites will be interacting with water molecules. Khouzami et al.[14] have calculated the coordinates of atoms in hydrated SAPO–11. The results show only four water molecules per unit cell of $AlPO_4$–11 . The rest of the water molecules may be mobile in the pores of $AlPO_4$–11 framework. IR studies[13] also have shown the presence of free water molecules. Hence, the XRD studies on their own is not capable of explaining the nature and location of all the adsorbed water.

3.3.3.b. Solid State MASNMR

A single resonance line at 34 ppm was observed in the ^{27}Al MASNMR spectrum of the as–synthesized form (AS) (cf. Chapter 2).

Fig. 3.5a and b are the ^{27}Al spectra for CD and FH sample, respectively. The signal at 34 ppm is present in both. However, the additional signal in sample CD at 32.3 ppm

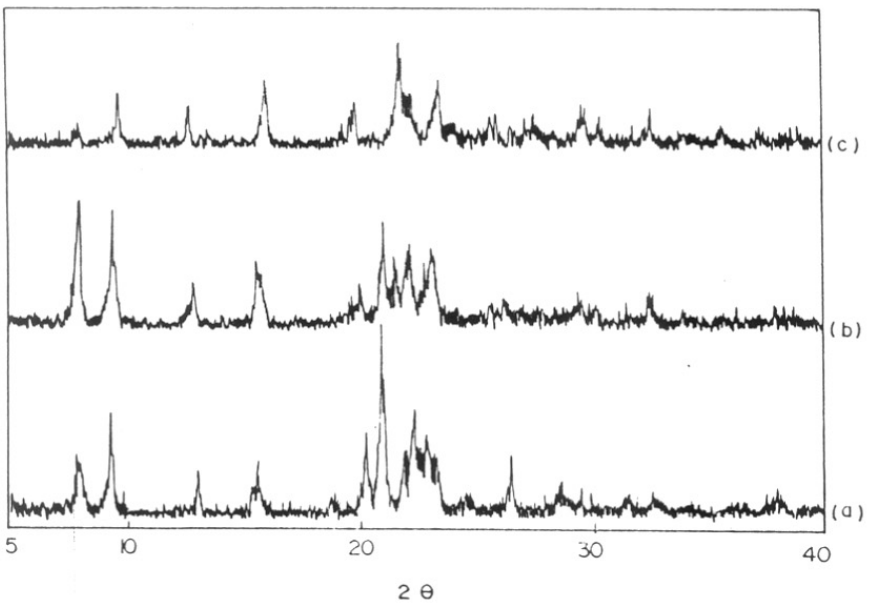

Fig. 3.4 ▷ XRD patterns for (a) as-synthesized; (b) Calcined and dehydrated; (c) Calcined rehydrated $AlPO_4$–11.

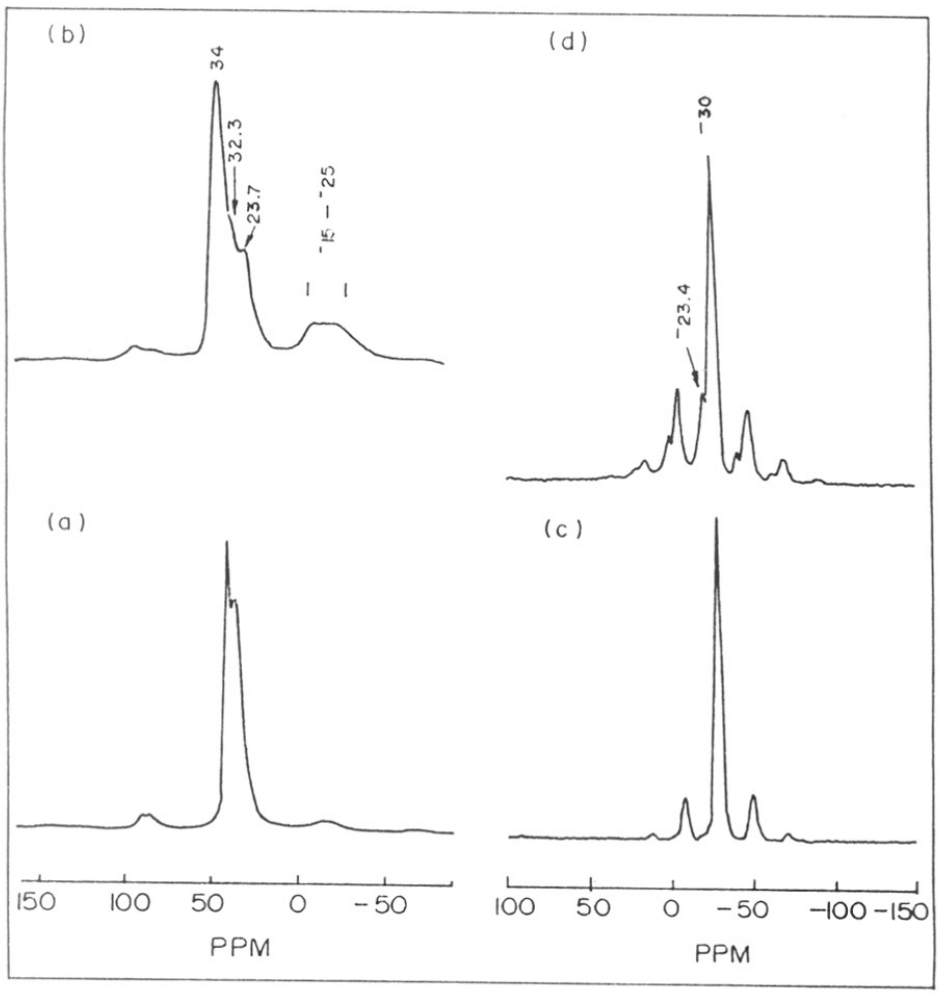

Fig. 3.5 ▷ (a) ^{27}Al MASNMR spectra for calcined and dehydrated; (b) Calcined and rehydrated $AlPO_4$–11. (c) ^{31} PMASNMR spectra for calcined and dehydrated; (d) Calcined and rehydrated $AlPO_4$–11.

appears only as a shoulder in the sample FH which also shows an additional peak at 23.7 ppm. These signals and the additional broadening observed in FH most probably arise on account of the quadrupole interaction with the non–zero electric field gradient (e.f.g.) on the aluminium nuclei with 5/2 spin[29].

In a ^{27}Al MASNMR study of zeolite ZSM–5 and Y, Kentgens et al.[29] have observed that quadrupole broadening is most prominent in the latter case (zeolite Y) which has high Al content. This broadening was found to depend on the nature of the charge–compensating cation, chemical shift distribution and the intensity of magnetic field applied. In the case of $AlPO_4$–11, which has a high Al content but no charge–compensating cation, a similar broadening can be expected. The presence of water molecules leads to increased e.f.g. at the Al nucleus and hence, peak broadening is observed in the FH sample.

In addition to the peaks in the tetrahedral region, a broad peak appeared in the high field in the region of -15 to -25 ppm in the case of FH sample. A peak in this region is characteristic of 6–coordinated Al species in the framework and has been reported in the case of related materials such as $AlPO_4$–11 and SAPO–34[9], $AlPO_4$–17[10], $AlPO_4$–5[8], $AlPO_4$–H3[25], and VPI–5[20]. This broad peak is typical of interaction of water molecules with AlO_4 tetrahedra[28] and is recognized as evidence for the presence of chemisorbed water molecules in hydrated $AlPO_4$'s. The existence of this peak was confirmed by quantitatively analyzing the integrated area of the peak. The integrated area of the peak in the range 6 to -70 ppm is considerably larger than the area of the other spinning side band in the low field region 67 – 112 ppm. The corrected area corresponding to the 6–coordinated Al represents 20% of the total area under the ^{27}Al signal.

In the ^{31}P MASNMR spectra, a single peak at -30 ppm was observed for the AS sample (cf. Chapter 2). This peak was unaffected by calcination and dehydration in sample CD (Fig. 3.5c). In sample FH, an additional peak appeared at -23.4 ppm(Fig. 3.5d). The area corresponding to this additional peak is 20% of the total area. This signal is typical of the framework phosphorus interacting with water molecules in $AlPO_4$ molecular sieves[14,30].

3.3.3.c. Modelling Studies

The structure of calcined $AlPO_4$–11 was refined by Rietveld profile analysis[18] in the range $d = 0.86 - 3.91$ Åin two space groups: Icmm assuming no ordering of tetrahedral Al and P, and Icm2 assuming strict ordering of Al and P on tetrahedral nodes. A view of structure of $AlPO_4$–11 corresponding to Icm2 space group is shown in Fig. 3.6. The structure comprises of six crystallographically distinct tetrahedral sites (3Al and 3P). T1 and T2 (T= tetrahedral Al or P) are located at the junction of 10–, 6– and 4–membered rings while the T3 is located at the junction between 10–, 6– and 6–membered rings.

For each of the tetrahedra, the different possibilities of water approaching the T–site through its oxygen end are considered. A typical cluster model representing the water adsorbed at a TO_4 unit is shown in Fig. 3.7a. The calculations were carried out for the water molecule, bare tetrahedral cluster(Td) and tetrahedral clusters with the H_2O molecule adsorbed(adsorption complex). The adsorption energy of water (ΔH_{ads}) at different sites is calculated as mentioned below:

$$\Delta H_{ads} = T.E_{Complex} - (T.E_{Td} + T.E_{Water})$$

In all the adsorption complexes, the distance between the tetrahedral atom and the oxygen of water molecule (T–atom of H_4TO_4 and oxygen of H_2O) is kept at 1.5 Åuniformly.

The total energy calculated for the six crystallographically distinct T–sites (3Al and 3P) modelled by H_4TO_4 cluster is given in Table 3.5. Calcined and dehydrated $AlPO_4$–11(CD) show a tendency for rapid uptake of water molecules. Since $AlPO_4$–11 framework is a neutral one, there are no compensating cations present to interact with water. Hence, water could be assumed to interact with the framework oxygens through hydrogens and with framework T–sites through oxygen. Four different modes of interaction of a water molecule with TO_4 group is considered as shown in Fig. 3.7 (a to d). The results of the calculations on these model clusters are summarized in Table 3.6.

The interactions between the atoms of water molecule and $AlPO_4$–11 framework are qualitatively estimated from the values of the net charge density on the atoms and bond

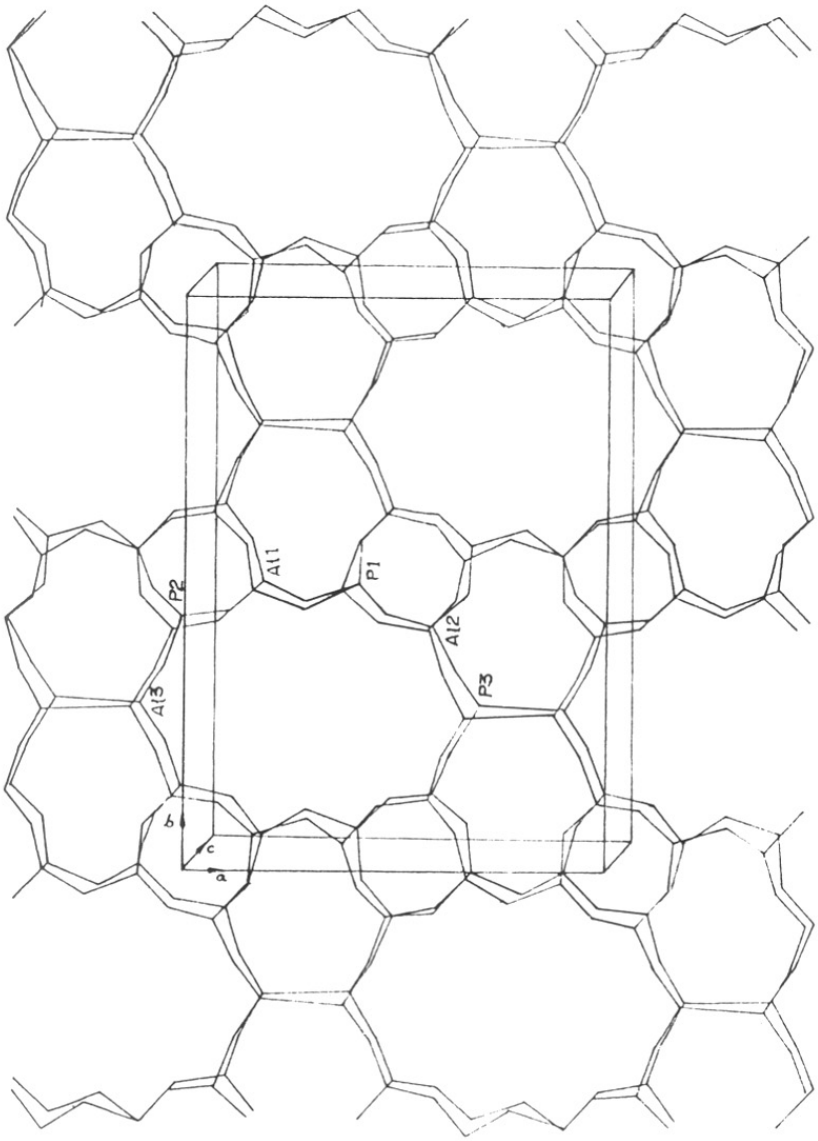

Fig. 3.6 ▷ The framework structure of $AlPO_4$–11. The edges of unit cell are shown and the view is along the c–axis.

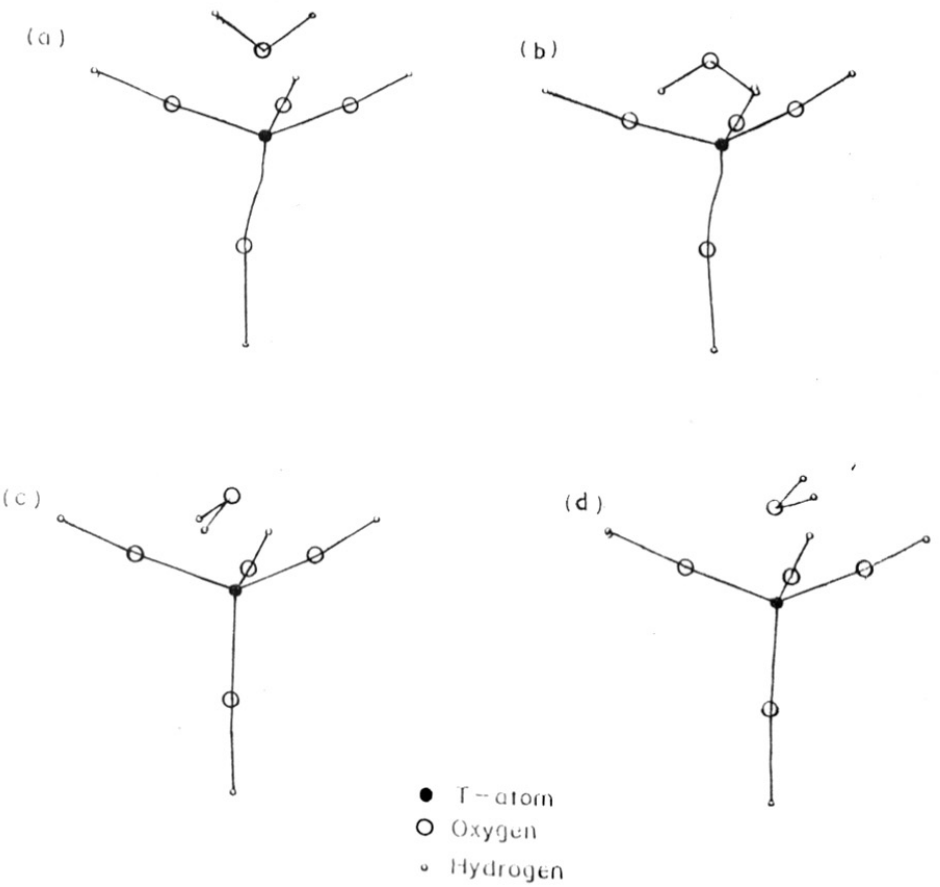

Fig. 3.7 ▷ Typical cluster models showing different modes of adsorption of water over a TO_4 group.

T–site	Oxygen sites	Total energy	Net charge on T–site
Al1	O1, O4, O5′, O6′	−1380.32	0.91
Al2	O2, O5, O6, O7	−1380.73	1.01
Al3	O3, O7′, O7′, O8	−1383.31	0.91
P1	O1, O4, O5, O6	−1476.03	1.47
P2	O2, O5′, O6′, O7′	−1477.97	1.65
P3	O3, O7, O7, O8	−1473.84	1.81

TABLE 3.5. **Electronic Properties of H_4TO_4 (where T = Al or P) Clusters Representing Different Sites in $AlPO_4$–11 Framework.**

Mode of interaction of water	Adsorption energy (eV)	Interaction of hydrogen atoms of water with oxygen of framework	Interaction of oxygen atom of water with T–site of framework
H_2O in the plane of O–T–O with oxygen atom towards T–site (Fig. 3.7a)	+8.80	strong	strong
H_2O in the plane of O–T–O with oxygen atom away from T–site (Fig. 3.7b)	+27.09	strong	weak
H_2O in a plane perpendicular to O–T–O plane with hydrogen atoms towards oxygen of TO_4 group (Fig. 3.7c)	+20.48	strong	medium
H_2O in a plane perpendicular to O–T–O plane with hydrogen atoms away from oxygen of TO_4 group (Fig. 3.7d)	+12.74	weak	medium

TABLE 3.6. **Different Modes of Interaction of Water with the TO_4 Group in $AlPO_4$–11 Framework as Shown in Fig. 3.7 and the Values of Calculated Adsorption Energy for the Al3 Site is Given as a Typical Example.**

orders calculated. It is evident from the data in Table 3.6 that the mode of interaction shown in Fig. 3.7a is the energetically favourable mode. This mode of interaction with all the six TO_4 groups given in Table 3.5 and each individual site have been analyzed in detail.

Hereafter, all the water adsorption complexes will denote only the model shown in Fig. 3.7a. There are six ways the mobile water molecules can approach the T–site. The adsorption energy of water to a particular T–site is assumed to be an average of the six values of adsorption energy calculated for the six ways of adsorption of water around a T–site. For example, the different possibilities wherein the water molecule can lie in the plane of O–T–O for Al3 tetrahedron are illustrated below. Al3 is bonded to four oxygens namely O3, O8 and two O7′. The six possible planes through which oxygen molecule can approach the Al3 site are those planes containing three atoms as shown: O3Al3O8, O3Al3O7′, O7′Al3O8, and O7′Al3O7′(O3Al3O7′and O7′Al3O8 are repeated). The results of the calculation on the above cluster models as well as for the cluster models representing water adsorption around P3 site are given in Table 3.7. The absolute values of calculated adsorption energy reflect the inherent negative charge on AlO_4 and positive charge on PO_4 tetrahedra. In reality when AlO_4 and PO_4 are lying adjacent, the charges will be uniformly distributed over all atoms leading to a comparable adsorption energy. Hence, only a the qualitative trend on the strength of adsorption over Al and P sites could be derived from the results of present calculations (Table 3.7).

The average adsorption energy for adsorption of water molecule over Al3 site is calculated from the values in Table 3.7 as 9.97eV. The magnitudes of adsorption energy are dependent on the distance of water molecule from the T–site and size of the cluster model. A small cluster model is chosen to study the interaction of water molecule with a single T–site and the T– – –$O(H_2O)$ distance is uniformly kept at 1.5 Å for comparative purposes. Thus the complex having the smallest positive value of ΔH_{ads} will be the energetically favourable mode of adsorption. The magnitude of adsorption energy given here are for qualitative ordering of adsorption sites only. The values of adsorption energies are

Three atoms of the plane in which the water molecule is present	Adsorption energy of water (ev)	Net charges on		
		oxygens of the framework	T–site	oxygen of H_2O
O3–Al3–O7′(×2)	10.12	−0.72− 0.65	+1.11	−0.07
O3–Al3–O8	8.80	−0.74− 0.72	+1.14	−0.07
O7′–Al3–O7′	10.16	−0.65− 0.63	+1.11	−0.04
O7′–Al3–O8 (×2)	10.31	−0.66− 0.67	+1.14	−0.03
O3–P3–O7 (×2)	−17.46	−0.84− 0.33	+1.62	−0.06
O3–P3–O8	−17.78	−0.87− 0.46	+1.74	−0.02
O7–P3–O7	−13.66	−0.63− 0.84	+1.88	−0.16
O7–P3–O8 (×2)	−12.33	−0.80− 0.91	+1.94	−0.18

TABLE 3.7. **Electronic Properties of Water Adsorbed Over T3 (where T = Al or P) site. T3− − −O of H_2O is 1.5 Å.**

found to depend on the polarization of the O–Al–O bonds. When the net negative charge on the framework oxygen atoms and the net positive charge on the aluminium atom are maximum, say as in the case of O3Al3O8 plane shown in Table 3.7, the adsorption is favoured. Oxygen of the water molecule gains the maximum negative charge in this case. The adsorption of water is found to take place by the transfer of electrons from the TO_4 group. The net charges on various atoms themselves are found to depend on the geometry of TO_4 group which is discussed below.

The procedure mentioned above is followed and the values of adsorption energy for water at the rest of the four T–sites were also calculated. The average adsorption energy of water obtained from six values for each site is given in Table 3.8. The values of adsorption energy in Table 3.8 indicates that Al3 and P3 are the preferred sites among the aluminium and phosphorus, respectively, for the adsorption of water. The geometric reasons for the preference of T–sites is obvious since these sites have the largest T–O–T angles, thus posing minimum steric hindrance to the approaching water molecules. Further to the steric factor, the electronic factor is also favourable where the T–O–T angles are maximum and the T–O distances are minimum.

Topologically, Al3 and P3 sites occur at the junction of 10– and two 6–membered rings as mentioned earlier. Statistically, T3 sites represent 20% of the T–sites (where T is either Al or P) since there are two T1 and T2 sites each, for every single T3 site.

It is pertinent to recall the NMR results which show that on hydration of $AlPO_4$–11, 20% of the Al and P sites are affected. Sites affected in this manner can be directly related to the number of T3 sites per unit cell. By a quantitative analysis, ratios of intensities of the two signals in the NMR spectra of the hydrated sample has been calculated. These ratios, which correspond to the ratios of of the intensities of the additional peaks (arising from water adsorption) to the corresponding tetrahedral peaks for Al and P is $\approx 20 : 80$, an observation consistent with interaction of water molecules with the T3 site causing distortion of the framework.

Site	Average T–O–T angle (degrees)	Average adsorption energy of water(eV)	Net charges on			
			oxygen of the frame-work	T–site	oxygen of H_2O	Hydrogen of H_2O
Al1	146.0	11.93	−0.56	+0.93	−0.12	+0.22
Al2	158.0	11.35	−0.61	+1.00	−0.12	+0.20
Al3	171.8	9.97	−0.68	+1.13	−0.05	+0.17
P1	147.5	−13.21	−0.70	+1.64	−0.27	+0.27
P2	157.3	−13.88	−0.66	+1.69	−0.15	+0.26
P3	171.3	−15.17	−0.71	+1.85	−0.06	+0.27

TABLE 3.8. **The Geometric and Electronic Properties of Water Adsorbed Over All the Six T–sites.**

3.4 CONCLUSIONS

1. The largest pore molecular sieve, VPI–5 transforms to $AlPO_4$–8 by heating or drying at 388 K. The transformation is found to be irreversible.
2. The synthesis systems and crystallization conditions for VPI–5 and $AlPO_4$–8 are identical.
3. The transformation of both H1(GTRI) and VPI–5 to $AlPO_4$–8 provides evidence to show that the former two represent same crystalline phase. H1(GTRI) and $AlPO_4$–8 are examples of synthesis of microporous crystalline $AlPO_4$'s in the absence of organic additives.
4. For the hydrated $AlPO_4$–11, ^{27}Al and ^{31}P MASNMR spectra show additional signals at around ≈ -20 and -23.4 ppm respectively, indicating interaction of the T–sites with water molecules.
5. Water adsorbs on the TO_4 group as shown in Fig. 3.7a.
6. Among the different T–sites, T3 (where T=Al or P) shows favourable adsorption energy for water due to its geometry (wide T–O–T angles).

3.5 REFERENCES

1. F. D'Yvoire, *Bull. Soc. Chim. Fr.*, 1961, **p. 1762.**
2. J.W. Richardson. Jr., J.V. Smith and J.J. Pluth, *J. Phys. Chem.*, **94**, 3364, 1990.
3. S.T. Wilson, B.M. Lok and E.M. Flanigen, U.S. Pat. 4310440, 1982.
4. N. Rajic, D. Stojakovic and V. Kaucie, *Zeolites*, 10, 802, 1990.
5. K. Sorby, R. Szostak, J.G. Ulan and R. Gronsky, *Catal. Lett.*, **6**, 209, 1990.
6. S. Prasad and I. Balakrishnan, *Inorg. Chem.*, **29**, 4830, 1990.
7. B. Duncan, R. Szostak, K. Sorby and J.G. Ulan, *Catal. Lett.*, **7**, 367, 1990.
8. R. Meinhold and N.J. Tapp, *J. Chem. Soc. Chem. Comm.*, 1990, **p. 219.**
9. M. Goepper, F. Guth, L. Delmotte, J.L. Guth and H. Kessler, *Stud. Surf. Sci. Catal.*, **49B**, 857, 1989.
10. C.S. Blackwell and R.L. Patton, *J. Phys. Chem.*, **88**, 6134, 1984.
11. H.L. Zubowa, E. Alsdorf. R. Fricke, F. Neissendorfer, J.R. Menden, E. Scheirer, D. Zeigan and B. Zibrowius, *J. Chem. Soc. Faraday Trans. 1.*, **86**, 2307, 1990.
12. D. Hasha, L.S. de Saldarriaga, C. Saldarriaga, P.E. Hathaway, D.F. Cox and M.E. Davis, *J. Am. Chem. Soc.*, **110**, 2127, 1988.
13. N.J. Tapp, N.B. Milestone, M.E. Bowden and R.H. Meinhold, *Zeolites*, **10**, 105, 1990.
14. R. Khouzami, G. Coudurier, F. Lefebvre, J.C. Vedrine and B.F. Mentzen, *Zeolites*, **10**, 183, 1990.
15. L. Maistrian, Z. Gabalica and E.G. Derouane, *Appl. Catal.*, **67**, L11, 1991.
16. S. Prasad, V.G. Gunjikar and I. Balakrishnan, *Thermochim. Acta, in press.*
17. M.J.S. Dewar and W. Thiel, *J. Am. Chem. Soc.*, **99**, 4899, 1977.
18. J.W. Richardson Jr., J.J. Pluth and J.V. Smith, *Acta. Crystallogr.*, **B44**, 367, 1988.
19. R.S. Mulliken, *J. Phys. Chem.*, **23**, 1833, 1955.
20. P.J. Grobet, J. Martens, I. Balakrishnan, M. Mertens and P.A. Jacobs, *Appl. Catal.*, **56**, L21, 1989.
21. M.E. Davis, C. Montes, P.E. Hathaway and J.M. Garces, *Stud. Surf. Sci. Catal.*, **49A**, 189, 1989.
22. E.T.C. Vogt and J.W. Richardson Jr., *J. Solid. State. Chem.*, **87**, 469, 1990.
23. D. Muller, E. Jahn, G. Ladwig and U. Haubenreisser, *Chem. Phys. Lett.*, **109**, 382, 1984.
24. M.E. Davis, C.E. Montes, P.E. Hathaway, J.P. Arahncet, D.L. Hasha and J.M. Garces, *J. Am. Chem. Soc.*, **111**, 3919, 1989.

25. J.A. Martens, B. Verlinden, M. Mertens, P.J. Grobet and P.A. Jacobs, *ACS. Symp. Ser.*, **398**, 305, 1989.

26. J.O. Perez, N.K. McGuire and A. Clearfield, *Catal. Lett.*, **8**, 1991, 145.

27. L.B. McCusker, Ch Baelocher, E. Jahn and M. Bulow, *Zeolites*, **11**, 1991, 308

28. R. von Ballmoos and J.B. Higgins, *Collection of simulated XRD patterns for zeolites, Zeolites*, **10(5)**, 328 S, 1990.

29. A.P.M. Kengens, K.F.M.G. Scholle and W.S. Veeman, *J. Phys. Chem.*, **87**, 4357, 1983.

30. D. Muller, I. Grunze, E. Hallas and G.Z. Ludwig, *Anorg. Allog. Chem.*, **500**, 80, 1983.

31. E. Jahn, D. Muller and K. Becker, *Zeolites*, **10**, 151, 1990.

CHAPTER 4

TRANSITION METAL SUBSTITUTED $AlPO_4$-11

4 TRANSITION METAL SUBSTITUTED $AlPO_4$–11

4.1 INTRODUCTION

In the $AlPO_4$'s, isomorphic substitution for a large number of elements for Al^{3+} and/or P^{5+} has been claimed[1,2]. There are three possible mechanisms for substitution of Si in $AlPO_4$. These are substitution of Si for Al^{3+}, P^{5+} or for Al^{3+} and P^{+} in patches[1]. Metals substitute preferentially for Al^{3+} in $AlPO_4$ lattice. As many as 13 metals have been successfully incorporated into $AlPO_4$ lattice[2]. The most studied of these substitutions are those of Mg^{2+}, Co^{2+}, Mn^{2+}, and Fe^{3+}. Several workers have reported framework incorporation of Co^{2+} in $AlPO_4$–5[3–6]. The existence of redox centres in CoAPO–5 have been reported[6]. TPD measurements have shown the presence of acid sites in CoAPO–11 implying substitution of Co^{2+} for Al^{3+} [7]. ESR spectra recorded at 4.2 K revealed the oxidation of Co^{2+} to Co^{3+} during calcination in CoAPO–34 and CoAPO–5[5]. In MnAPO–5, the large anisotropy manifested in the numerous side bands of the ^{31}P and ^{27}Al spectra have been attributed to the interaction of Mn^{2+} with ^{31}P and ^{27}Al nuclei[8]. The ESR spectrum of the calcined dehydrated sample showed hyperfine splitting characteristic of 6-coordinated $Mn^{2+}(H_2O)_6$. These studies supported the existence of framework as well as extra framework Mn^{2+} in MnAPO–5.

FeAPO–n materials, unlike the Si or divalent metal substituted $AlPO_4$, do not exhibit catalytic properties. Fe^{3+} substitutes for Al^{3+}, producing no net framework charge. FeAPO–5, has been characterized by Mossbaüer and ESR measurements[9,10]. As in the case of zeolites, the broad signal at $g = 2$ has been attributed to Fe species occluded in the pores and the sharp signal at $g = 4.3$ to framework substitution[9]. However, isotropic resonance with $g = 4.3$ is possible for both tetrahedral and octahedral Fe^{3+} depending on the ligand distortion the Fe^{3+} ion. Mossbaüer spectroscopic studies[10] has shown that

only a small part of iron is actually incorporated into the tetrahedral site of FeAPO–5 the remaining being present as an amorphous iron aluminium phosphate.

Very few catalytic reactions have been reported with MeAPO's as catalysts. These include the methanol conversion[11] and skeletal isomerization reactions of hydrocarbons reported by Pellet et al.[12,13].

This chapter describes the synthesis, characterization and some of the catalytic properties of CoAPO–11. These results are compared with $AlPO_4$–11 and MnAPO–11. The usefulness of n–dibutylamine (DBA) as organic additive for the synthesis of metal–$AlPO_4$–11 as for $AlPO_4$–11[14] has been confirmed.

4.2 EXPERIMENTAL

4.2.1 Synthesis

To a solution of 24.2 g of aluminium isopropoxide in 22.5 g of water was added a solution of 13.4 g of H_3PO_4 in 12 g of water. 7.6 g of n–dibutylamine was added to the mixture. 1.3 g of cobalt acetate was added as a solution in 2 g of water to get a gel composition of 0.085 CoO. Al_2O_3. P_2O_5. DBA. $40H_2O$. The gel was treated at 428 K in closed autoclaves in a preheated oven under static conditions for 24 hours. The reaction was quenched to ambient and the blue crystals washed with water and air dried. A sample of MnAPO–11 was synthesized in a similar manner; 1.4 g of manganese acetate was substituted for cobalt acetate.

4.2.2 Characterization

The samples were characterized by XRD, MASNMR, TGA/DTA, TPD etc. The experimental details are given in Chapter 2.

4.2.3 Catalysis

Catalytic reactions such as dehydration, oligomerization and cracking were carried out in conventional down–flow silica reactor. Aqueous and gaseous products were analyzed by

GC (Shimadzu R 16A) using Porapak N and n–Octane–Porasil–C columns. Organic liquid products were analyzed on a Bentone 34 (5%) + DIDP(5%) on chromosorb W column.

4.3 RESULTS AND DISCUSSION

4.3.1 Synthesis

Cobalt–incorporated samples had an intense blue colour where as Mn–incorporated ones were white. CoAPO–11 had a chemical composition of $Co_{0.06}$ $Al_{0.46}$ $P_{0.48}$ and MnAPO–11 had a composition of $Mn_{0.06}$ $Al_{0.46}$ $P_{0.48}$.

4.3.2 Characterization

4.3.2.a. X–ray Diffraction

The X–ray diffraction patterns of CoAPO–11 and MnAPO–11 are given in Fig. 4.1. They are similar to the pattern of $AlPO_4$–11[11]. Attempts to increase the concentration of cobalt resulted in a decrease in X–ray reflection intensities. This may be due to a large excess of cobalt going into extra framework positions as observed in the case of $AlPO_4$–5[4].

4.3.2.b. Solid State MASNMR

Only one peak is observed in ^{27}Al or ^{31}P MASNMR spectra of CoAPO–11 characteristic of Al or P, respectively (Fig. 4.2). In ^{27}Al spectra, the intensity of the side bands increases upon calcination. In the ^{31}P MASNMR spectra for CoAPO–11, a broad single resonance line is observed. No P–OH defect groups could be detected under CP conditions at different contact times. However, a shoulder peak at −22 ppm appeared upon calcination. The intensity of this signal increased under CP conditions indicating interaction of framework P with OH^-/H_2O[15].

The ^{27}Al and ^{31}P MASNMR spectra of MnAPO–11 (Fig. 4.3) show considerable anisotropy due to paramagnetic shifts induced by Mn^{2+}. An increase in side band intensity is also observed, similar to that observed in MnAPO–5[8]. On calcination, narrowing of the individual lines occurred. Side bands are observed upto 100 and 200 KHz wide in

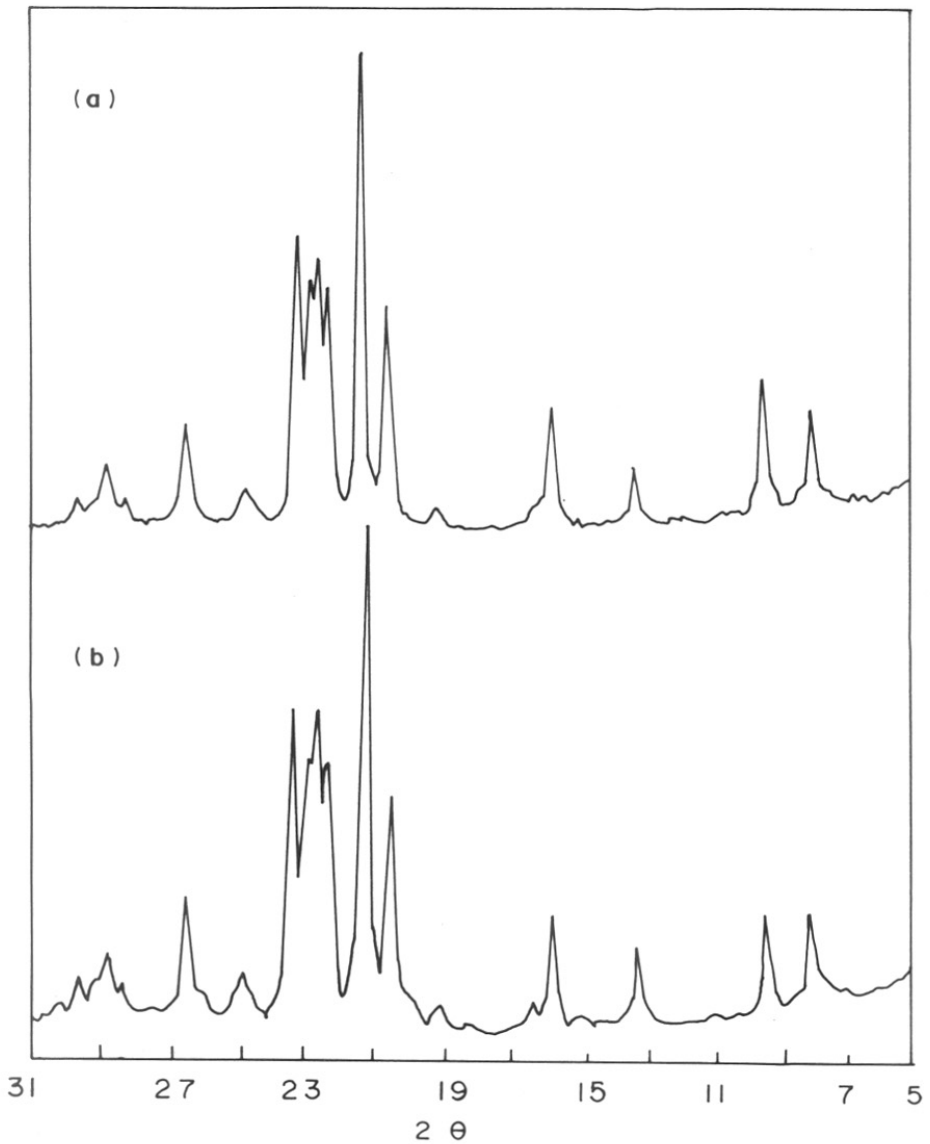

Fig. 4.1 ▷ XRD patterns for (a) CoAPO–11; (b) MnAPO–11.

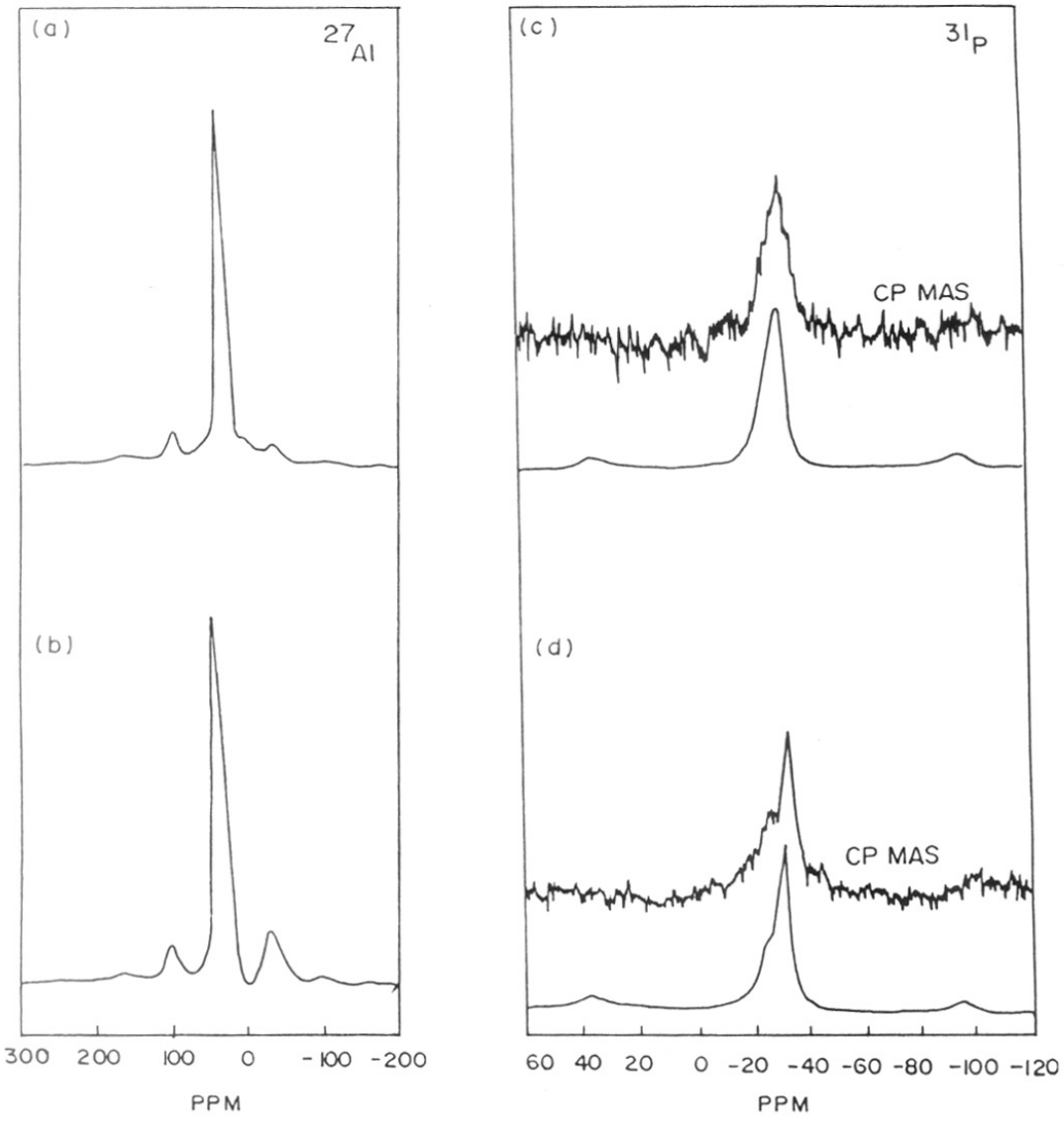

Fig. 4.2 ▷ ^{27}Al MASNMR spectra for (a) as–synthesized; (b) Calcined CoAPO–11. ^{31}P MASNMR spectra for (c) As–synthesized; (d) Calcined CoAPO–11.

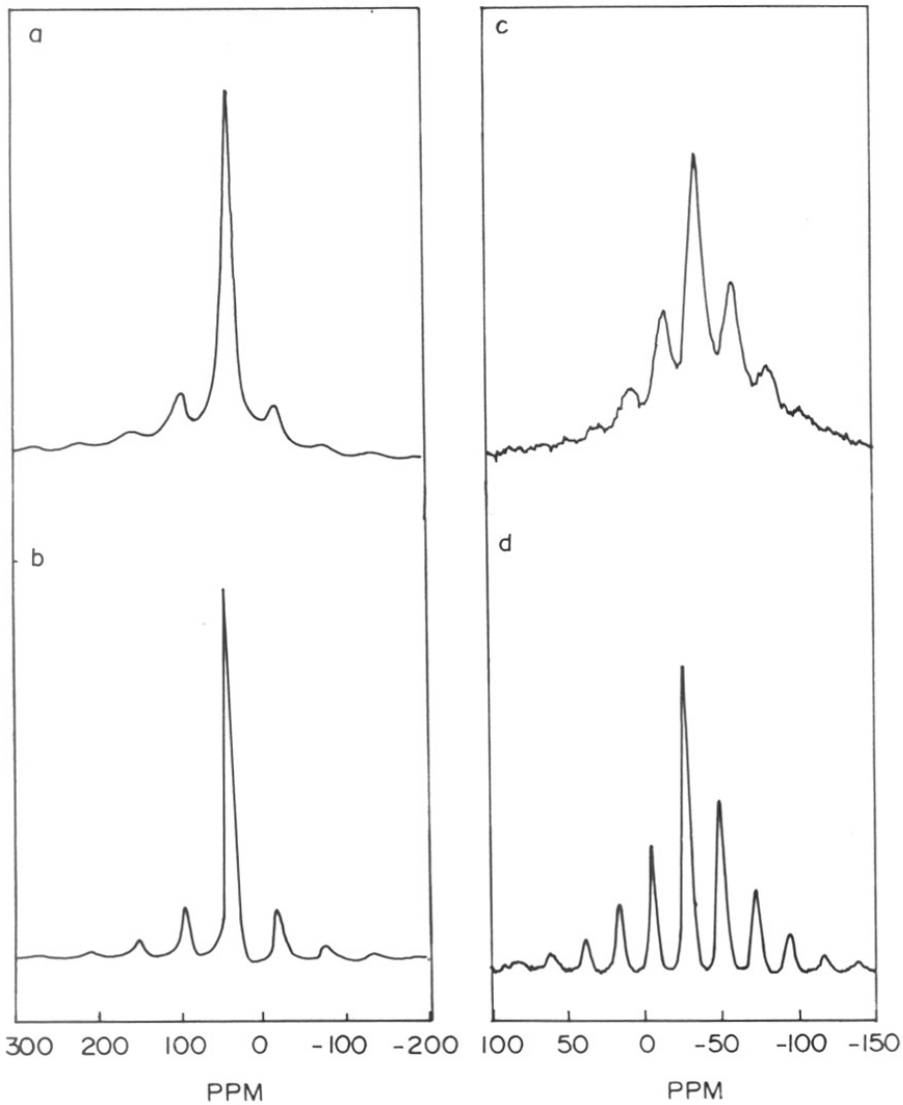

Fig. 4.3 ▷ ^{27}Al MASNMR spectra for (a) as–synthesized; (b) Calcined MnAPO–11. ^{31}P MASNMR spectra for (c) As–synthesized; (d) Calcined MnAPO–11.

^{27}Al and ^{31}P spectra respectively. The greater width in the ^{31}P spectrum indicates shorter distance between the Mn^{2+} and ^{31}P nuclei[11] and hence substitution of Mn^{2+} for ^{27}Al in MnAPO–11. It may be noted that splitting of the ^{27}Al peak in the tetrahedral region is not observed in calcined metal substituted $AlPO_4$–11 which is unlike in the case of $AlPO_4$–11(Chapter 3). The presence of intense spinning side bands and the broadening of the peaks suggests that in transition metal $AlPO_4$–11 some of the ^{27}Al and ^{31}P nuclei are closer to Mn^{2+} and Co^{2+} supporting their location in the framework. Similar observations with respect to MASNMR spectral data have been made by other workers in the case of CoAPO–5[6] and MnAPO–5[8].

4.3.2.c. Characterization of Co^{3+} in the framework of CoAPO–11.

Exothermic peak observed in the temperature range of 553–623 K in the DTA curve (Fig. 4.4) is indicative of template removal. The associated change in color of CoAPO–11 from blue to green–yellow indicates that atleast a part of cobalt is in a higher oxidation state in the calcined sample[5,6].

The blue colour was restored on reduction with hydrogen or on exposure to methanol vapour even at room temperature. In the latter case, methanol was oxidized to formaldehyde by framework co^{3+}. Formation of formaldehyde by Co^{3+} occurs by a mechanism suggested by Iton et al.[5]. In this mechanism, formation of a free radical involving electron transfer from CH_3OH to Co^{3+} is the first step:

$$CH_3OH + Co^{3+} \longrightarrow CH_3O. + Co^{2+} + H^+ \qquad (1)$$

this is followed by oxidation of the methoxy radical to formaldehyde.

$$CH_3O. + Co^{3+} \longrightarrow CH_2O + Co^{2+} + H^+ \qquad (2)$$

The two anionic framework sites created by reduction of the two Co^{3+} cations (per methanol molecule) are compensated by protons produced through steps 1 and 2.

The as–synthesized MnAPO–11, white in colour, turned pink to purple blue upon

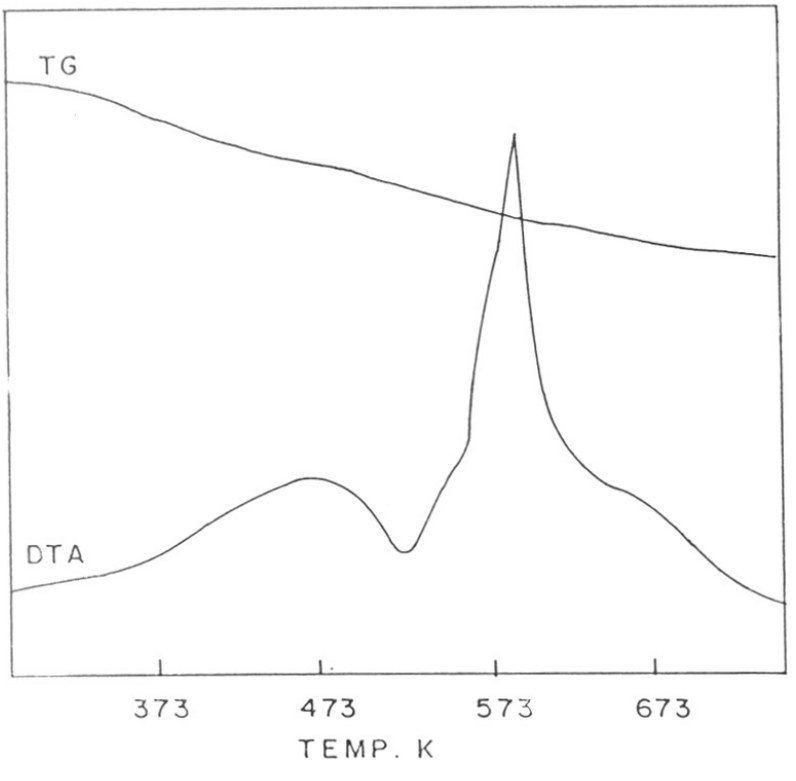

Fig. 4.4 ▷ Thermoanalytical curves for CoAPO–11.

calcination, an indication of the presence of $Mn(H_2O)_6^{2+}$ [8]. The white colour was not restored on exposure of the calcined sample to methanol vapour unlike calcined CoAPO–11 which showed a change in colour from green–yellow to blue.

4.3.2.d. Temperature Programmed Desorption

The TPD chromatogram of ammonia in the temperature range of 343–693 K exhibited peaks due to desorbed ammonia in CoAPO–11(Fig. 4.5). This may be attributed to to the presence of acidity in the sample as extraneous oxides and hydroxides do not contribute to acidity[16]. CoAPO–11 shows greater Lewis acidity than Brönsted acidity[17]. About 75% of Co^{2+} is oxidized to Co^{3+}[5]. The residual Co^{2+} present in the calcined CoAPO–11 contribute to Brönsted acidity in the present case. The strength of acid sites in CoAPO–11 is considerably weaker as compared to the corresponding sites in zeolites for which the temperature maximum of the peak representing the strong acid sites occur above 673 K. The weaker acid strength of the material favours improved selectivities in certain catalytic reactions such as isomerization reactions by eliminating side reactions[13].

4.3.3 Catalysis

4.3.3.a. Isopropanol Dehydration

Table 4.1 compares the product distribution pattern for $AlPO_4$-11 and CoAPO–11. While the major reaction over $AlPO_4$–11 is only dehydration, higher hydrocarbons are also formed over CoAPO–11.

Alkene oxidation over cobalt catalysts involves formation of an ion radical as an intermediate in a mechanism proposed by Bawn[18]. This mechanism may be extended to the reaction over CoAPO–11 as shown below:

$$CH_3 - CH(OH) - CH_3 \xrightarrow{\text{dehyd.}} CH_3 - CH = CH_2 + H_2O$$

$$CH_3 - CH = CH_2 + Co^{3+} \longrightarrow CH_3 - C^+H - \dot{C}H_2 \leftrightarrow CH_3 - \dot{C}H - C^+H_2 + Co^{2+}$$

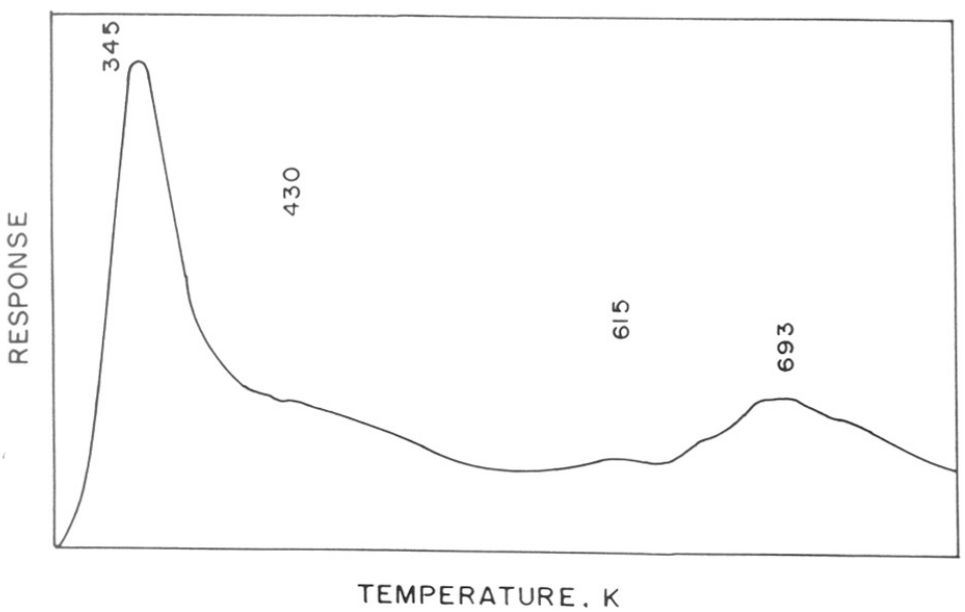

Fig. 4.5 ▷ TPD chromatogram for CoAPO–11.

Catalyst ▷	$AlPO_4$–11	CoAPO–11
Isopropanol Conversion	97.50	100.00
Product distribution (wt%)		
Ethane and ethylene	0.01	0.10
Propylene	98.21	84.21
Butanes and butenes	0.08	0.57
C_5^+ hydrocarbons	1.71	15.11

TABLE 4.1. **Comparison of $AlPO_4$–11 and CoAPO–11 in Isopropanol dehydration. Conditions : Temp.= 673 K; WHSV = 3.5; Time on stream = 3 hours.**

$$CH_3 - \dot{C}H - C^+H_2 \longrightarrow C_5^+ \quad \text{Hydrocarbons} + H^+$$

$$Co^{2+} + H^+ \longrightarrow Co^{3+} + \frac{1}{2}H_2$$

The conversion of isopropanol and selectivities towards higher hydrocarbons decreased on increasing space velocity (Table 4.1).

4.3.3.b. Propylene Oligomerization

Table 4.2 compares the catalytic activities of $AlPO_4$–11, CoAPO–11 and MnAPO–11 in the oligomerizaton of propylene. $AlPO_4$–11 was hardly active for this reaction. The higher hydrocarbons formed inside the pores cracks leading to higher selectivity to C_2 and C_4 hydrocarbons at longer contact time (low GHSV). Increasing the GHSV increased the C_5^+ selectivity. MnAPO–11 showed higher activity as compared to CoAPO–11.

4.3.3.c. Cumene Cracking

Table 4.3 compares the cumene cracking activity and selectivity to benzene for $AlPO_4$–11 and transition metal $AlPO_4$–11. The cracking activity increases with temperature in the metal substituted $AlPO_4$–11. $AlPO_4$–11 is inactive even at high temperatures. MnAPO–11 exhibited higher activity. The activity for cumene cracking indicates the presence of Brönsted activity in metal substituted $AlPO_4$–11.

4.4 CONCLUSIONS

1. Transition metal substituted $AlPO_4$–11, CoAPO–11 and MnAPO–11 have been synthesized with n–dibutylamine as organic additive.
2. Bifunctional catalytic centres have been identified in CoAPO–11 using conversion of methanol to formaldehyde and cumene cracking as test reactions.
3. MnAPO–11 showed higher activity in catalytic test reactions.

Catalyst ▷	$AlPO_4$–11	CoAPO–11		MnAPO–11
GHSV	450	450	1200	450
Propylene conversion	2.30	35.80	30.30	41.10
Product distribution (wt%)				
Ethane and ethylene	0.01	0.31	0.01	0.76
Propane	3.07	7.06	4.70	7.70
Propylene	94.89	61.47	67.04	56.20
Butanes and butenes	0.07	9.90	5.80	23.00
C_5^+ hydrocarbons	2.40	18.50	20.80	11.10

TABLE 4.2. **Comparison of $AlPO_4$–11 and Transition metal–$AlPO_4$–11 for Propene oligomerization. Conditions : Temp.= 723 K; Time on stream = 3 hours. Feed 97.3% propylene, 2.7% propane.**

Catalyst ▷	$AlPO_4$–11	CoAPO–11		MnAPO–11
Temp.(K)	673	673	723	673
Cumene Conversion (wt%)	1.60	11.50	14.90	18.90
Product distribution (wt%)				
Propane and propylene	–	1.50	1.80	1.80
Benzene	0.57	8.05	10.5	13.10
Toluene	–	0.02	0.04	0.21
Ethylbenzene	0.36	0.27	0.29	0.59
Cumene	98.4	89.41	86.10	81.10
N–Proplybenzene	0.55	0.31	0.30	0.90
Butylbenzenes & Others	0.04	0.50	0.70	1.50

TABLE 4.3. **Comparison of $AlPO_4$–11 and Transition metal $AlPO_4$–11 in Cumene cracking. Conditions : WHSV = 3.5; Time on stream = 3 hours.**

4.5 REFERENCES

1. B.M. Lok, C.A. Messina, R.L. Patton, R.T. Gajek, T.R. Cannan and E.M. Flanigen, *J. Am. Chem. Soc.*, **106**, 6092, 1984.
2. E.M. Flanigen, R.L. Patton and S.T. Wilson, *Stud. Surf. Sci. Catal.*, **37**, 13, 1988.
3. R.A. Schoondeydt, R. De Vos, J. Pilgrims and H. Leeman, *Stud. Surf. Sci. Catal.*, **49A**, 559, 1989.
4. V.P. Shiralkar, C.H. Saldarriaga, J.O. Perez, A. Clearfield, M. Chen, R.G. Antony and J.A. Donohue, *Zeolites*, **9**, 474, 1989.
5. L.E. Iton, I. Choi, J.A. Desjardines and V.A. Moroni, *Zeolites*, **9**, 535, 1990.
6. C. Montes, M.E. Davis, B. Murray and M. Narayana, *J. Phys. Chem.*, **94**, 6425, 1990.
7. N.J. Tapp, N.B. Milestone and J.M. Wright, *J. Chem. Soc. Chem. Comm.*, 1985, **p. 1801**.
8. D. Goldfarb, *Zeolites*, **9**, 509, 1989.
9. H.X. Li, J.A. Martens, P.A. Jacobs, S. Schubert, F. Schmidt, H.M. Zeithen and A.X. Trantwein, *Stud. Surf. Sci. Catal.*, **37**, 75, 1988.
10. C.M. Cardile, N.J. Tapp and N.B. Milestone, *Zeolites*, **10**, 90, 1990.
11. N.B. Milestone and N.J. Tapp, *Stud. Surf. Sci. Catal.*, **36**, 553, 1987.
12. P.J. Pellet, G.N. Long and J.A. Rabo, *Proc. 7th Int. Zeo. Conf.*, Tokyo, Japan (Eds. Y. Murakami et al.), 1986, **p. 843**.
13. P.J. Pellet, P.K. Coughlin, E.S. Shamshoun and J.A. Rabo, *ACS. Symp. Ser.*, **398**, 512, 1989.
14. I. Balakrishnan and S. Prasad, *Appl. Catal.*, **62**, L7, 1990.
15. R. Khouzami, G. Croudrier, F. Lefebrve, J.C. Vedrine and B.F. Mentzen, *Zeolites*, **10**, 183, 1990.
16. E.M. Flanigen, B.M. Lok, R.L. Patton and S.T. Wilson, *Pure and Appl. Chem.*, **58**, 1351, 1986.
17. N.J. Tapp, N.B. Milestone and D.M. Bibby, *Stud. Surf. Sci. Catal.*, **37**, 393, 1988.
18. L.E.H. Bawn and J.A. Sharp, *J. Chem. Soc.*, 1957, **p. 1854**.

CHAPTER 5

THE NATURE OF THE ORGANIC TEMPLATE MOLECULES IN AS-SYNTHESIZED $AlPO_4$-11

5 THE NATURE OF THE ORGANIC TEMPLATE MOLECULES IN AS–SYNTHESIZED $AlPO_4$–11 LATTICE

5.1 INTRODUCTION

It has been found by earlier workers[1,2] that only secondary alkyl amines act as template molecules in the synthesis of $AlPO_4$–11. Tapp et al.[2] have predicted that only secondary amines having length comparable to the unit cell dimension along the c–axis(ie.8.44 Å) are required for successful synthesis. However, Chapter 2 of the present work reports successful use of secondary alkyl amines whose length exeeds the unit cell c–dimension in the synthesis of $AlPO_4$–11.

Molecular modelling studies are useful to study the structural features and adsorption of molecules on molecular sieves. Surface acid–base property and water adsorption of $AlPO_4$ clusters by semi–empirical method have been included in an early phosphate study[3]. Carson et al.[4] by using STO–3G basis have found that optimized T–O–T angle for $AlPO_4$ is smaller than predicted for silicate, aluminosilicate units. Derouane et al.[5] have investigated the stability of SiOAl, SiOP and AlOP linkages by using *ab initio* method with STO–3G basis. The calculations predict AlOP linkage to be stabler than SiOAl or SiOP linkages in agreement with the high stability of $AlPO_4$ framework structures. Si preferentially substitutes P in $AlPO_4$ structure. The calculations also suggest that bridging –OH groups in $AlPO_4$, originating from non–stochiometry, defects or Si incorporation should show acidic property.

In this chapter, the results of molecular modelling and quantum chemical calculations are used to study the nature of the occluded template molecules and to interpret the relation between pore architecture of $AlPO_4$–11 and structural as well as electronic properties of template molecules. The results of ^{13}C MASNMR studies are presented which provide information regarding the dynamic nature of the amines inside the pores of $AlPO_4$–11.

5.2 METHODS AND EXPERIMENTAL

Standard force fields are used in the energy minimization calculations[6]. All geometrical degrees of freedom such as bond length, bond angle and dihedral angles are varied. In this process all atoms are moved and the molecule reaches a final geometry, where the molecular potential energy is minimum. From these calculations, and the dimensions of the amines at their minimum energy conformations, the strain energy involved in the conformational changes from their equilibrium geometry can be obtained.

Semi–empirical quantum chemical calculations using MNDO (Modified Neglect of Differential Overlap) technique[7] was used to study the electronic structure of the amines, cluster models of $AlPO_4$–11 framework and the ammonia adsorption complexes over the oxygen sites in $AlPO_4$–11. The values of electronic and total energy are used to decide the favourable adsorption sites. The analysis of molecular orbital energy as well as the contributions of various atomic orbitals to molecular orbitals and the electron distribution and partial charges calculated are also useful to know the nature of interaction between amines and $AlPO_4$–11 framework.

^{13}C CP MASNMR spectra were recorded in a Bruker MSL 300 spectrometer (7T magnetic field, ^{13}C frequency 75.47 MHz). A contact time of 1 ms, a pulse length of 5μ s and a spinning speed of 3KHz were employed. The chemical shifts were measured relative to ^{13}C signal of –CH group in adamantane.

5.3 RESULTS AND DISCUSSION

5.3.1 Geometrical Properties of Amines

The equilibrium geometry of the amine molecules were obtained by molecular force field method described by Gelin and Karplus[8] using an integrated molecular modelling package[6]. The dimensions calculated for various secondary amines in their equilibrium conformation are given in Table 5.1.

From the molecular modelling methods, a general relation has been derived to determine the dimension of amine molecules based on their van der Waal's radii. For a typical

Channel/molecule	dimension (Å)	Charge density on N	Charge density on H_N
10-membered channel	6.40×3.90		
	6.40×4.90		
6-membered channel	3.40×2.15		
4-membered channel	1.40×0.90		
NH_3	—	-0.24	0.08
Me_2NH	4.25×2.75×2.25	-0.29	0.15
Et_2NH	6.75×2.75×2.25	-0.29	0.15
n–Pr_2NH	9.25×2.75×2.25	-0.29	0.15
i–Pr_2NH	6.75×4.25×3.25	-0.29	0.11
n–Bu_2NH	11.75×2.75×2.25	-0.30	0.15
i–Bu_2NH	9.25×4.25×3.25	-0.29	0.11
n–Pe_2NH	14.25×2.75×2.25	-0.29	0.15
i–Pe_2NH	11.75×4.25×3.25	-0.29	0.11
i–Bu, n–PrNH	9.25×4.25×3.25	-0.31	0.11
i–Pe, n–PrNH	10.50×4.25×3.25	-0.31	0.11
n–$HexNH_2$	8.25×4.75×4.00	-0.30	0.10
Et_3N	6.00×6.00×6.00	-0.36	–

TABLE 5.1. **Dimensions† of the Pores in $AlPO_4$–11 as well as Certain Amine Molecules and Their Electronic Properties.**

† *For amine molecules length, width and height are given based on their Van der Waals radii.*

amine molecule RNHR′, where R ≠ R′, the length $L_{RNHR'}$ could be derived as,

$$L_{RNHR'} = L_{RNHR}/2 + L_{R'NHR'}/2 \quad (1)$$

where L_{RNHR} and $L_{R'NHR'}$ are reported in Table 5.1 for different alkyl groups varying from methyl to pentyl.

In a secondary amine molecule of the type RNHR′, where R and R′ are alkyl groups, the substitution of n–alkyl group by an iso–alkyl group reduces the length of the molecule by 1.25 Å. The width and height of both normal and iso–alkyl groups are well within the limits of the pore dimensions of the 10–member channel in $AlPO_4$–11(Table 5.1). The 10–member straight channel has side-pockets which are double 6–member channels (Fig. 5.1) and these side-pockets can easily accommodate a terminal methyl group carbon of the alkyl chains in the amines as could be seen from the values given in Table 5.1. There is a rotational freedom for the amine molecules along the N–C bonds. Conformational analysis was carried out on various secondary amine molecules given in Table 5.1. For the equilibrium conformation, rotation along the N–C bond was tried. For a rotation of ±30° along the N–C bond, the overall increase in energy did not exceed 5.0 K cal/mol for any of these secondary amine molecules. Within this flexible range of ±30°, the decrease occurring in the length of the amine molecules is ≈ 1.5 Å.

It has been reported[9] that there is approximately one template molecule present in each channel unit (8.44 Å along the straight channel) in the as–synthesized molecular sieve. The present simulation studies have shown that even secondary amine molecules which are longer than 8.44 Å can fit into a channel unit of $AlPO_4$–11 due to conformational flexibility.

5.3.2 Electronic Properties of Amine Molecules.

Semi–empirical MNDO calculations were carried out on different amine molecules in order to study the electronic factors involved in the specificity of secondary amines as templates. The net electron charge density on nitrogen as well as hydrogen attached to nitrogen (H_N)

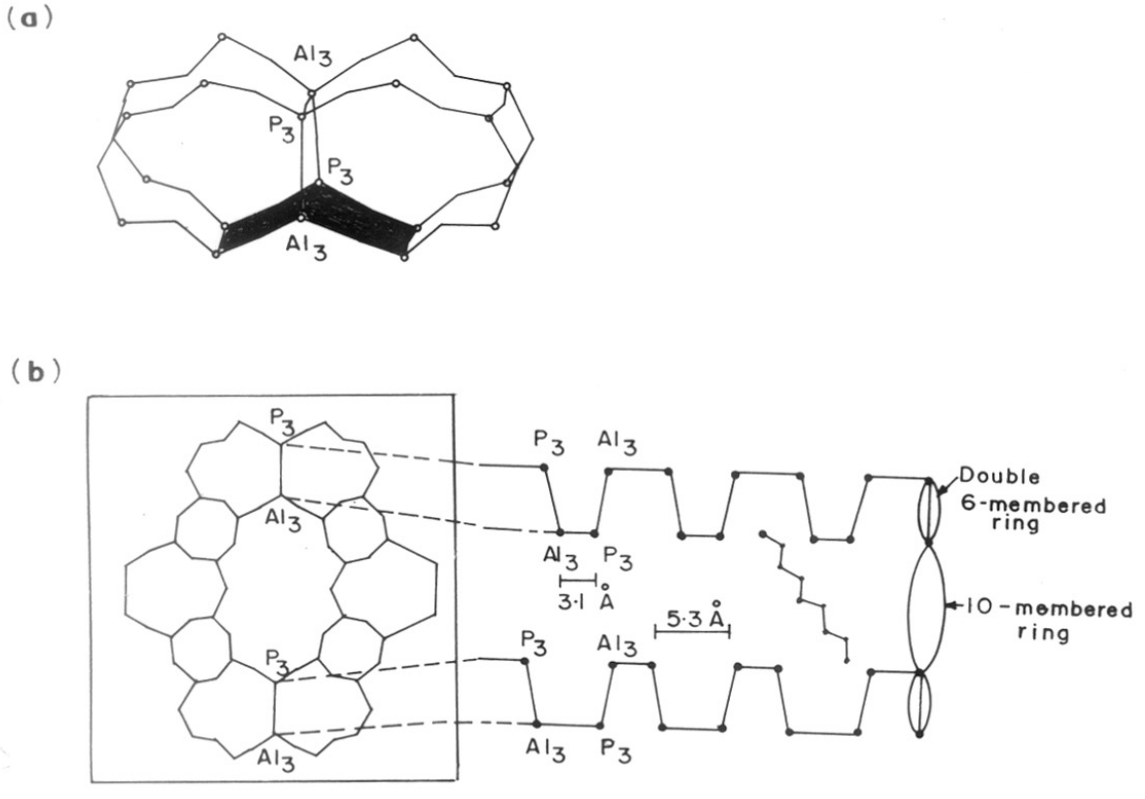

Fig. 5.1 ▷ (a) The geometry of side–pocket which is a double 6–member ring. The opening from the 10–membered ring is shown shading; (b) Schematic view of channels along c–axis (box) and a–axis. Model amine molecule skeleton (n–dibutylamine) is also shown. The figure is not drawn to scale.

of the amine molecules are given in Table 5.1. The electron charge density on nitrogen increases in the order primary $\leq$ secondary $<$ tertiary amines. The absence of hydrogen attached to nitrogen in the case of tertiary amine and almost zero charge on the hydrogens of methylene and methyl group of tertiary and primary amines are partial reasons for their failure to act as templating agent for the synthesis of $AlPO_4$–11 framework.

The net charge on nitrogen in secondary amines is found to be ≈ -0.30, independent of the dimension and nature of the alkyl groups. However, the n–alkyl groups are more efficient than iso-alkyl groups in withdrawing electrons from the hydrogens attached to nitrogen. Among all the atoms, the hydrogen attached to the nitrogen is the atom with maximum positive charge and hence it is expected to have strong bonding interaction with the oxygen atoms of the $AlPO_4$–11 framework. The electron distribution among the methylene and methyl groups are almost constant for all the secondary amines. Overall these amine molecules are less polar with a typical dipole moment value of 1.25 Debyes. Hence these molecules are expected to be weakly bonded to the framework. Tapp and Milestone[9] reported that the template molecules desorbed at $\approx$473 K which is in agreement to the predicted weak binding by the above calculation. Calculation was carried for ammonia also, since ammonia was used as the model compound to study the interactions between amine molecules and the bridging oxygen in $AlPO_4$–11 lattice.

5.3.3 Dimeric Cluster Models of the $AlPO_4$–11 Lattice

Altogether, there are 11 possible bridging oxygen sites which are crystallographically distinct in the ordered $AlPO_4$–11 structure[10]. The repeating unit cell containing 6 unique T–sites and the 11 oxygens attached to them are shown in Fig. 5.2. The inset shows the lattice of $AlPO_4$–11 formed by the presence of such repeating units. All the 11 unique oxygen sites in $AlPO_4$–11 are simulated by suitable cluster models. Dimeric cluster models [$(OH)_3$ T1–O–T2 $(OH)_3$] where T1=P and T2=Al were selected to model all the bridging oxygen sites in $AlPO_4$–11 crystal structure reported by Richardson et al.[10]. The hydrogen atoms needed to maintain neutrality of the clusters are located at the nearest neighbour T–sites. A typical cluster model is shown in Fig. 5.3a. Electronic structure of these clus-

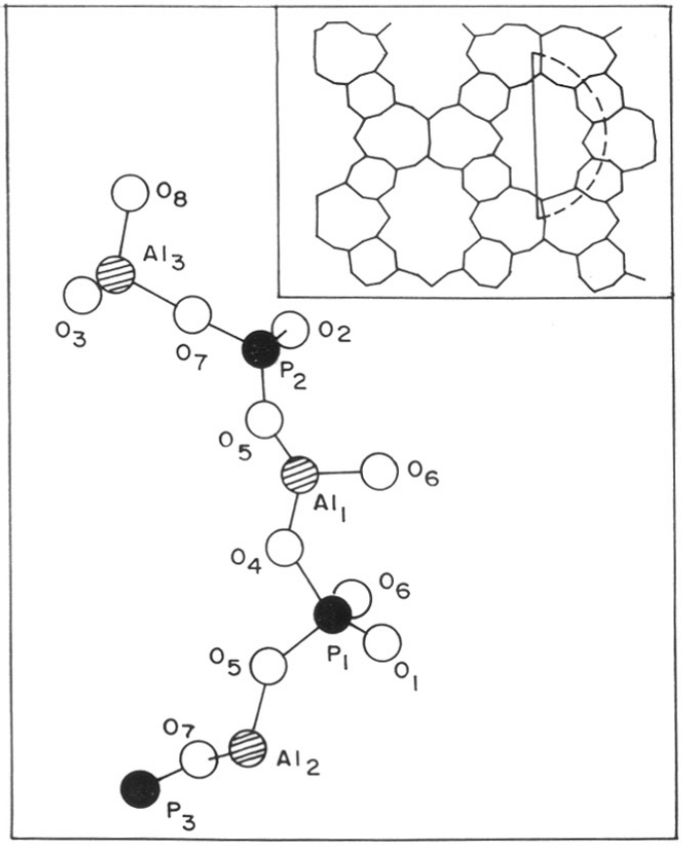

Fig. 5.2 ▷ **A repeating unit of $AlPO_4$–11 structure showing all the bridging oxygen sites. The inset is a schematic representation of $AlPO_4$–11 lattice.**

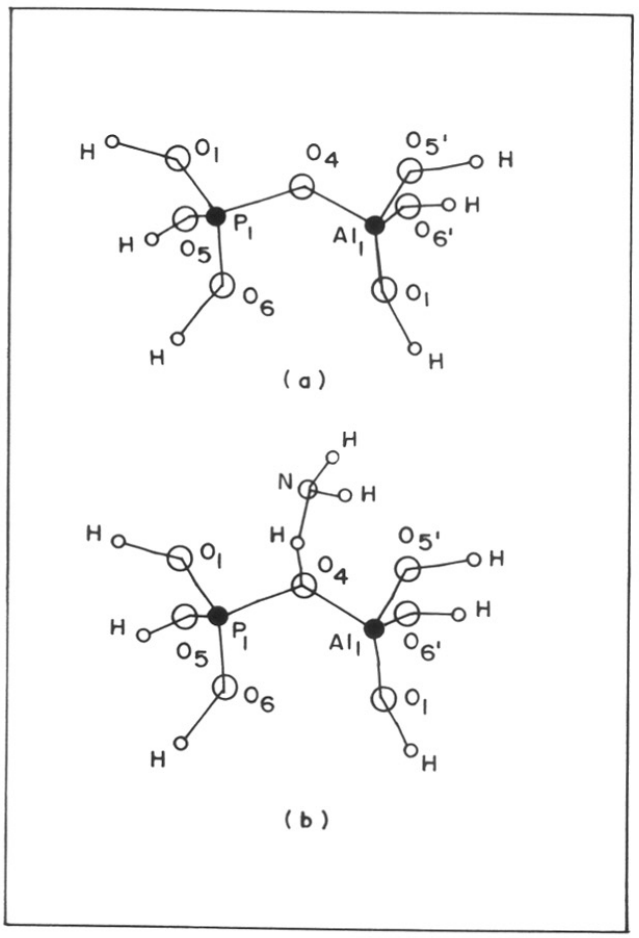

Fig. 5.3 ▷ (a) A typical representation of cluster model showing the bridging oxygen site O4; (b) The geometry of the dimeric cluster–ammonia adsorption complex.

ters are calculated by MNDO method. Cluster models, their total energy and the electron density on the bridging oxygen are reported in Table 5.2. The net electron density on the bridging oxygen atoms is found to increase with increasing T–O–T angle and decreasing T–O distance. The calculated electron density on bridging oxygen atoms indicates how strongly the oxygen atom can interact with the hydrogen atom of ammonia.

5.3.4 Ammonia Adsorption Complexes

The electronic structure of amines indicate that the major interaction of the amine with framework is expected to occur through the hydrogen attached to nitrogen and its nearest neighbors. Hence, ammonia adsorption over different oxygen sites in $AlPO_4$–11 will have corollary results as far as electronic interactions are concerned. A neutral ammonia molecule adsorbed through one of its hydrogen atoms to the bridging oxygen site of $AlPO_4$–11 cluster is considered. Ammonia is positioned in such a way that O–NH_2 bond lies at the centre of T–O–T angle on the obtuse side. The typical cluster model representing the ammonia adsorption complex is shown in Fig. 5.3b. The binding energy of ammonia to the 11 different oxygen sites in $AlPO_4$–11 lattice is calculated and given in Table 5.2. The binding energy of ammonia to the oxygen sites are calculated as follows:

$$B.E_{NH_3} = T.E_{complex} - (T.E_{dimeric\ \ cluster} + T.E_{NH_3})$$

where B.E and T.E are binding energy and total energy respectively. The binding energy of ammonia is a positive value which is an artifact of the small cluster model. However, the binding energy gives the trend of the strength of adsorption of ammonia at various oxygen sites which is expected to be the same for the amine molecules also. The analysis of molecular orbitals of the cluster models show that the Highest Occupied Molecular Orbitals (HOMO) are contributed by the 2p orbitals of oxygen and aluminium, while the Lowest Unoccupied Molecular Orbitals (LUMO) are contributed by the 1s orbital of hydrogen and 2p orbitals of oxygen and phosphorus. The 1s orbital of hydrogen in ammonia is contributing to the frontier HOMO in the adsorption complex. Since PO_4 groups are having unoccupied orbitals, the electron donation from amines to PO_4 group is expected to occur.

Cluster Model	T–O–T angles (degrees)	Total energy of the cluster (eV)	Charge density on the bridging oxygen	Total energy for ammonia adsorption complex (eV)	Adsorption energy of ammonia (eV)	Charge density on ammonia
P1–O1 –Al1	167	–2519.21	–0.63	–2767.16	2.29	–0.04
P1–O4 –Al1	131	–2519.86	–0.50	–2768.69	1.41	–0.02
P1–O5 –Al2	140	–2519.85	–0.61	–2768.44	1.65	–0.05
P1–O6 –Al2	152	–2517.75	–0.63	–2766.24	1.75	–0.06
P2–O2 –Al2	174	–2521.07	–0.66	–2768.36	2.95	0.00
P2–O7'–Al3	168	–2524.15	–0.62	–2772.22	2.17	–0.02
P2–O5'–Al1	147	–2519.14	–0.62	–2767.78	1.60	–0.02
P2–O6'–Al1	140	–2519.59	–0.64	–2768.18	1.65	–0.04
P3–O3 –Al3	172	–2518.78	–0.66	–2766.03	2.99	–0.05
P3–O7 –Al2	166	–2517.29	–0.68	–2765.21	2.32	–0.05
P3–O8 –Al3	175	–2518.38	–0.69	–2765.24	3.38	–0.04

TABLE 5.2. **Results of MNDO Calculations on the Cluster Models of $AlPO_4$–11 Lattice and the Ammonia Adsorption Complexes.**

The favourable adsorption sites for ammonia are found to be O4, O5, O5′ and O6′. Incidentally, the values of T–O–T angles for these oxygen sites are minimum (Table 5.2). The ammonia prefers to adsorb on oxygen sites where the steric hindrance for ammonia to approach oxygen site is minimum and this argument is applicable to the secondary amines also. The amine molecule may undergo multiple site adsorption with the hydrogen atoms of the alkyl groups having interactions with other oxygen atoms of the framework. The topographic analysis of the framework indicates that the favourable oxygen adsorption sites predicted by electronic structure calculations lie at different positions of the framework. O6′ is on the wall common to 4–member and 6–member channels and hence the template molecule can not physically approach this site. O4 is on the wall common to 6–member and 10–member channels, while O5 and O5′ are on the walls common to 4–member and 10–member channel as could be made out from the Fig. 5.2. It is encouraging to note that the present findings are in correspondence with the studies[11] on the crystal structure analysis of the as–synthesized MnAPO–11 material, which show that the diisopropylamine is located inside the pore in such a way that nitrogen lies closer to O4 and O5 of the framework.

5.3.5 ^{13}C MASNMR Studies

The ^{13}C CP MASNMR spectroscopic studies on as–synthesized $AlPO_4$–11 with n–dipropylamine, n–dibutylamine and n–dipentylamine template molecules indicate that they are chemically intact without undergoing any dissociation as shown in Fig. 5.4. The asymmetric doublet pattern($\approx$55 ppm) arising in ^{13}C NMR spectra of carbons bonded to nitrogen can be attributed due to ^{14}N – ^{13}C quadrupolar effects as explained by Naito et al.[12]. Otherwise unsplitted signals for the methylene and methyl carbon indicate that both the alkyl groups in dialkylamines are in an uniform environment inside the $AlPO_4$–11 framework and both alkyl groups are in same conformation.

When the as–synthesized samples are dried at higher temperatures, the NMR spectrum shows a split in the methyl group signal. This is shown in Fig. 5.5. for $AlPO_4$–11 synthesized using n–dibutylamine dried at 373 K. Such a solid–state splitting could be

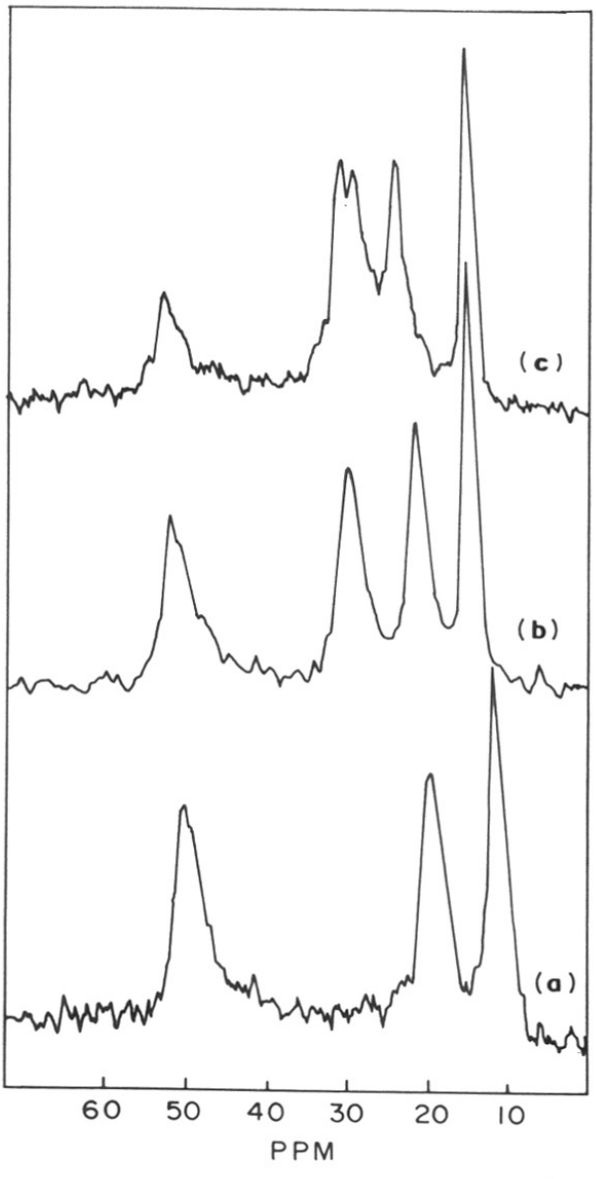

Fig. 5.4 ▷ ^{13}C CP MASNMR spectra for as–synthesized $AlPO_4$–11 with (a) n–dipropylamine; (b) n–dibutylamine; (c) n–dipentylamine as templating molecules.

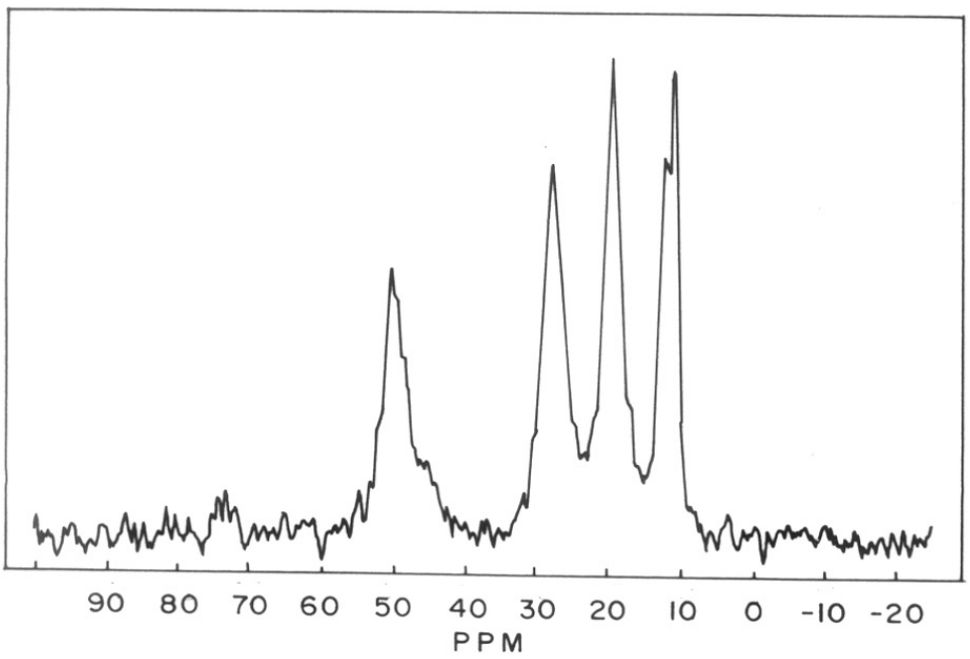

Fig. 5.5 ▷ ^{13}C CP MASNMR spectrum for $AlPO_4$–11 synthesized using n–dibutylamine dried at 373 K.

due to environmental changes or due to conformational changes occurring to the occluded species. In the earlier studies[13,14], it was reported that templating molecules existing in uniform environment inside ZSM–5 and ZSM–11 framework give rise to unsplitted signals. Boxhoorn et al.[14] have provided evidence from ^{13}C MASNMR studies that in the case of TPA ion inside ZSM–5 framework, the species undergoes conformational changes on heat treatment.

Conformational changes between the two alkyl groups is expected to cause splitting in the methyl as well as the methylene group signals. However, since the splitting occurs only in the signal of methyl group (Fig. 5.4), the fact that the terminal methyl group alone is present in a different environment is brought out. These results indicate that the template molecules are still chemically intact and they possess freedom for the dynamic behaviour inside the neutral $AlPO_4$–11 framework. The amines may have more than one favourable adsorption site and the values of adsorption energy are expected to be comparable, thus facilitating its migration from one to another favourable site. This observation is in correlation with the findings from electronic structure calculation that there are three oxygen sites for adsorption of basic molecules with comparable adsorption energy (Table 5.2). As mentioned earlier, one of the terminal methyl group carbon could enter a double 6–member side pocket of the 10–member straight channel and thus exist in a different environment.

5.4 CONCLUSIONS

The following observations are the outcome of the present study:

1. The favourable oxygen sites for the adsorption of amine molecules are O4, O5 and O5′ as predicted by the electronic structure calculations. It is also observed that the results are consistent with the findings from single crystal powder diffraction studies of as–synthesized MnAPO–11, that the diisopropylamine is hydrogen bonded to O4 and O5.
2. The occluded amine molecules in as–synthesized $AlPO_4$–11 samples are chemically intact. At higher temperatures, they have a dynamic freedom inside the pores as indicated by NMR studies.

3. In deciding the role of these amine molecules as templates the geometric factor plays a relatively insignificant role compared to the electronic factor because of the conformational flexibility and the possibility of accommodating the methyl groups in side–pockets.
4. As far as the electronic factor, there is a small but subtle difference in the electron density distribution among the various primary, secondary, and tertiary amines. It appears that the different amines may also play a role only in modifying the pH of the precursor gel thereby facilitating the synthesis to different extents. It is difficult to estimate the pH modifier role played by template molecules from the present study. In the formation of $AlPO_4$–11, the electronic influence of amine molecules seems to be greater than the geometric factor.

5.5 REFERENCES

1. S.T. Wilson, B.M. Lok, C.A. Messina and E.M. Flanigen, *Proc. Int. Zeo. Conf.*, Butterworths, Guildford, 1984, **p.97**.
2. N.J. Tapp, N.B. Milestone, D.M. Bibby, *Zeolites*, **8**, 183, 1988.
3. J.B. Moffat, R. Vetrivel and B. Viswanathan, *J. Mol. Catal.*, **30**, 171, 1985.
4. R. Carson, E.M. Cooke, J. Dwyer, A. Hinchliffe and P.J. O'Mallay, *Stud. Surf. Sci. Catal.*, **46**, 39, 1989.
5. J.G. Fripiat, E.G. Derouane and R. von Ballmoos, *J. Phys. Chem.*, **94**, 1687, 1990.
6. *"Molecular Modelling Package: Quanta and charm – Release 2.1, 1990"*, developed by Polygen Corporation, U.S.A.
7. M.J.S. Dewar, W. Thiel, *J. Am. Chem. Soc.*, **99**, 4899, 1977.
8. B.R. Gelin, M. Karplus, *Proc. Natl. Acad. Sci. USA*, **72**, 2002, 1975.
9. N.J. Tapp, N.B. Milestone, *Stud. Surf. Sci. Catal.*, **36**, 639, 1988.
10. J.W. Richardson Jr., J.J. Pluth, J.V. Smith, *Acta. Crystallogr.*, **B44**, 376, 1988.
11. J.J. Pluth, J.V. Smith, J.W. Richardson Jr., *J. Phys. Chem.*, **92**, 2734, 1988.
12. A. Naito, S. Ganapathy, C.A. McDowell, *J. Chem. Phys.*, **74**, 5393, 1981.
13. J.B. Nagy, Z. Gabelica, E.G. Derouane, *Zeolites*, **3**, 43, 1983.
14. G. Boxhoorn, R.A. van Santen, W.A. van Erp, G.R. Hays, N.C.M. Alma, R. Huis, A.D.H. Claque, *Proc. 6th Int. Zeo. Conf. Reno, USA*, (Eds.D. Olson, A. Bisio), Butterworths, 1984, **p. 694**